Liquid Crystalline Phases of Anisotropic, Polymer Functionalized Nanoparticles

Dissertation
zur Erlangung des Grades
„Doktor der Naturwissenschaften“
im Promotionsfach Chemie
am Fachbereich Chemie, Pharmazie und Geowissenschaften
der Johannes Gutenberg-Universität Mainz

vorgelegt von

Stefan Meuer
geboren in
Bad Soden am Taunus

Mainz, 2008

Die vorliegende Arbeit wurde unter Betreuung von XXXXXXXXX in der Zeit von Oktober 2005 bis September 2008 am Institut für Organische Chemie der Johannes Gutenberg-Universität Mainz angefertigt.

Dekan:	XXXXXXXXXXXXX
Erster Berichterstatter:	XXXXXXXXXXXXX
Zweiter Berichterstatter:	XXXXXXXXXXXXX

Tag der mündlichen Prüfung:

Deutsche Zusammenfassung

Diese Arbeit beschäftigt sich mit der Polymerfunktionalisierung formanisotroper Nanopartikel wie TiO_2 Nanostäbchen oder Kohlenstoff Nanoröhren. Dies dient der Solubilisierung und sterischen Stabilisierung in organischen Medien, da diese ionenfrei hergestellt werden können, was eine Nutzung für nanoskopische, elektrische Schaltkreise ermöglicht. Die Polymere wurden mittels der RAFT (reversible addition-fragmentation chain transfer) Polymerisation mit engen Molekulargewichtsverteilungen hergestellt. Im Detail wurden Ankergruppen in Blockcopolymere und an der Alphaposition eingeführt, welche eine Anbindung an die Nanopartikeloberfläche ermöglichen. Die Polymere wurden durch Variation der verschiedenen Blocklängen für eine bestmögliche Adsorption optimiert. Die so gewonnenen Polymer funktionalisierten Nanopartikel zeigten eine gute Löslichkeit in organischen Medien und zeigten zudem eine lyotropes, flüssigkristallines Phasenverhalten. Dies war aufgrund der Formanisotropie zu erwarten, zeigte jedoch ebenfalls ein unerwartetes thermotropes Verhalten, welches durch die Polymerhülle erzeugt wurde. Die Flüssigkristalle wurden eingehend mittels polarisierter Mikroskopie und Differential Scanning Calorimetry (DSC) untersucht. Die flüssigkristallinen Phasen aus Nanostäbchen und –röhren wurde dann zur Orientierung der anisotropen Nanopartikel benutzt und es konnten makroskopisch geordnete Proben hergestellt werden. Die Polymerhülle um die Nanopartikel ermöglichte es ebenfalls diese in Polymerfilme einzuarbeiten und so Nanopartikelverstärkte Kunststoffe herzustellen.

Schlagwörter:

Anisotrope Nanopartikel, TiO_2 Nanostäbe, Kohlenstoff Nanoröhren, Polymer Synthese, RAFT Polymerisation, Flüssig Kristall, Makroskopische Orientierung.

English Abstract

This thesis focuses on the polymer functionalization of anisotropic nanoparticles like TiO_2 nanorods and carbon nanotubes. The polymer corona is used to stabilize the nanoparticles sterically and to dissolve them in organic media. These media are highly desired as they are intrinsically ion-free, which allows their use for the fabrication of nano-scaled electronic devices. The polymers were synthesized with the reversible addition-fragmentation chain transfer (RAFT) polymerization with low polydispersities. Anchor units were incorporated in block copolymers or at the alpha position of homoblock polymers, which allows the specific binding to the nanoparticle surface. The polymers were optimized by variation of the block lengths for maximal adsorption. The resulting polymer functionalized nanorods and –tubes were well soluble in organic media and a lyotropic liquid crystalline behavior. This was expected from their shape anisotropy, but they showed an additional, unexpected thermotropic behavior induced by the polymer corona. The liquid crystals were investigated by polarizing microscopy and differential scanning calorimetry (DSC). The lyotropic liquid crystalline phases from nanorods and –tubes were used for the orientation of the anisotropic nanoparticles and macroscopically oriented samples were produced. The polymer corona did also allow to incorporate the nanoparticles into polymers resulting in nanoparticles reinforced plastics.

Keywords:

Anisotropic nanoparticles, TiO_2 nanorod, Carbon nanotube, polymer synthesis, RAFT polymerization, liquid crystal, macroscopic orientation.

A Introduction

A.1 Liquid Crystals

Liquid crystals are partially ordered, anisotropic fluids. They are thermodynamically located between the three-dimensionally ordered solid crystal and the totally unordered liquid state. They usually show ordering in one or two dimensions in space while the other dimensions are unordered and give mobility to the system. For instance, a liquid crystal (LC) may flow like a liquid, but have the molecules in the liquid arranged and oriented in space. There are many different varieties of liquid crystalline phases known according to their degree of order and the impact of temperature and/or concentration. Liquid crystals were first found by the Austrian botanical physiologist Friedrich Reinitzer in 1888, working at the German University of Prague, who was extracting cholesterol from carrots to establish its chemical formula. He investigated the properties of various derivatives of cholesterol and found a strange behavior for cholesteryl benzoate. The substance showed two “melting points”: around 145.5℃ it melted into a cloudy liquid, and at 178.5℃ it melted again and the cloudy liquid became clear. Nowadays we know that the first transition was from crystalline to liquid crystalline and the second one from liquid crystalline to isotropic, also called the clearing point. At that time this phenomenon was not understood and Reinitzer sent samples to Otto Lehmann in Karlsruhe. He was a well known expert on crystallography and observed the same behavior Reinitzer described. Lehmann developed the revolutionary concept that a new, previously undescribed, state of matter was found and used the names “living crystal” or “liquid crystal” for the first time. His concept was heavily attacked by the scientific communities which argued that impurities induced this strange behavior. It took a while until Daniel Vorländer from the University of Halle found that the molecular

shape of a substance correlates to the existence of a LC. He revealed that among different isomers of aromatic substances, the para substituted were the only ones showing LC behavior.

The liquid crystal phase is also called a mesophase from the Greek word “meso” – “in between” the classical crystal and liquid phases. The building blocks of liquid crystals, called mesogens, are classified by their shape, as this is the origin of the mesophase behavior. The shape has to be anisotropic which can be realized by rod-like, disc-like and lath-like molecules. Liquid crystals formed by rod-like molecules are called calamitic, by disc-like molecules discotic and by lath-like molecules sanidic. Another important classification of liquid crystals is done by the variable inducing the liquid crystalline phase. One is temperature and these liquid crystalline phases are called thermotropic and the other is volume fraction in solution and those are called lyotropic liquid crystals.

For the liquid crystalline behavior of rod-like particles many theories have been developed by Onsager, Flory and Alben.[1,2,3] In these theories, a simple hard body interaction was used to explain the packing of rods for given volume fractions or in more general given partial pressures. It is obvious that the packing-volume needed by many rods can be minimized by aligning the rods parallel to each other, which directly leads to the creation of an anisotropic phase. There is also an impact of the aspect ratio: as spheres (aspect ratio = 1) pack best in an isotropic phase, one can imagine that there is a minimal aspect ratio needed to form an anisotropic packing. The minimal aspect ratio (length to width of the rods) found by the different models differ from 3.5 for the oldest and up to 6.5 for the latest model of Flory. This minimal aspect ratio is lowered when additional attractive interactions are present. They couple neighboring rods to similar orientations in space and the rods behave as if their aspect ratio is increased. This can be anisotropic interactions like dipolar or

induced dipolar moments as they are present for all organic molecules (their aspect ratios are usually much smaller than 6.5) possessing a liquid crystalline phase. The critical volume fractions of rods needed for a liquid crystalline phase is a function of the aspect ratio and decreases with increasing volume fraction. Flory's calculation gave a volume fraction of 1 for an aspect ratio of 6.5 and 0.36 for an aspect ratio of 20. These values are also affected by additional attractive interactions and reduce the minimal volume fraction needed for a liquid crystalline phase.

For calamitic liquid crystals three major phases are known and George Friedel introduced their nomenclature: the nematic (from "nema" (Greek) = thread), the cholesteric (derived from cholesteryl derivatives) and the smectic (from "smegma" (Greek) = soap) phases. In the nematic phase the rod-like objects are aligned in one direction (called director), but without any correlation of the centers of mass. The molecules are distributed randomly in space as in an ordinary liquid and are therefore usually less ordered than other liquid crystalline phases. Their degree of order can be quantified by the order parameter $\boldsymbol{S}$, which has a value of one for perfect order and zero for no order. It is calculated by the following formula:

Equation A.1
$$\boldsymbol{S} = \left\langle \frac{3\cos^2\theta - 1}{2} \right\rangle$$

with θ, the angular difference to the average orientation, the director. A typical value for a well ordered nematic phase is 0.7 but decreases rapidly down to 0.3 close to the clearing point.

The cholesteric phase is the chiral version of the nematic phase. It also possesses the orientational order of the chiral rods, but shows a spontaneous macroscopic helical superstructure with the helical axis perpendicular to the local director. It can be imagined as a stack of nematic layers, which are continuously twisted with respect to each other. The helical pitch of the cholesteric phase often lies

in the range of visible light, which leads to selective reflectance of certain colors as it was observed for cholesteryl benzoates by Reinitzer.

The smectic phases are showing not only a directional order but also a positional order of the mesogens into a layered structure. Smectic phases are subdivided into more liquid like phases smectic A and C (the mesogens are distributed randomly within the layers), the hexagonal phases smectic B, I and F (short range hexagonal order within the layers) and crystal like smectic J, G, E, K and H phases with increasing degree of order within the layers, but without interlayer correlation. Most phases are very difficult to find and it is hard to distinguish them. The more common phases are the smectic A (S_A) and smectic C (S_C) phases. A schematic overview of nematic, cholesteric, S_A and S_C phases can be found in figure A.1.

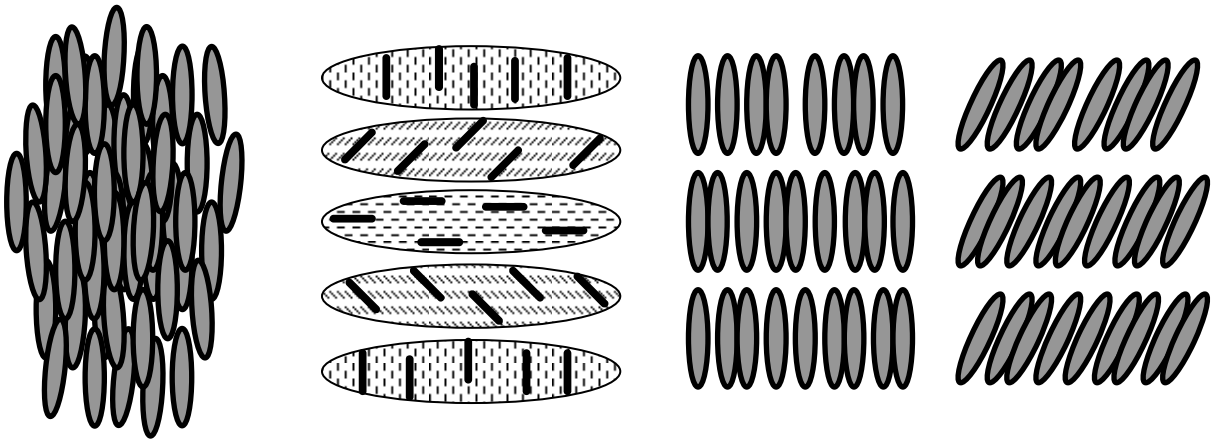

Figure A.1: Scheme of nematic, cholesteric, smectic A and smectic C liquid crystalline phases.

One way to distinguish the different liquid crystalline phases is to analyze them by polarizing microscopy. The textures found between crossed polarizers are usually typical for one phase, but a final determination should be done by X-ray scattering. A

typical texture for a nematic liquid crystal is for example the Schlieren texture. The birefringent domains are separated by dark lines flowing into dark point defects. Depending on the nature of the point defect, two or four dark lines are emanating from that spot. These points are defects in the director field and the dark lines are created as the director flows around these points being locally parallel to the analyzer or polarizer pair (see figure A.2). Smectic A phases often show the formation of batônnets when cooling from the isotropic phase and a fan-shaped texture is often found. Both texture show elongated homogeneously birefringent domains that are built up by the smectic layers (see figure A.2).[4]

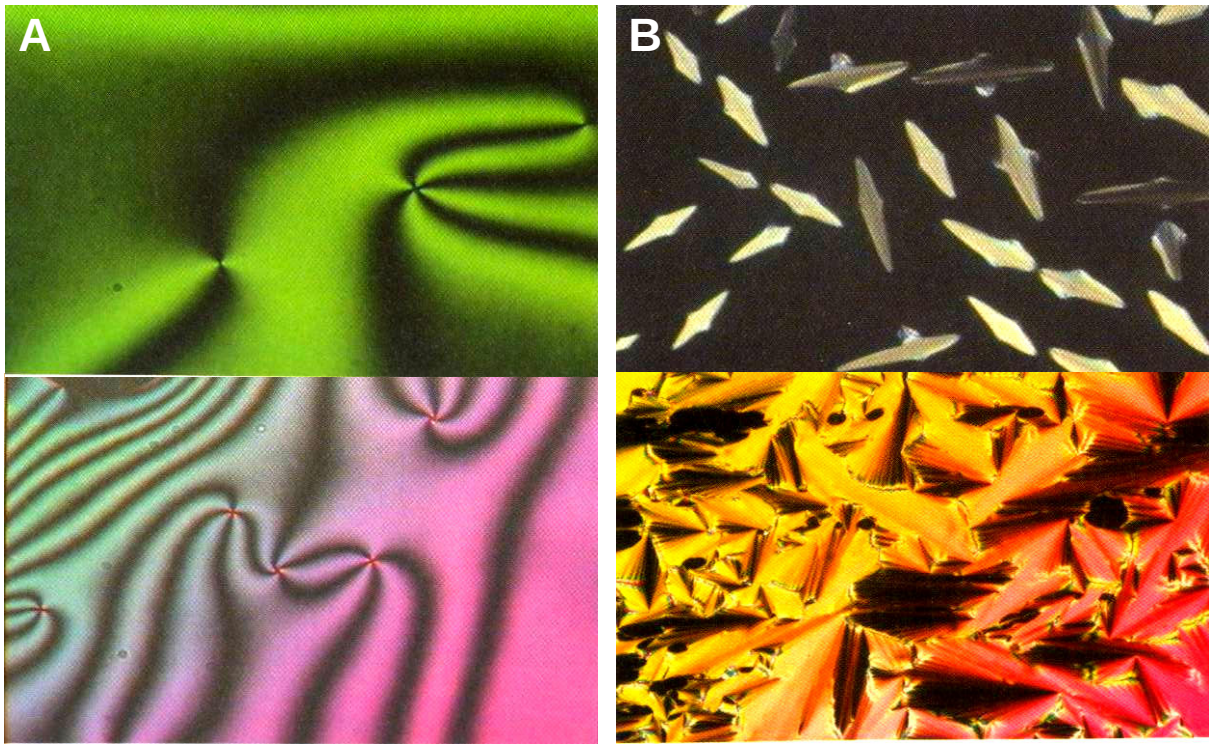

Figure A.2: A: nematic Schlieren textures; B: upper image: smectic batônnets, lower image: smectic fan-shaped texture presented in lit. 4.

All these different phases can be found for both thermotropic and lyotropic phases. The term lyotropic liquid crystal is used in literature for two very different systems: for surfactants in water and for dissolved / dispersed rod-like molecules, polymers,

colloids or nanoparticles in solvents. In the first system, surfactants are dissolved in water well above their critical micelle concentration and depending on the surfactant, anisotropic micelles are formed. These micelles (superstructures of small molecules) behave like the rod-like objects and liquid crystalline phases can be found.[5] In the other system, a solvent is used to change the volume fraction and thus the mobility of the rods. For organic molecules and polymers this is sometimes needed as the crystalline to liquid crystalline transition temperatures are beyond the decomposition temperature (see figure A.3).

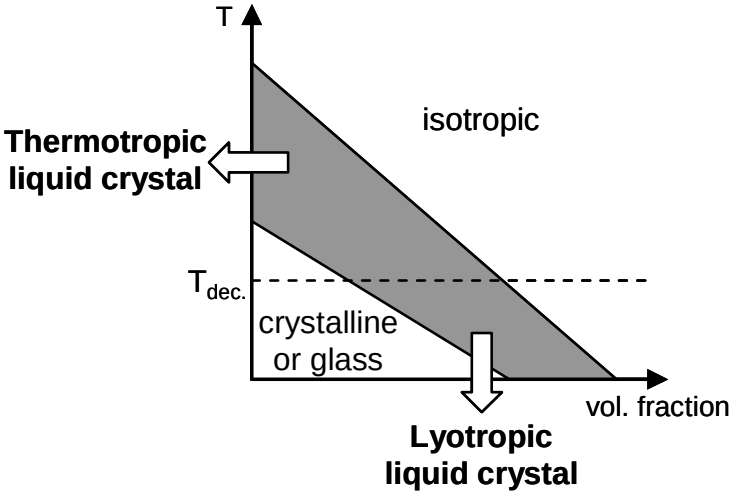

Figure A.3: Impact of volume fraction and temperature on the accessibility of a liquid crystalline phase for organic molecules or polymers.

The solvent acts as a plasticizer and reduces the transition temperatures below the decomposition temperature by increasing the mobility of the system. Especially for anisotropic colloids or nanoparticles the mobility of the rods has to be increased as they are usually totally immobile in their pure state. As already claimed by the theories, the volume fraction of solvent cannot be increased infinitely without losing the liquid crystalline phase. In the case of temperature dependant solvent-rod interactions one can accept an additional effect of temperature on the phase behavior.

A.2 Anisotropic Nanoparticles

Starting from the discovery of carbon nanotubes in 1991 by Iijima,[6] various anisotropic nanoparticles have been found. A broad range of oxidic, metallic and organic nanorods or nanotubes is available nowadays as their unique structural versatility as well as anisotropic chemical and physical properties are highly interesting. Due to nano-confinement effects known from spherical nanoparticles, the short nanorod axis differs significantly from the long axis leading to anisotropic optical, electrical, mechanical and chemical properties. Thus, expectations concerning the application of nanomaterials are rising as the technological limits of today's microdevices are already becoming apparent. Downscaling conventional technologies by at least an order of magnitude is necessary as the next logical step, and nanoparticles are the perfect building blocks for this purpose.

There are two general classes of anisotropic nanoparticles: nanotubes and nanorods. Carbon nanotubes (CNT) have been the first anisotropic nanoparticles that were found as mentioned above and nowadays a variety of nanotubes made from carbon, V_2O_5, TiO_2, SiO_2, NbS_2, WS_2, MoS_2, CdS, CdSe, GaS, PbS and many other materials are available. All of them have unique properties like being extremely mechanically tough (e.g. CNT)[7], being semiconductors (e.g. TiO_2) or being efficient lubricants (e.g. MoS_2).[8] The synthetic methods vary from catalyzed chemical vapor depositions (e.g. CNT), templated sol-gel methods (e.g. TiO_2) or even CNT templated growth methods (e.g. SiO_2).[9]

The other major class of anisotropic nanoparticles are nanorods. Over the last years, many metallic, oxidic as well as chalcogenic nanorods were synthesized. The variety includes fluorescent CdSe nanorods, semiconducting TiO_2 nanorods and highly conductive gold nanorods. The synthetic routes are quite different for each

material and there is no general approach. CdSe nanorods can be easily made by changing the surfactants used for a normal CdSe nanoparticles synthesis, enhancing the speed of growth of different crystal sites. Gold nanorods are usually produced in an aqueous surfactant solution and the surfactant micelles template the nanorods growth.[9]

A.2.1 TiO_2 Nanorods

Titanium dioxide is a well known commercial product accounting for ≈ 70% of the total pigment production volume of the world. It is often used as additive in sun blocker, as TiO_2 is a white and highly scattering solid (refractive index of 2.8) and it adsorbs UV radiation (band gap = 3.0 eV = 410 nm). It is also used for waste water treatment as TiO_2 is a strong photo-oxidizer. The same property is used for self-cleaning surface coatings which are always clean, sterile and non-fouling. Another property of titanium dioxide was used by Grätzel et al. who produced a cheap and efficient solar cell concept based on TiO_2 as semiconducting material for electron transport.[10] In this concept, the TiO_2 also acts as scattering back mirror of the cell enhancing the light harvesting.

Titanium dioxide nanorods used for this work were synthesized using a sol-gel method under very acidic conditions. The pH-value together with a temperature of 140 ℃ directs the rutile crystal growth towards a rod-like shape. Rutile crystallizes in an elongated tetragonal crystal lattice and has therefore chemically different crystal sites. Therefore it is possible to favor the growth of certain crystal sites by controlling pH-value and temperature. The resulting nanorods are polydisperse in length and width, but at a stable aspect ratio around 5.5. The length averages of these nanorods are $<L_n>$ = 71 nm and $<L_w>$ = 90 nm resulting in an polydispersity index ($<L_w>/<L_n>$)

of 1.3. To obtain this distribution, we analyzed 350 rods from SEM and TEM images and used the length distribution (see figure A.4) to calculate the average surface per nanorod (= 3800 nm^2) and their average volume (= 15000 nm^3). With these values and the known density of rutile (4260 kg/m^3) one can calculate the average surface and the average number of rods present per mg powder to $\langle S \rangle_{1mg} = 9.6*10^{16}$ nm^2 and $\langle N \rangle_{1mg} = 8.8*10^{13}$.

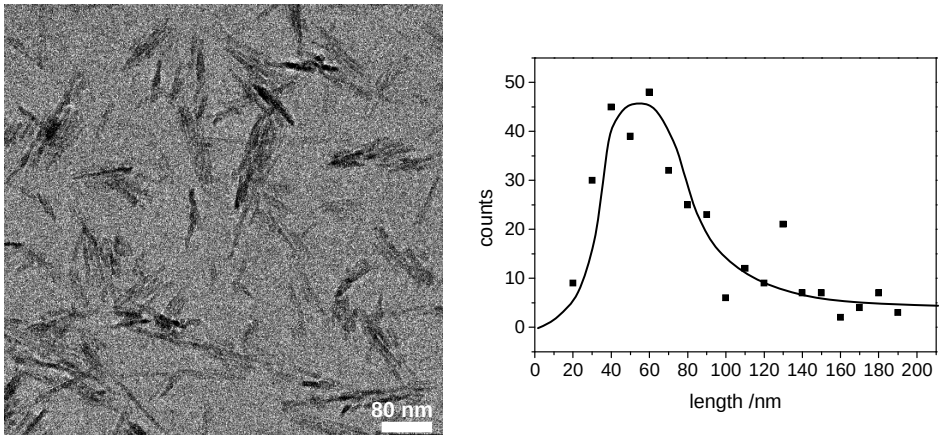

Figure A.4: TEM image and length distribution of TiO_2 nanorods (the line is only a guide to the eyes).

The distribution of the nanorods shows a peak at 60 nm and a long decay of the length up to almost 200 nm. The distribution function looks like a Schulz-Flory distribution known from polymer science.

A.2.2 Carbon Nanotubes

There are two major classes of CNTs: Single-walled and multi-walled CNTs. Single-walled CNTs (SWCNT) can be imagined as a rolled sheet of graphene. The way the graphene sheet is wrapped is represented by a pair of indices (n,m) called the chiral vector. The integers n and m denote the number of unit vectors along two directions in the honeycomb crystal lattice of graphene. If m=0, the nanotubes are called "zigzag" (helical, non-chiral) and if n=m, the nanotubes are called "armchair" (non-helical, non-chiral). Otherwise, they are called "chiral" (helical, chiral; see figure A.5).

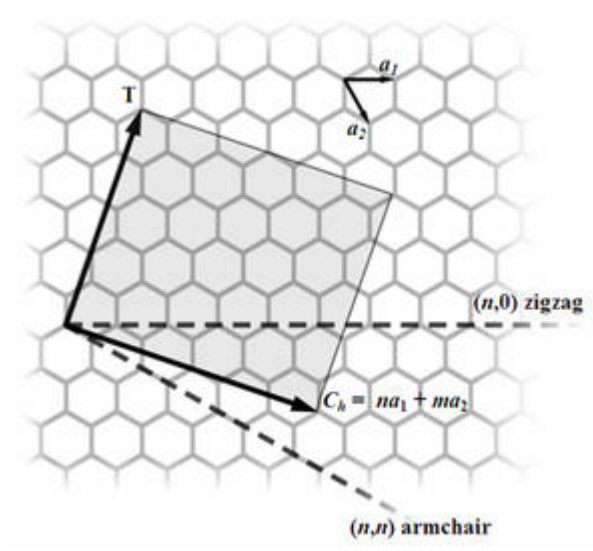

Figure A.5: Visualization of the chiral vector of an unrolled SWCNT.

SWCNTs have very unique electronic properties which are directly correlated to their chiral vector: For a given (n,m) CNT, if $^{(n-m)}/_3$ is a natural number, then the nanotube is metallic, otherwise the nanotube is a semiconductor. Thus theoretically, one third of all (n,m) CNTs is metallic. In more detail, all armchair (n=m) nanotubes are metallic, while some zigzag or chiral nanotubes are semiconducting, some metallic. In theory, metallic nanotubes have an electrical current density more than 1,000

times larger than metals such as silver and copper. This fact combined with extreme mechanical properties as young modules of 0.8 – 0.9 TPa (Kevlar: 0.25 TPa, stainless steel: 0.2 TPa) and tensile strengths of 10 – 150 GPa (Kevlar: 3.5 GPa, stainless steel: 1 GPa) makes them a highly interesting material.[11] As a drawback, the synthesis of SWCNTs is not up-scalable to large quantities (kg, or ton scale) so far.

Multi-walled CNTs are built up out of several CNTs fitting exactly into the next wider tube. A nice comparison can be done by looking at the famous Russian Matryoshka doll, which contains of several wooden dolls fitting all one into each other (see figure A.6).

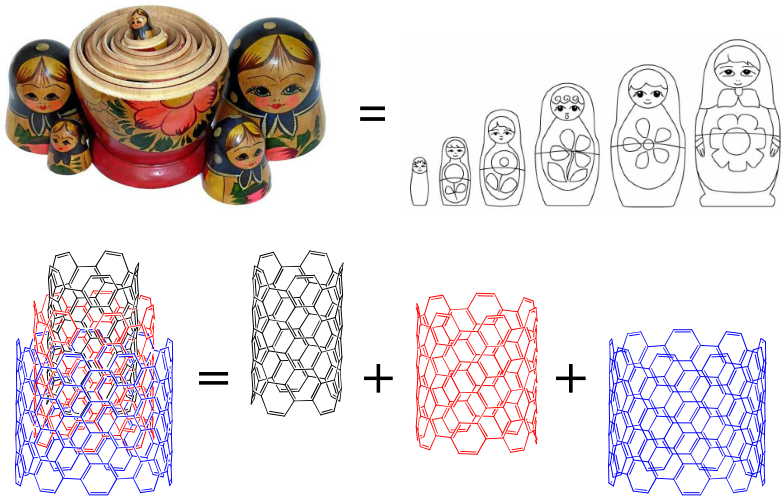

Figure A.6: Build-up of the Russian Matryoshka doll and of multi-walled carbon nanotubes.

The spacing in between two CNTs inside a multi-walled CNT (MWCNT) is usually around 3.3 Å, which is exactly the same spacing as between two graphene sheets in natural graphite. The reason for that is obvious, as the lowest energy of packing is achieved at this distance. Their mechanical properties are similar to those of SWCNT and the electronic conductivities are also comparable.

The MWCNTs used in this work are Baytubes® C 150 P which were kindly donated by Bayer MaterialScience AG. Their tensile strength is larger than 10 GPa, the young modulus is larger than 1 TPa, the thermal conductivity is larger than 2000 W/mK and the electric conductivity is around 10^4 S/cm. They are produced via a metal catalyzed chemical vapor deposition method and are collected as highly entangled aggregates of roughly 0.5 mm (see figure A.7).

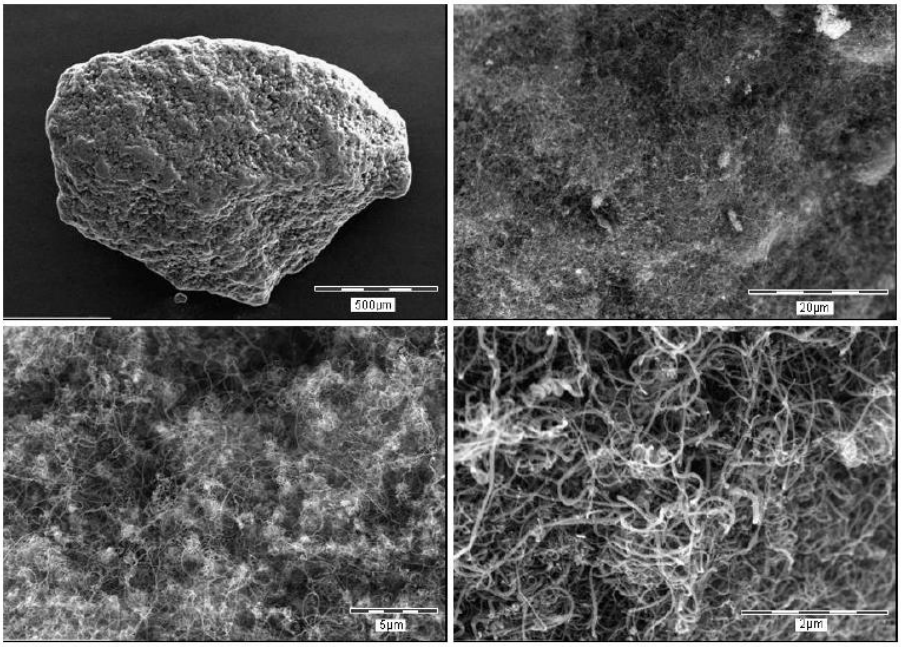

Figure A.7: SEM images of Baytube® aggregates.

The CNTs are highly pure as no amorphous carbon can be found and the carbon purity is larger than 95 %. The MWCNTs have between 3 to 15 walls with an outer diameter between 5 and 20 nm and have a length between 1 and 10 µm. Their aspect ratio is therefore very large, making them prominent materials for liquid crystalline phases.

A.3 Controlled Radical Polymerization

Controlled radical polymerization techniques were developed at the end of the 1980s. At that time, most scientific research on radical polymerization ceased as the polymerization control was too poor, compared to living anionic polymerization, to produce well defined systems desired by the scientific community. The reasons for this are side and termination reactions leading to highly polydisperse systems. On the other hand, living ionic polymerization is highly limited concerning functional monomers. This opened the desire to combine the advantages of both systems leading to well defined polymers of functional monomers. The first approach used so called “Iniferters” (initiation – transfer – termination agent) as additives to a normal radical polymerization. Effectively, these agents reduced the speed of polymerization by reducing the number of radical (= free chain ends) via the creation of an equilibrium between the normal active chain end and a dormant species (see figure A.8).[12]

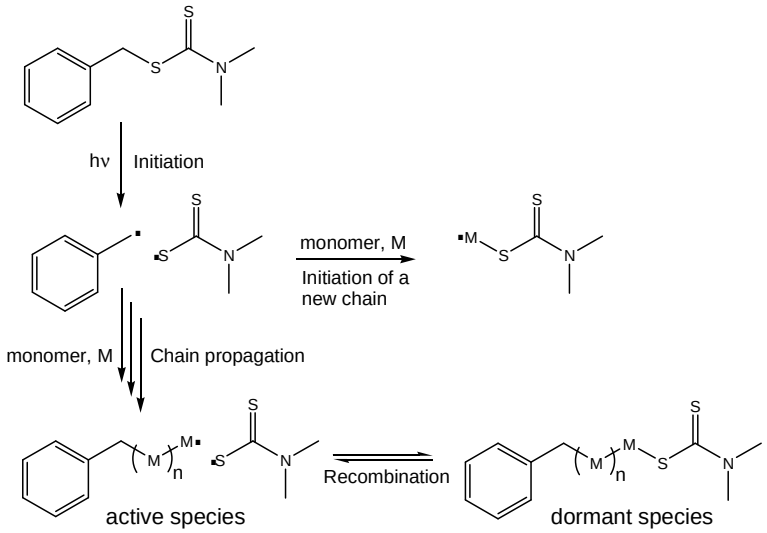

Figure A.8: Mechanism of an iniferter mediated polymerization.

This method worked quite well for the suppression of termination reactions but still leads to a broad molecular weight distribution as initiation of new chains occurs, besides the mediation, at any time. Thus, initiation of new growing chains must also be inhibited to achieve a narrow and predictable molecular weight distribution as found for anionic polymerization.

Out of this first system three major controlled radical polymerization techniques evolved: the ATRP (atom transfer radical polymerization), the NMP (nitroxide mediated polymerization) and RAFT (reversible addition fragmentation chain transfer) polymerization techniques. All methods use an equilibrium reaction between an active and a dormant chain end, controlling the polymerization. How this equilibrium controls the polymerization is different for ATRP and NMP compared to RAFT: For ATRP and NMP, the free radical concentration is significantly lowered, leading to the loss of termination reactions (the free radical concentration squared enters in the speed of termination) but also the speed of polymerization is significantly lowered. The control for RAFT polymerization is achieved by a fast chain transfer while termination reactions occur as in conventional radical polymerization. As a side effect of chain growth control, all methods allow the build-up of block copolymers by reactivation of the dormant chain end.

A.3.1 Atom Transfer Radical Polymerization

This polymerization technique was invented by the group of Matyjaszewski in 1998 at the Carnegie Mellon University in Pittsburgh, Pennsylvania.[13] It uses a reversible transfer of halogen atoms (therefore the name atom transfer…) between a catalyst and the active chain end getting dormant when receiving the halogen atom. The

catalyst is usually a transition metal which allows a reversible addition and removal of the halogen atoms by a redox reaction (see figure A.9). Typical examples are metal organic copper(I) complexes stabilized by 2,2'-bipyridines, tetramethyl ethylendiamine (TMEDA) or triphenyl phosphane. Copper is not the only transition metal used for ATRP but the most commonly used one. The choice of the ligand sphere needs to be optimized for the solvent as well as the monomer used making it hard to adopt this method for new monomers. So far, polymerizations of the following monomers were performed: styrene and styrene derivatives, acrylates, methacrylates, acrylnitril, methacrylamide and methacrylic acid.[13]

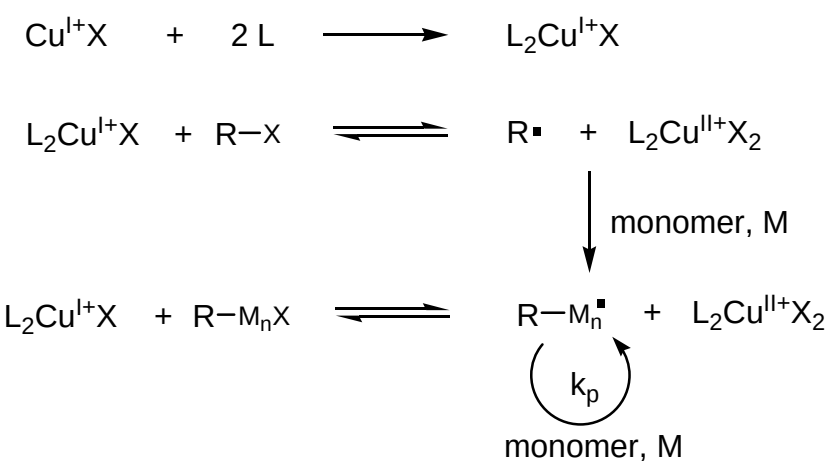

Figure A.9: Mechanism of ATRP.

The halogen atom usually used is bromine, but also others are known. Concerning the purification of these polymers, residual transition metal complexes have to be removed, which can be difficult depending on the system used.

A.3.2 Nitroxide Mediated Polymerization

The nitroxide mediated polymerization technique was developed by Hawker et al.[14] 1997 after primary research by Georges et al. 1993.[15] Similar to the ATRP, a reversible equilibrium between dormant and active species is used for control. In the first experiments performed by George et al., a stable free radical – a nitroxide – is added to a normal polymerization. After initiation, the nitroxide radical can combine with a radical chain end, resulting in a dormant species. The nitroxide to chain end bond is thermo reversible and the active chain end is recovered (see figure A.10).

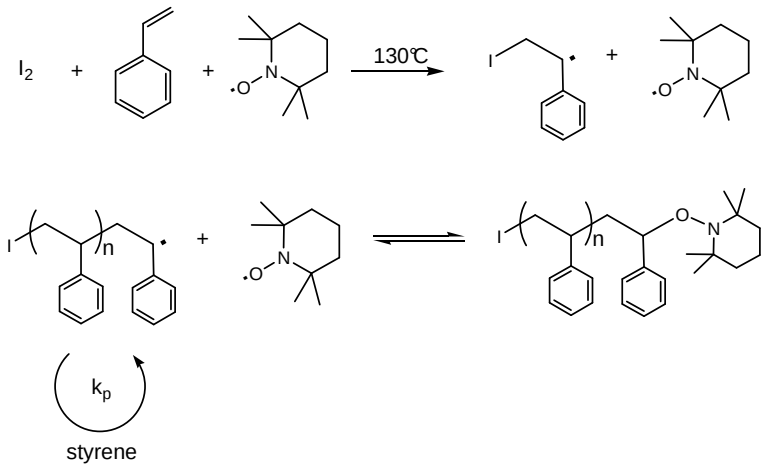

Figure A.10: Mediation of a radical polymerization by the addition of nitroxides.

This first experiment yielded a polymer with lower polydispersity than 1.5, but overall the polymerization was not well controlled. The initiation is rather undefined in this bimolecular system of initiator and control agent. Therefore, a monomolecular approach was investigated by Hawker et al., leading to a better controlled system. The idea was to mimic the dormant chain end obtained by George's approach, which can then be activated to the active species with a perfect 1:1 ratio of active chain ends and stable free radical in solution (see figure A.11).

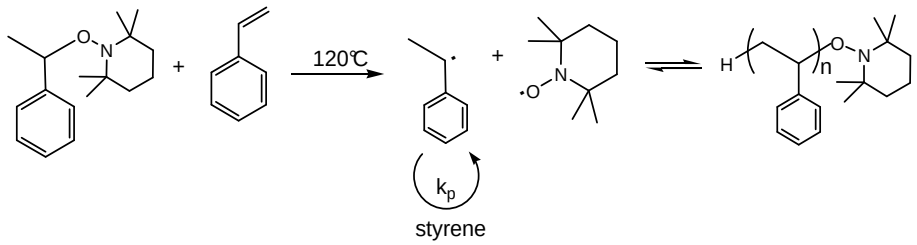

Figure A.11: Mechanism of an unimolecular nitroxide mediated polymerization.

This approach was successful and yielded well defined polymers based on styrene. Following the same approach, multifunctional starters can be synthesized opening the field to star polymers. But TEMPO (2,2,6,6-Tetramethyl-1-piperidin-1-oxyl) was suitable only for the polymerization of styrene and styrene copolymer with large styrene content. Other monomers can only be polymerized with modified nitroxides. The best performance is achieved by acyclic nitroxides having a α-hydrogen and they allow polymerization of styrene, acrylate, methacrylate, acrylamide, acrylnitrile and 1,3-diene with polydispersities of 1.05 (see figure A.12).[16,17] Obviously, the design of the nitroxide has a large impact on the polymerization leading to the necessity to modify the initiator for new monomers.

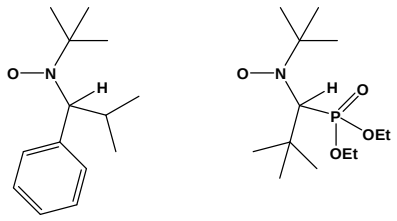

Figure A.12: Efficient nitroxides for the polymerization of most vinyl monomers.

A.3.3 Reversible Addition-Fragmentation Chain Transfer Polymerization

The first reports on radical addition-fragmentation reactions appeared in the early 1970s[18] but the first direct use of addition-fragmentation transfer agents was reported by Rizzardo et al. in the late 1980s.[19] A very recent review on "radical addition-fragmentation chemistry in polymer science" by Moad, Rizzardo and Thang in 2008[20] summarizes the research progress on the mechanism of RAFT polymerization, RAFT agents and polymerizable monomers. The general build-up of a RAFT agent is shown in figure A.13.

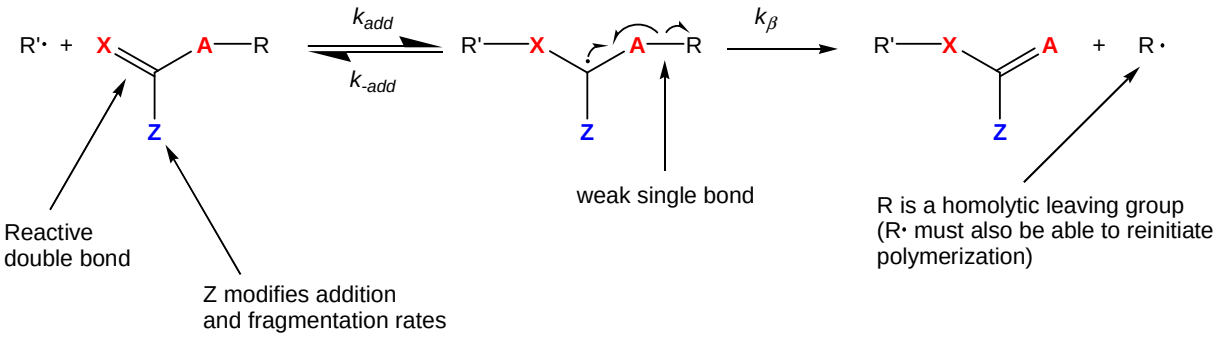

A.13: Build-up and function of a RAFT agent.

As the C=X double bond must be reactive towards radical addition, X is most often CH_2 or sulfur. The Z-group affects the reactivity of the RAFT agent towards the propagation of the radical and the stability of the intermediate radical species (middle structure of fig. A.13). Examples of A-units are CH_2, CH_2=$CHCH_2$, oxygen and sulfur. The created radical R• must be suitable for the reinitiation of polymerization and needs to be chosen correctly for each monomer.

In terms of rate constants, an efficient RAFT polymerization is performed when the RAFT agent possesses the following properties: It must be equipped with a reactive C=X double bond leading to a high k_{add}. The intermediate radicals should

fragment rapidly having a high k_β and weak X-R bond and perform no side reactions. The intermediate radical must partition in favor of products with $k_\beta \geq k_{add}$ and the resulting radical R• has to be able to reinitiate polymerization (see figure A.14).

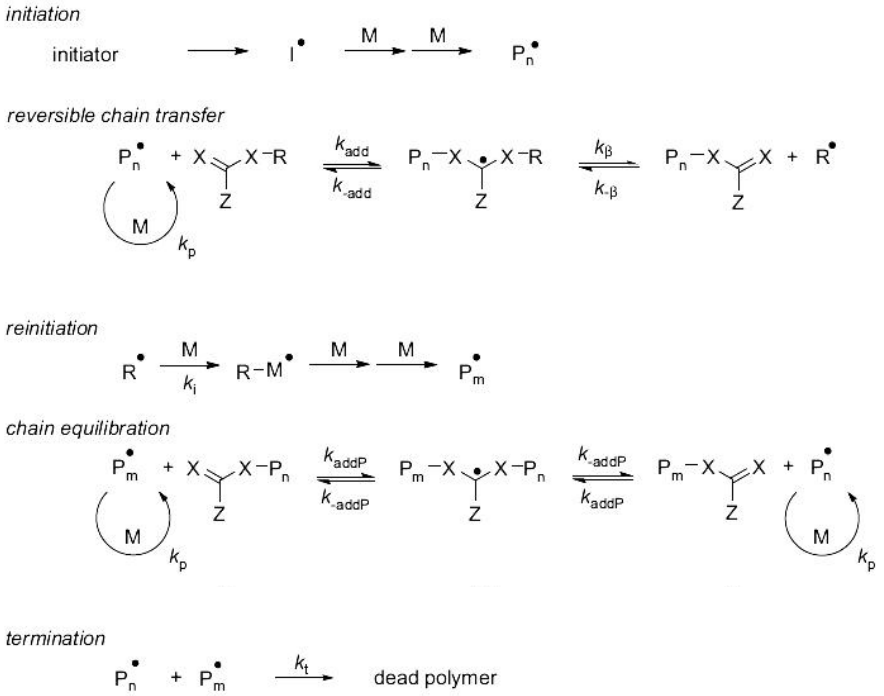

Figure A.14: Mechanism of RAFT polymerization given in literature 20.

The termination processes are not directly suppressed by the RAFT process leading to almost undisturbed radical polymerization kinetics. Living characteristics can therefore only be achieved when the molecular weight of the polymer formed is much lower than the molecular weight formed without RAFT agent and when the amount of polymers with RAFT agent capped ends far exceeds terminated chain ends. This can only be fulfilled for very efficiently transferring RAFT agents. Therefore RAFT agents are typically analyzed for their transfer constants $\boldsymbol{C_{tr}} = \frac{\boldsymbol{k_{tr}}}{\boldsymbol{k_p}}$ with $\boldsymbol{k_{tr}}$, the rate of chain transfer, defined by $\boldsymbol{k_{tr}} = \frac{\boldsymbol{k_\beta}}{\boldsymbol{k_{-add}} + \boldsymbol{k_\beta}} \cdot \boldsymbol{k_{add}}$ and $\boldsymbol{k_p}$, the rate of polymerization. It was

shown that a significant lowering of the polydispersity can only be achieved for C_{tr} >> 10 (see figure A.15). Very efficient RAFT agents usually have transfer constants C_{tr} much larger than 100.[21]

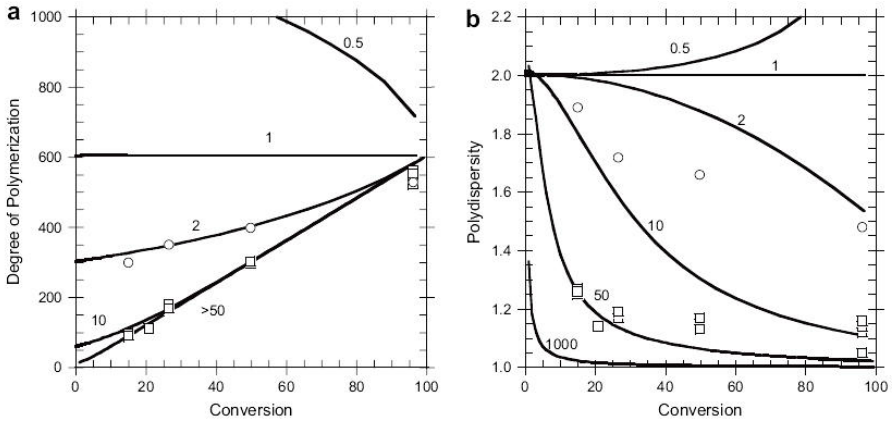

Figure A.15: Impact of C_{tr} on the degree of polymerization and polydispersity presented in lit. 21 (open symbols are experimental results and lines calculated).

Very efficient RAFT agents are thiocarbonlythio compounds (X = A = sulfur) including dithioesters, trithiocarbonates, xanthates and dithiocarbamates. For all classes, the choice of the Z and R group is substantial for addition and fragmentation rates and an overview is shown in figure A.16.

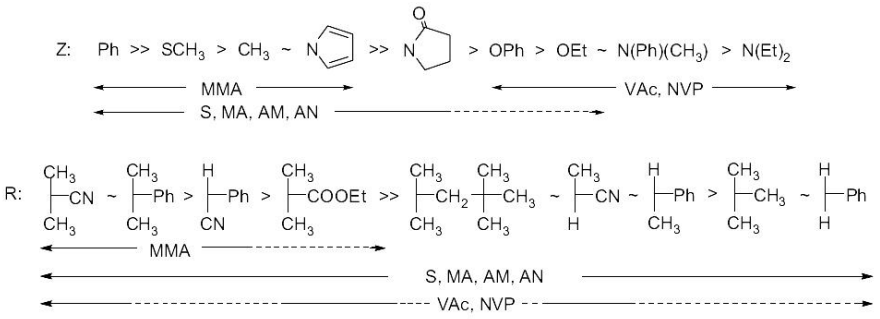

Figure A.16: Guidelines for selection of RAFT agents for various polymerizations presented in lit. 20.

Figure A.16 shows trends for Z- and R-groups: For Z, addition rates decrease and fragmentation rates increase from left to right. For R, fragmentation rates decrease from left to right.

Among the most active RAFT agents are the dithiobenzoates (Z = Ph) which can be – for appropriate R – used very generally for polymerizations of acrylates, methacrylates, styrene and styrene derivatives. The R-unit can carry functional units as hydroxyl, carboxylic acid / carboxylate, sulfonic acid / sulfonate, azide, olefin and siloxane groups. A very often used functional RAFT agent is 4-(4-cyanovaleric acid) dithiobenzoate as etherification of the valeric acid leads to various functional derivatives.

A.4 References

1 L. Onsager, *Ann. N. Y. Acad. Sci.*, **1949**, 51, 627.

2 P. J. Flory, G. Ronka, *Mol. Cryst. Liq. Cryst.*, **1979**, 54, 289-310.

3 R. Alben, *Mol. Cryst. Liq. Cryst.*, **1971**, 13, 193-231.

4 I. Dierking, "Textures of liquid crystals", **2003**, WILEY-VCH, Weinheim, Germany.

5 R. G. Laughlin, *Curr. Opin. in Colloid & Interface Science*, **1996**, 1, 384-390.

6 S. Iijima, *Nature*, **1991**, 354, 56.

7 B. I. Yakobson, P. Avouris, "Mechanical Properties of Carbon Nanotubes" in "Carbon Nanotubes - Synthesis, Structure, Properties, and Applications", M. S. Dresselhaus, G. Dresselhaus, P. Phaedon (Eds.), Topics in Applied Physics, Vol. 80, **2001**, Springer, Heidelberg, Germany.

8 L. Rapoport, Y. Feldman, M. Homyonfer, H. Cohen, J. Sloan, J. L. Hutchison, R. Tenne, *Wear*, **1999**, 229, 975; M. Chhowalla, G. A. J. Amaratunga, *Nature*, **2000**, 407, 164; C. Drummond, N. Alcantar, J. Israelachvili, R. Tenne, Y. Golan, *Adv. Funct. Mater.*, **2001**, 11, 348.

9 G. R. Patzke, F. Krumeich, R. Nesper, *Angew. Chem. Int. Ed.*, **2002**, 41, 2446-2461.

10 M. Grätzel, *Nature*, **2001**, 414, 338-344.

11 S. Belluci, *Phys. Stat. Sol. C*, **2005**, 2, 34-47; H. G. Chae, S. Kumar, *Journal of Applied Polymer Science*, **2006**, 100, 791-802; B. G. Demczyk, Y. M. Wang, J. Cumings, M. Hetman, W. Han, A. Zettl, R. O. Ritchie, *Materials Science and Engineering A*, **2002**, 334, 173-178; M. Meo, M. Rossi, *Composites Science and Technology*, **2006**, 66, 1597-1605; S. B. Meo, R. Andrews, *Crit. Rev. Solid State Mater. Sci.*, **2001**, 26, 145-249.

12 T. Otsu, M. Yoshida, *Macromol. Chem. Rapid Commun.*, **1982**, 3, 127-132; T. Otsu, *J. Polym. Sci. Chem.*, **2000**, 38, 2121.

13 K. Matyjaszewski, J. Xia, *Chem. Rev.*, **2001**, 101, 2921-2990.

14 C. J. Hawker, A. W. Bosman, E. Harth, *Chem. Rev.*, **2001**, 101, 3661-3688.

15 M. K. Georges, R. P. N. Veregin, P. M. Kazmaier, G. K. Hamer, *Macromolecules*, **1993**, 26, 2987-2988.

16 D. Benoit, S. Grimaldi, S. Robin, J. P. Finet, P. Tordo, Y. J. Gnanou, *J. Am. Chem. Soc.*, **2000**, 122, 5929.

17 D. Benoit, E: Harth, P. Fox, R. M. Waymouth, C. J. Hawker, *Macromolecules*, **2000**, 33, 363.

18 B. Giese, "Radicals in organic synthesis: formation of carbon-carbon bonds", **1986**, Pergamon Press, Oxford;. W. B. Motherwell, D. Crich, "Free radical chain reactions in organic synthesis", **1992**, Academic Press, London.

19 G. F. Meijs, E. Rizzardo, *Die Makromol. Chem., Rapid Commun.*, **1988**, 9, 547-551; G. F. Meijs, E. Rizzardo, S. H. Thang, *Macromolecules*, **1988**, 21, 3122-3124; P. Cacioli, D. G. Hawthorne, R. L. Laslett, E. Rizzardo, D. H. Solomon, *J. Macromol. Sci. A*, **1986**, 23, 839-852.

20 G. Moad, E. Rizzardo, S. H. Thang, *Polymer*, **2008**, 49, 1079-1131

21 Y. K. Chong, J. Krstina, T. P. T. Le, G. Moad, A. Postma, E. Rizzardo, *Macromolecules*, **2003**, 36, 2256-2272.

B Objective of this Work

Nanoparticles have very unique properties, which originate from their small size. A typical nanoparticle has a size much too small for the creation of an electronic band structure but is much larger than a single molecule. The result is a unique mixture of molecular and bulk properties making them a highly interesting material. Especially anisotropic nanoparticles are very interesting as they have directional properties as well. In some cases, one length scale of the nanorods / -tubes is large enough to show a “normal” electronic band structure while the other nano-sized lengths show typical molecular properties like fluorescence. But to use the different properties of the nanoparticle, they need to be oriented in space. Not only the single nanoparticle have to be oriented, but best all together in the same direction leading to a macroscopic accessibility of the nanoscopic properties. This is highly desired for the build-up of nano-scaled electronic devices as conventional downscaling of devices has reached its limits.

To realize this, the nanoparticles have to be solublized. This can be done e.g. by using surfactants or by chemical modification of the nanoparticle surface to create surface charges. Very stable aqueous dispersions can be realized this way. Unfortunately, they cannot be used for the build-up of electronic devices, as ions (free surfactant and/or counter ions) will create short cuts and leaking currents. Therefore organic (intrinsically ion-free) dispersions are required which can be realized using steric stabilization and the concept of “hairy rods” (see figure B.1). In this concept, a hard and insoluble core (originally rigid rod polymers, in this case the nanorod) is solublized by hairs (originally alkyl chains, in this case polymer chains).

Therefore, the objective of this thesis was to establish routes for the preparation of “hairy rod” structures from various anisotropic, inorganic nanoparticles,

to characterize their properties in solution and to search for anisotropic ordering in concentrated solution.

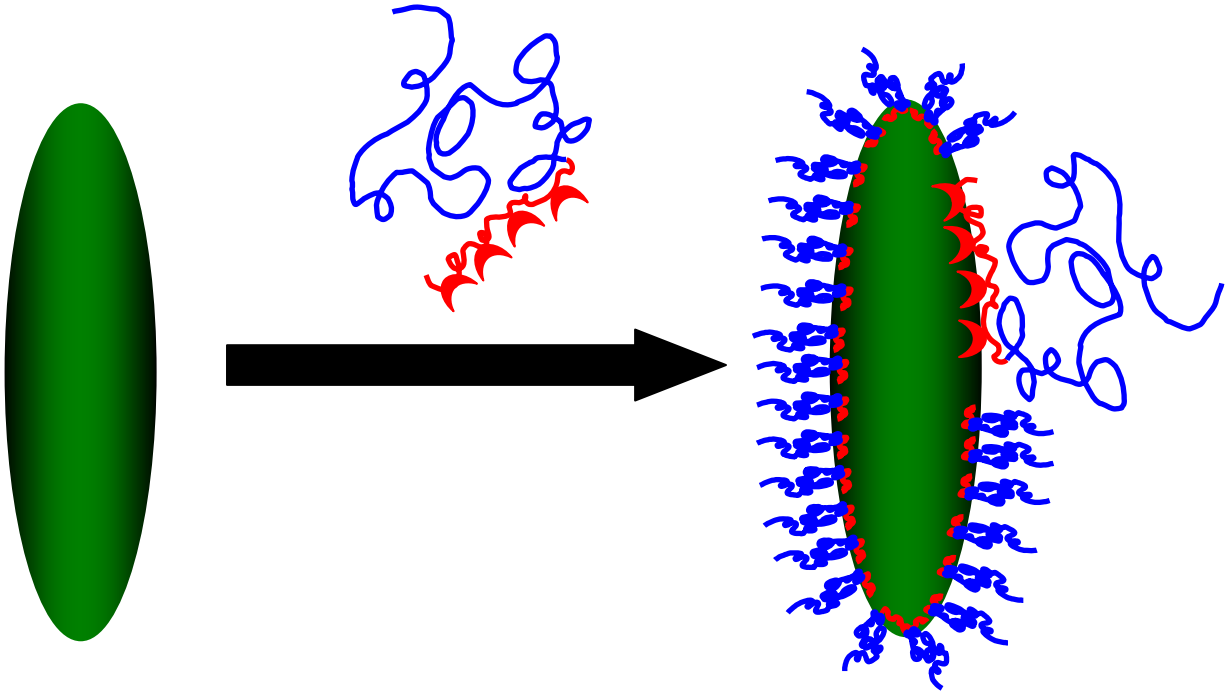

Figure B.1: Polymer functionalization of anisotropic nanoparticles following the "hairy rod" approach.

To stabilize organic dispersions of inorganic anisotropic nanoparticles by the "hairy rod" approach, functional polymers need to be synthesized. They must have specific anchor units incorporated either as an anchor block or as alpha functionality to ensure a good interaction with the nanorod / nanotube surfaces and a soluble block for the steric stabilization and organic solubility. This requires the use of controlled radical polymerization techniques allowing the build-up of block copolymers with low polydispersities. The functional polymers need to be optimized concerning architecture and block lengths in order to maximize the adsorption. It is important to optimize the steric stabilization as well as the solubility of the polymer coated nanoparticles. The functional polymers shall then be used to functionalize the anisotropic nanoparticles to prepare stable dispersions in organic media. Their

stability must be investigated using light scattering and/or electron microscopy to visualize the dispersed nanoparticles. Desired are aggregate-free dispersions containing single nanoparticles since aggregates are undefined assemblies of nanorods. In addition to classical solvents, polymeric solvents are important, as they offer the potential to incorporate the nanoparticles into polymer films. Once stable dispersions are achieved, the concentration of the nanoparticles must be increased to investigate their self-organization. Ideally, the anisotropic nanoparticles should show liquid crystalline behavior, fully analogous to anisotropic small molecules or rigid rod polymers. Liquid crystallinity shall be investigated using polarizing microscopy combined with differential scanning calorimetry. If they show liquid crystalline behavior, the impact of temperature and volume fraction (thermotropic and/or lyotropic behavior) upon the liquid crystalline phases should be investigated. Finally, the macroscopic orientation of the anisotropic nanoparticles shall be investigated.

C Results & Discussion

C.1 General Principle of Polymer Functionalization

In general, dispersions of nanoparticles can be obtained following very different routes. For aqueous systems, electrostatic stabilization can be obtained by oxidation of the surface, which leads to charged surface species or by adsorbing charged molecules (for example surfactants) on their surface. These approaches are the best methods to disperse nanoparticles in aqueous solutions. But as charges are involved, ions are always present (loose surfactants or counter ions of surface charges) which limits the use of such dispersions for electronic applications. Short cuts and leaking currents are usually the drawbacks.

Dispersions in organic media are therefore highly interesting and they can also be obtained following different approaches but usually the same principle: As charges cannot be used, steric stabilization is used. Usually this is done by following the idea of “hairy rods”, which was originally used for the solubilization of stiff insoluble main chain liquid crystalline polymers by adding soluble alkyl chains (the hairs) to the polymer backbone (the rods). Alkyl chains are therefore often used to stabilize nanoparticles in organic solvents. Usually surfactants having a binding moiety and a long alkyl chain are used. Those systems give usually very stable dispersions and have been investigated extensively since many years.

On the other side polymers are also used and offer advantages compared to surfactants: polymers themselves are objects of nanometer dimensions. Therefore polymer coated surface are stabilized sterically up to distance of nanometers and not just for angstroms as with alkyl chains. Polymer chains have also a lot of free volume inside, which can be filled by solvent. This large interaction volume between solvent and functionalized surface leads to good solubility in solvents for the polymer. In

addition, new polymers designed for surface functionalisation can have multiple anchor units for surface attachment. Therefore adsorption-desorption equilibria reactions are avoided, and a robust fixation of the multi-dentate polymer ligand to the surface can be achieved. Another point is the variability of chemical functions beyond solubility. Stimuli responsive or conductive polymers can be used to functionalize the surface leading to highly interesting hybrid systems. And as a final point, polymer functionalized nanoparticles can be incorporated well into polymer films, which is impossible for surfactant stabilized nanoparticles. They are usually expelled from the polymer matrix as they are not miscibility with polymers.

The general principle used in this thesis is the use of functional polymers for the surface functionalization of inorganic nanorods and nanotubes. To realize this, three questions have to be solved: The first one is: Which anchor unit is suitable for the surface functionalization? It should have a strong binding energy to the surface but how can it be incorporated into the polymer backbone?

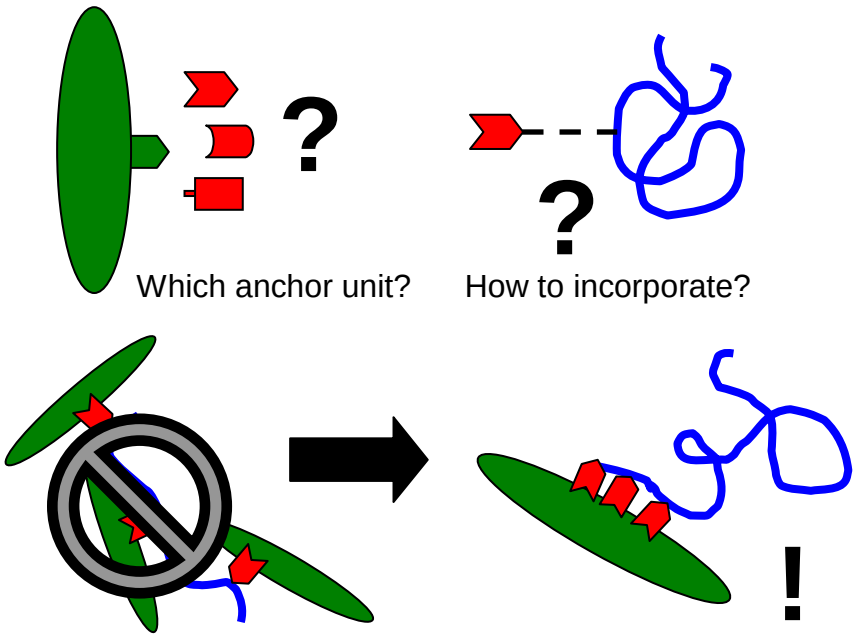

Figure C.1: Visualization of necessities for surface active polymers.

Then the question of polymer architecture must be solved, as one could generally think of a statistical copolymer of anchor units and soluble units or a block copolymer with a distinct anchor unit block and a soluble block. As one can imagine, the statistical one is easier to synthesize but has a critical drawback as the polymer could bind to more than one nanoparticle leading to interparticle cross-linking (see figure C.1). Therefore the diblock copolymer is the better choice as the anchor block (assumed it is not too long) should only be able to bind to a single nanorod. The anchor block length is also a critical parameter for the grafting of a surface: The larger the anchor block is, the more surface will be occupied by it and this will limit the density of grafted chains. On the other hand, it should have a certain length to ensure a stable connection to the surface. The soluble polymer chain's entropy is lowered when the anchor block binds to the surface. Thus, the polymer's entropy pay must be matched by the binding energy of the anchor block. The binding energy scales with the number of anchor units binding.

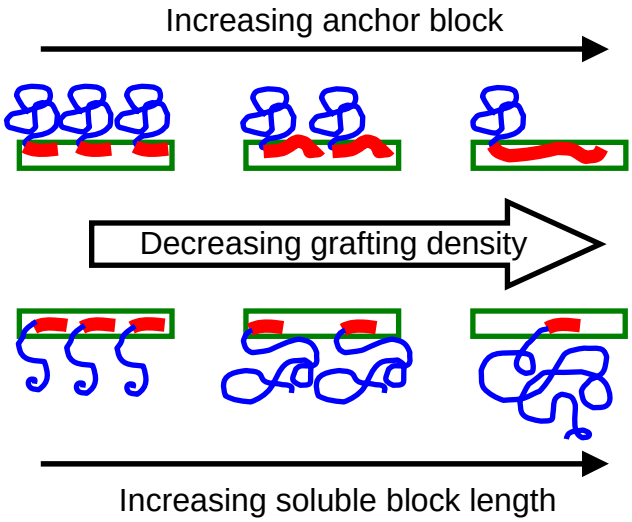

Figure C.2: Expected impact of block lengths on grafting density.

Combining both trends, there should be an optimal situation for a short (10 to 20) anchor block. On the other hand, the chain's entropy is also a function of soluble

block length and thus the length of the soluble block should be sufficiently long for the steric stabilization, but not longer. The grafting density for a given anchor block length should also be a function of the soluble block length: As the functionalization is usually done from solution, the soluble block forms a polymer coil in solution. This coil radius should limit the accessibility to the surface and therefore the grafting density on the surface (see figure C.2).

The realization of these demands requires a well controllable polymerization method suitable for the build-up of block copolymers. Our choice was the RAFT polymerization as it fulfills these requirements and allows the use of functional monomers. For the incorporation of the anchor units either a reactive monomer was used for the build-up of the second block or a functional RAFT agent was used to incorporate exactly one anchor unit. The synthetic approach is shown in figure C.3.

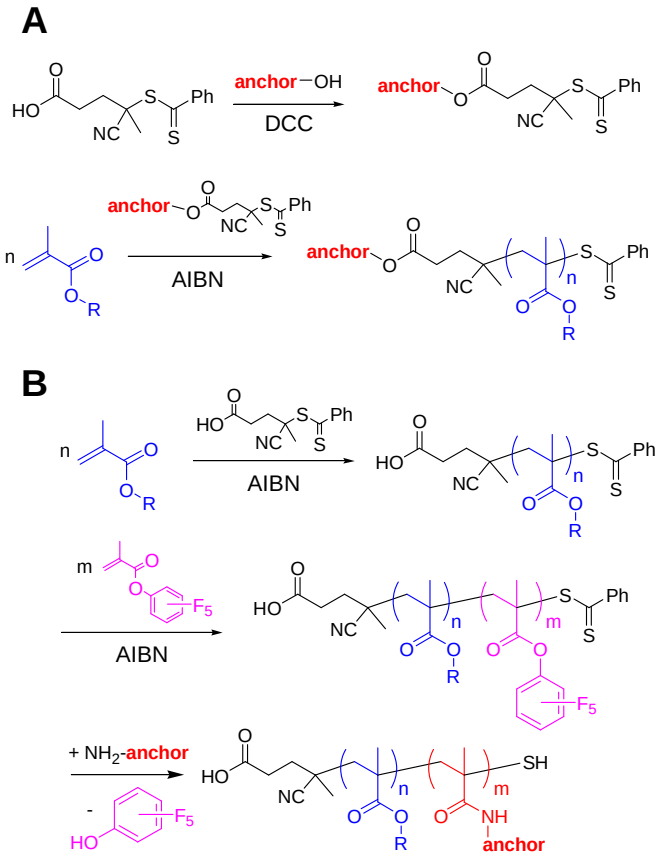

Figure C.3: Synthesis of anchor unit containing polymers: A: Route to alpha anchor unit functionalized polymers; B: Route to anchor block copolymers.

C.2 Polymer Functionalized TiO_2 Nanorods

Anchor units suitable for the functionalization of TiO_2 nanorods are carboxylic acids, anhydrides and catecholes. These anchor units use unsaturated Titanium species on the surface to form a complex. Titanium is very oxygenophilic and binds preferentially to anchor units with two oxygen atoms forming a tetragonal or even octagonal complex. Catecholes have been found by Messersmith et al. to be highly effective to bind on most oxidic surfaces and are naturally used as adhesive moiety (in mussel adhesive proteins). A suitable amino functionalized species of a catechole is dopamine. It can be reacted easily with the reactive ester approach presented in figure C.3, but cannot be used for the alpha anchor functionalized polymer approach (via a catechole functionalized RAFT agent controlling the radical polymerization), as catecholes are radical inhibitors.

C.2.1 Impact of Block Lengths on the Adsorption Behavior

The block length of the soluble and of the anchor block should have an impact on the adsorption behavior of the polymer as shown in figure C.2. Therefore we investigated the adsorption of dopamine functionalized PMMA block copolymers on TiO_2 nanorods. We varied the block lengths of both blocks and measured the adsorption by adding a polymer solution to the nanorods, washed unbound polymer away and investigated the polymer functionalized nanorods by thermo gravimetry (TGA). In a TGA experiment, the sample is heated up to 900 °C and the weight loss is recorded as a function of temperature. As the TiO_2 nanorods withstand these temperatures without weight loss, only the decomposition of the organic polymer is monitored. Out of the weight loss (usually around 300 to 500 °C), the amount of bound polymer per mg nanorods can be calculated. Knowing the molecular weight of the polymer,

nanorod surface and nanorod density, one can calculate the amount of bound chains per single nanorod and the distance between two polymer chains. These numbers are of course only rough estimates as many assumptions must be made but the relative adsorption behavior can be shown quite efficiently. The following publication shows, that the number of adsorbed chains increases when the anchor block as well as the soluble block length decreases and found an optimal situation for approx. 20 anchor units and 40 to 100 soluble repeat units.

The following publication is a joined publication together with M. Zorn and both authors contributed equally to the publication. The results can be summarized as follows: It focuses on three major points: First, the detailed investigation on adsorption behavior as a function of block lengths (mostly S. Meuer). Second, the generalization of the concept of polymer functionalization on various oxidic and chalcogenic nanorods (mostly M. Zorn) and third, the general formation of lyotropic liquid crystalline phases from polymer functionalized nanorods (S. Meuer and M. Zorn). The parts of the publication can be separated as follows: all results concerning block copolymers based on polymethyl methacrylate (PMMA) and poly(diethyleneglycol monomethyl ether methacrylate) (PDEGMEMA) used for the functionalization of TiO_2 nanorods are part of this thesis. All results concerning polystyrene (PS) based block copolymers used for the functionalization of TiO_2, ZnO, SnO_2 and CdTe were contributed by M. Zorn. In more detail, the following experiments and results were contributed by S. Meuer:

First, the analysis of the length distribution of TiO_2 nanorods found by counting SEM and TEM images and presented in table C.1 and figure C.5. Second, the synthesis and characterization of all **PMMA X/Y dopamine** and **PDEGMEMA X/Y dopamine** block copolymers presented in figure C.6 and table C.2. Third, the adsorption kinetic of **PMMA 70/30 dopamine** on TiO_2 nanorods (investigated by UV-

Vis spectroscopy) shown in figure C.7A. Forth, the preparation and execution of TGA experiments of all **PMMA X/Y dopamine** and **PDEGMEMA X/Y dopamine** TiO_2 functionalized nanorods partially shown in figure C.7B. Fifth, the calculations based on equations C.1, C.2 and C.3 leading to the following parameters describing the adsorption: number of chains / nanorod, Area per adsorbed chain A_{chain}, the interpolymer distance *s* and the reduced coverage σ^* for all **PMMA X/Y dopamine** and **PDEGMEMA X/Y dopamine** TiO_2 functionalized nanorods (shown in table C.3). Sixth, the visualization and summary of all results in figure C.8 and seventh, the preparation and investigation of lyotropic liquid crystalline textures found for **PMMA 70/30 dopamine** functionalized TiO_2 nanorods in PEG 400 as “solvent” and for **PDEGMEMA 40/30 dopamine** functionalized TiO_2 nanorods in excess **PDEGMEMA 40/30 dopamine** as “solvent” presented in figure C.11 A-D.

C.2.1.1 Publication in Journal of Materials Chemistry 2008, 18, 3050–3058

Liquid crystalline phases from polymer functionalized semi conducting nanorods

Matthias Zorn[1], Stefan Meuer[1], Muhammad Nawaz Tahir, Yuriy Khalavka, Carsten Sönnichsen, Wolfgang Tremel, Rudolf Zentel

[1] both authors contributed equally to this article.

Summary

The orientation of semi conducting nano-materials is a hot topic in optoelectronic applications. Liquid crystallinity offers the potential to orient inorganic anisotropic nanorods, if they can be solubilised sufficiently as realized by polymer functionalisation. In this work we functionalized TiO_2, SnO_2, ZnO and CdTe nanorods with PMMA, PS and PDEGMEMA (poly(diethylene glycol monomethyl ether) methacrylate) diblock copolymers via grafting to with anchor groups. The block copolymers were synthesized by RAFT polymerization (PDI ≈ 1.2) via reactive ester diblock copolymers, which were functionalized later with anchor units polymer analogously. The surface coverage of the nanorods (determined by TGA) is dependent on the block lengths and ratios and a maximal coverage is found for short anchor unit blocks. Stable dispersions are obtained for these hairy rod hybrids and they form liquid crystalline phases at suitable concentration in organic solvents as well as in oligomeric and polymeric matrices like oligo-PEG, oligo-PS and polymeric PDEGMEMA. Liquid crystalline textures are found in polarizing microscopy images.

Clearing temperatures were found between 60 and 230 ℃ depending on the length of the nanorods and the organic matrix.

Introduction

The use of nano-objects in the real macroscopic world requires – besides their preparation – also their macroscopic organization and orientation. The organization of nanometer sized objects can be realized in colloidal crystals[1] and lyotropic liquid crystals (LC)[2]. Generally the formation of lyotropic liquid crystals[3,4,5] from rigid-rod objects as result of form-anisotropy is well understood[6,7] and such phases offer the potential to orient anisotropic nanoparticles. In this respect the orientation of functional semi conducting nanoparticles is interesting for materials science and especially for photovoltaics.[8,9,10,11] E.g. oriented semi conducting materials might improve the device performance in solar cells by alignment of electron-carrying nanorods perpendicular to the electrode.[12] Following this concept it was shown by Alivisatos and co-workers that the efficiency of nanoparticle solar cells could be enhanced, if rod-shaped particles are chosen.[13] Research in this direction is, so far, limited by the solubility of functional nano-particles, which is needed to obtain the LC-phase at high concentration.

Historically lyotropic LC-phases in water have been observed for various rigid-rod objects like V_2O_5 ribbons,[14,15] tobacco mosaic viruses[16] and TiO_2 nanorods[17]. Aqueous solutions offer the opportunity to stabilize nano-objects electro statically by surface charges. But as a major drawback, the charges used to stabilize the system disable any electronic use. Therefore ion free mineral liquid crystals from uncharged anisotropic nanoparticles in organic solvents are needed.

This requires the “solubilisation” of the nano-objects in organic solvents. For this purpose the particles have to be surface functionalized with a soluble corona to

overcome the strong adhesion forces among them.[18,19] The concept of “hairy rods”, which was originally developed for stiff main chain liquid crystalline polymers, is very promising for such inorganic nano-objects too.[3] In that concept, a stiff insoluble core is solubilised by linking long chains (the hairs) on its surface. Alkyl chains are often used[20,21] to stabilize nanoparticles of sphere- or rod-like shape and they are also used for delaminated clay fragments.[22] In some cases they allow the preparation of highly concentrated solutions, which give rise to a liquid crystalline ordering, if anisotropic nanoparticles are used.

Polymeric surfactants[19,22,23] offer here advantages for the solubilisation of inorganic nano-objects: polymers themselves are objects of nanometer dimensions. Therefore polymer coated surface are stabilized sterically up to distance of nanometers and not just for angstroms as with alkyl chains. Then polymer chains have a lot of free volume inside, which can be filled by solvent. This large interaction volume between solvent and functionalized surface leads to good solubility in solvents for the polymer. In addition, new polymers designed for surface functionalisation have multiple anchor units for surface attachment. Therefore adsorption-desorption equilibria reactions are avoided, and a robust fixation of the multi-dentate polymer ligand to the surface can be achieved. Using this concept we could recently observe smectic and nematic phases in highly concentrated solutions of TiO_2 nanorods,[19] which were coated with block copolymers (see figure C.4). This concept could also be applied successfully to carbon nanotubes.[24] In addition we were able to solubilise TiO_2 nanorods in a functional organic matrix and thus to orient semi conducting inorganic nanorods in an organic hole conducting matrix by self-assembly.[25]

In order to see, if the concept to (i) solubilise anisotropic inorganic nano-particles with block copolymers and (ii) to observe LC-phases in highly concentrated

solutions can be generalized (see figure C.4), we extended our work to various semi conducting nano-particles, which require different anchor blocks and therefore more work in the polymer synthesis. Concerning the inorganic part we concentrated on nanorods from semiconductors like TiO_2, ZnO, SnO_2 and CdTe, which are discussed mostly for opto-electronic applications. Concerning the block copolymer synthesis we used RAFT polymerization and a reactive ester intermediate.[26] We focus here mostly on the surface functionalisation with newly synthesized block copolymers and describe first results concerning the observation of LC-phases in various solvents.

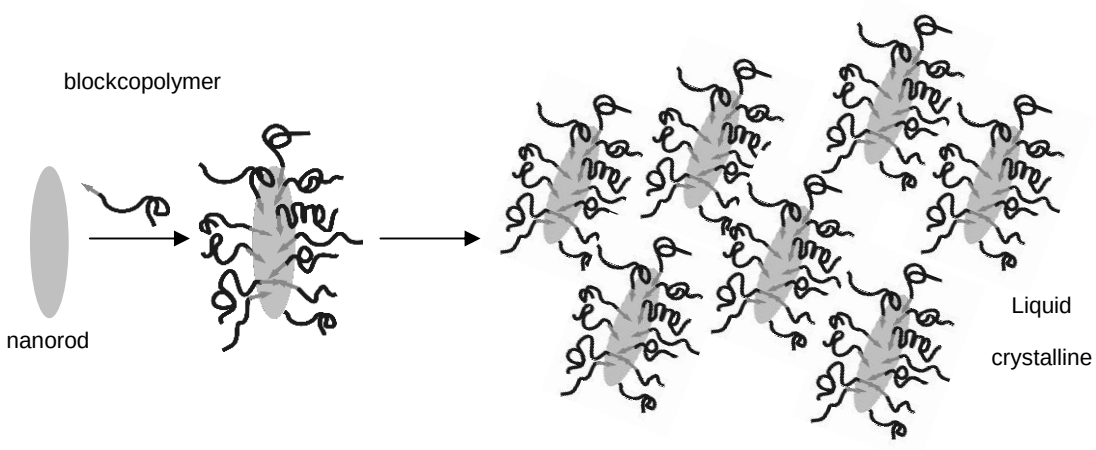

Figure C.4: Scheme for functionalisation and liquid crystalline ordering.

Results and Discussion

Semi conducting nanorods

The oxidic semi conducting nanorods were all prepared by hydrothermal methods.[27,28,29] This synthetic route can produce the particles in a high quantity and without any stabilizing surfactants on the nanorod surface. The products of these syntheses possess a narrow polydispersity for TiO_2 and SnO_2. The size distribution of ZnO nanorods is broader. CdTe was synthesized with TOPO as stabilizing ligand. Table C.1 collects the physical characterization like average size with respect to

length and width as well as the characteristic surface, which is the basis for the calculations of the surface coverage, described later in this work.

Table C.1: Physical properties of nanorods used in this study.

material	density [g/cm^3]	l [nm]	d [nm]	l/d	surface [nm^2]	nanorods / mg	surface [nm^2/mg]
TiO_2	4.26	31	6	5.2	600	$3.03*10^{14}$	$1.82*10^{17}$
ZnO	5.61	122	19	6.4	7800	$5.20*10^{12}$	$4.05*10^{16}$
SnO_2	6.95	20	4	5.0	280	$5.72*10^{14}$	$1.58*10^{17}$
CdTe	6.20	23	4	5.8	310	$5.58*10^{14}$	$1.75*10^{17}$

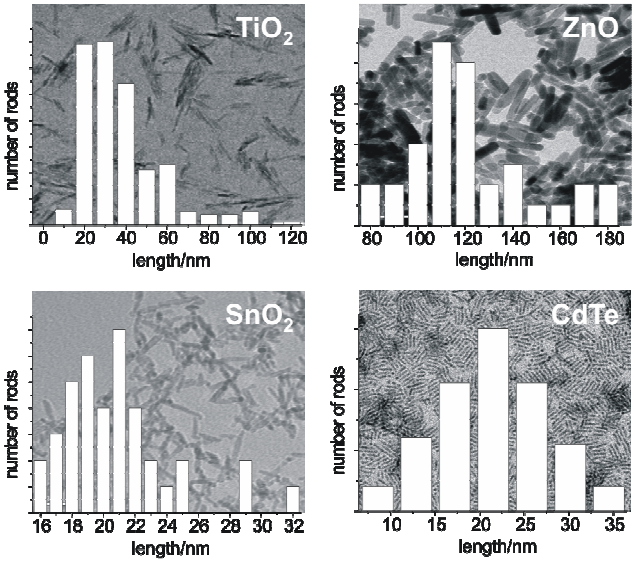

Figure C.5: Transmission electron microscopy (TEM) images of nanorods used in this study. The width of the images is 650 nm for TiO_2, 200 nm for SnO_2, 450 nm for ZnO and 870 nm for CdTe. The length distributions of the nanorods are inlayed.

Size distributions as well as TEM images can be found in figure C.5. In all cases the preparation methods allow to synthesize rods with high aspect ratios (length/width larger than 5), that posses the potential to act as mesogens, if a good mobility and solubility can be achieved by a polymeric corona as a shell around the particle.

Functional diblock copolymers

To synthesize the polymers, which are needed to solubilise the inorganic particles in organic solvents, reversible addition fragmentation transfer (RAFT) polymerization was chosen.[30] The block copolymers for the surface modification of the inorganic nanorods presented above were synthesized according to the scheme presented in figure C.6 as described in refs. 19 and 25. In the first step of the synthesis the block that acts as solubiliser is polymerized. It is made of methyl methacrylate, (diethylene glycol monomethyl ether) methacrylate or styrene. After purification of the first block it can be used as a macro initiator leading to a diblock copolymer. As a second block, we chose a reactive ester monomer (pentafluorophenole acrylate), which allows the introduction of various anchor groups by a polymer analogous reaction with any primary amine connected to an anchor group for the nanorod material.[26]

The block lengths of the soluble block were determined by GPC (determined with light scattering detector and known dn/dc ratios) and are therefore well accessible. The polydispersity index (PDI) of almost all polymers made is between 1.14 and 1.21. These are very good values for diblock copolymers after a polymer-analogous reaction. The polymers made from (diethylene glycol momomethyl ether) methacrylate have larger PDIs. This phenomenon might be due to diethylene glycol dimethacrylate (acts as a cross linker) impurities from the monomer synthesis.

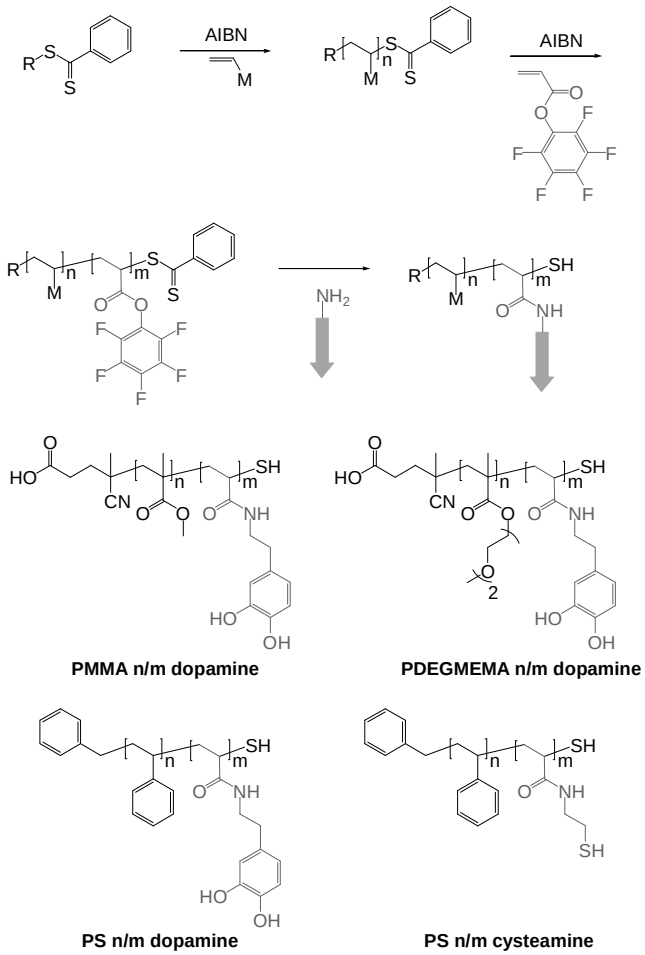

Figure C.6: Synthesis of reactive diblock copolymers and polymer analogous conversion to anchor unit functionalized polymers.

As an anchor group to functionalize the oxidic nanorods dopamine was chosen, which is known to bind preferentially to the unsaturated metal centers on the surface of the oxidic nanocrystal.[31] The conversion of the reactive block can be monitored by ^{19}F-NMR, IR and UV spectroscopy and is found to be quantitative.[26] The resulting block copolymers are somewhat amphiphilic, but well soluble in THF, which is a solvent for both blocks. For functionalisation of CdTe thiol groups were introduced by polymer analogous reaction of the reactive block copolymer with cysteamine. The reaction with cysteamine results in a total conversion as examined by IR spectroscopy and ^{19}F NMR spectra (disappearance of the three signals of the pentafluorophenole acrylate). All block copolymers are collected in table C.2.

Table C.2: block lengths, molecular weights and polydispersities of anchor unit functionalized diblock copolymers used in this study.

polymer m/n anchor	soluble units	anchor units	M_n [g/mol]	M_w [g/mol]	PDI
PMMA 100/20 dopamine	100	20	14,700	17,600	1.20
PMMA 100/40 dopamine	100	40	18,900	22,900	1.21
PMMA 100/60 dopamine	100	60	23,000	27,400	1.19
PMMA 110/20 dopamine	110	20	15,200	17,800	1.17
PMMA 110/40 dopamine	110	40	19,400	23,300	1.20
PMMA 110/60 dopamine	110	60	23,500	28,000	1.19
PMMA 140/20 dopamine	140	20	17,800	20,300	1.14
PMMA 140/40 dopamine	140	40	22,000	25,500	1.16
PMMA 140/60 dopamine	140	60	26,100	30,300	1.16
PMMA 70/30 dopamine	70	30	12,800	15,000	1.17
PDEGMEMA 40/30 dopamine	40	30	14,500	17,500	1.21
PDEGMEMA 190/30 dopamine	190	60	47,400	72,500	1.53
PS 90/10 dopamine	90	10	11,600	13,300	1.15
PS 90/10 cysteamine	90	10	11,100	13,000	1.17

Functionalized nanorods / Hybrid systems

For surface functionalisation of the inorganic nanorods anchor groups, which chemisorb strongly on oxidic or sulfidic surfaces are used. This functionalisation (grafting-to) is done in dilute solution (both polymer and nanorods) to prevent interparticle cross linking. Bidentate ligands containing enediol moieties such as dopamine serves as robust anchor group to many metal oxides[32] and it has been proved spectroscopically that such ligands convert the under-coordinated surface sites back to a bulk-like lattice structure, which results in a really robust binding.[33] Thus this anchor group chemisorbs strongly. The functionalisation kinetics can be monitored by UV-Vis spectroscopy as dopamine has a strong absorption band around 285 nm. We investigated the decrease of the polymer concentration in solution in presence of excess nanorods. Figure C.7A shows the adsorption of the block copolymer onto TiO_2 nanorods and the resulting property changes of the nanorods. For this purpose the absorption spectra of a dopamine functionalized polymer solution was recorded in a quartz cuvette with unfunctionalized TiO_2

nanorods lying at the bottom. UV-Vis spectra were taken and show a weakening of the absorption band over time. This is due to adsorption of the polymer on the TiO_2 nanorods at the bottom of the cell. After two days, the spectrum was run again and the signal of the dopamine units were found again in comparable strength to the beginning of the experiment but blue shifted to 269 nm. This effect can be explained by solubilised TiO_2 nanorods that started to diffuse freely in the cuvette. The dopamine units bind to the nanorod surface and form a charge transfer complex with unsaturated surface titanium ions. The electron density of dopamine is reduced in this complex (the HOMO is lowered), which corresponds to a blue shift in its absorption spectra (the HOMO – LUMO distance increased). The effect was observed without the use of ultra sound or stirring of the sample, which proves the solubility of these hairy rods.

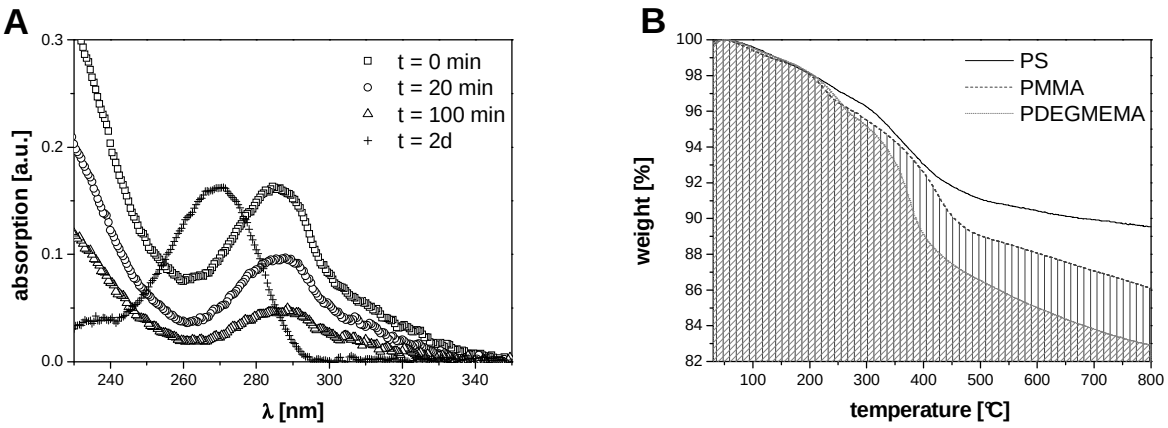

Figure C.7: **A**: Adsorption kinetic of **PMMA 70/30 dopamine** on TiO_2 nanorods monitored by UV-Vis spectroscopy; **B**: TGA analysis of PS, PMMA and PDEGMEMA coated TiO_2 nanorods.

To investigate the efficiency of the functionalisation process in detail, various diblock copolymers with PMMA, PS and Poly(diethylene glycol monomethyl ether) methyl

methacrylate as soluble block and dopamine or thiol units in the anchor blocks were used (see tab. C.2). These block copolymers formed the basis to study (i) the influence of the type of anchor group, (ii) the length of both blocks and (iii) the chemistry of the inorganic nanorod on the “grafting-to” efficiency, which determines the functionalisation of the inorganic nano-particle with polymer chains. The functionalisation was carried out in THF solutions with a weight ratio of TiO_2 nanorods to polymers of 2 : 1. The solutions were stirred over night and cleaned from unbound polymer by repeated centrifugation of the functionalized nanorods and removal of the supernatant solution.

The amount of bound polymer was measured using thermo gravimetry (TGA, see fig. C.8B). The samples were heated up to 800 °C under a nitrogen atmosphere and the weight loss was measured as a function of temperature. As TiO_2 withstands these temperatures, the weight loss is only due to the decomposition of the polymer (usually by depolymerisation). With known molecular weight (Tab. C.2) and nanorod surface (Tab. C.1) it is possible to calculate roughly the number of polymer chains per nanorod (see table C.3).

To study the influence of block-length mostly TiO_2 nanorods were used. They are in average 31 nm long and 5.6 nm wide, so that the nanorods have a surface of about 600 nm^2 and a volume of 770 nm^3 in average. Taking the density of crystalline rutile into account, $3*10^{14}$ nanorods are present per milligram powder (see tab. C.1). Thus the calculated surface of the nanorods is $1.82*10^{17}$ nm^2/mg or 1820 m^2/g.

Table C.3: Adsorption characteristics of diblock copolymers **PS, PMMA and PDEGMEMA X/Y dopamine** on TiO_2 nanorods.

soluble units **X**	anchor units **Y**	chains / nanorod	A_{chain} [nm^2]	s [nm]	R_g [nm]	σ*
70[a]	30	25	24.3	4.9	3.6	1.7
100[a]	20	21	28.6	5.3	3.8	1.6
	40	16	38.0	6.2	4.3	1.6
	60	9	65.8	8.1	4.8	1.1
110[a]	20	14	42.7	6.5	3.9	1.1
	40	17	35.3	5.9	4.4	1.7
	60	13	48.0	6.9	4.9	1.5
140[a]	20	15	40.2	6.3	4.2	1.4
	40	13	44.6	6.7	4.7	1.5
	60	10	58.4	7.6	5.1	1.4
40[b]	30	22	27.0	5.2	2.9	1.0
190[b]	60	3	254.4	15.9	5.9	0.4
90[c]	10	28	21.4	4.6	3.4	1.7

For A_{chain}, s and σ* see equations 1, 2 and 3. a: methyl methacrylate, b: diethylene glycol monomethyl ether) methacrylate, c: styrene

Table C.3 summarizes the calculated amounts of chains per TiO_2 nanorod for each block copolymer. Figure C.8 shows the dependence of the amount of adsorbed polymer chains on the length of anchor and soluble block. Independent of the nature of the soluble block (PS, PMMA, PDEGMEMA) the same trend is observed. The number of adsorbed chains per nanorod increases as the number of repeat units in the soluble block as well as in the anchor block decreases. Thus a maximum of adsorbed chains is found for block copolymers with about 10 to 30 repeat units in the anchor and 40 to 100 in the soluble block (see xz and yz trajectories in fig. C.8). As expected the number of adsorbed chains increases as the anchor block gets shorter. There should be – of course – a minimum length that is needed for a stable connection. But this length is obviously shorter than the shortest anchor blocks examined. On the other side, the length of the soluble block is also limiting the grafting density. When the coil diameter of the soluble block is larger than the area

accessible to the anchor block, the coils will hinder each other. Thus the grafting density gets down, when the soluble block is too large.

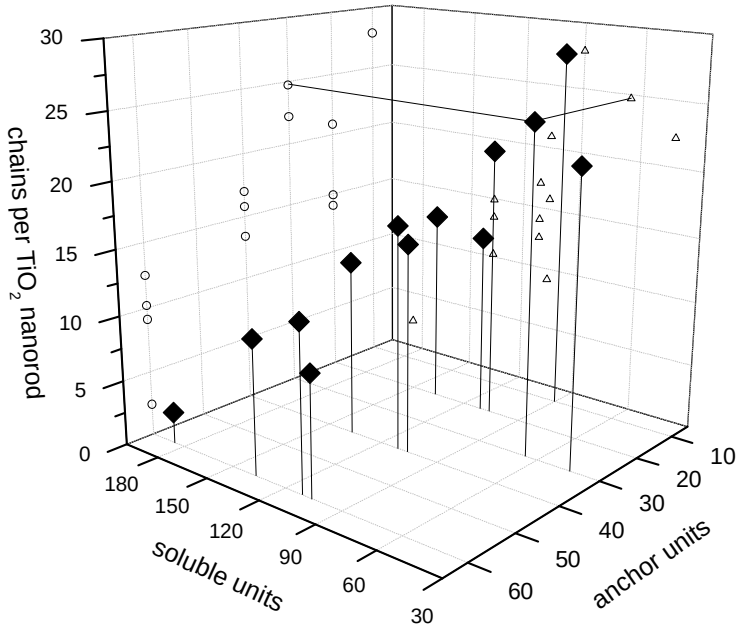

Figure C.8: Adsorbed chains per TiO_2 nanorod of **PS, PMMA and PDEGMEMA X/Y dopamine** diblock copolymers (the dark squares are the xyz points, the open spheres and triangles are the corresponding trajectories).

Equation C.1: $$A_{chain} = A_{nanorod} / N_{adsorbed\ chains}$$

Equation C.2: $$s = \sqrt{A_{chain}}$$

Equation C.3: $$\sigma^* = \pi R_g^2 / s^2 = \pi R_g^2 / A_{chain}$$

A more quantitative interpretation of these results on a molecular level can be obtained, if the area covered per polymer chain and the inter polymer distance are discussed.[34] The area that is covered per polymer chain is calculated by dividing the nanorod surface by the number of chains per nanorods (see equation C:1). The

interpolymer distance s is defined as the square root of this area (see equation C.2). Another useful ratio is known as reduced coverage σ* and is calculated with equation C.3 (R_g values were calculated from known R_g to M_w relations of PMMA and PS; the values for Poly(diethylene glycol monomethyl ether) methacrylate were estimated from Polyhexyl methacrylate).[35] This value resembles the degree of coverage: A value of two marks the onset of large steric interactions, which lead to deformed polymer coils on the surface (brush regime).[36] Values smaller than one corresponds to distances between two polymers on the surface that are larger than the cross section of that coil in solution. This regime of σ* values < 1 is also called mushroom regime (all calculated values are collected in tabs. C.3 and C.4). Almost all σ* values are between 1 and 2. Thus the polymer functionalized surfaces consists of close packed polymer mushrooms that fill the surface completely. In one case, a σ* value of 0.4 was found. In this case the surface morphology should consist of isolated mushrooms. The soluble block of that polymer had 190 and the anchor block 60 repeat units. Both values are not optimal when compared to the trends from the other diblock copolymers, so that such a low coverage is not astonishing. Considering these calculations one should consider that there might be various sources of errors, e.g. from asymmetry in polydispersity and therefore the absolute values are uncertain to some extend. However comparison with literature data presented below give comparable values. In addition all compared systems were treated identically. So the trends in these values are correct.

The interpolymer distances vary from 4.6 to 8.1 nm for the polymers from table C.3. Literature reports interpolymer distances from 2.8 to 25 nm with σ* values from 2.6 to 10.3 in cases where diblock copolymers with short anchor blocks were used.[34,37] These literature values were measured with planar and chemically

homogeneous surface like silicon or aluminum oxide while our experiments were carried out on nanorod surfaces.

Next the binding efficiency on different nanorods was studied for identical or – at least – very similar block copolymers. In order to functionalize TiO_2, ZnO and SnO_2 nanorods the block copolymer **PS 90/10 dopamine** (styrene with dopamine anchor) was used (see tab. C.4). The reduced coverages σ* from functionalized TiO_2 and SnO_2 are similar with a slight increase from TiO_2 (σ* = 1.7, s = 4.6 nm) to SnO_2 (σ* = 2.5, s = 3.8 nm). However the reduced coverage for ZnO particles is significantly larger (σ* = 9.1, s = 2.0 nm). This effect might be due to different crystal structure. TiO_2 and SnO_2 crystallize in a rutile structure whereas ZnO crystallized as wurtzite. All cations form stable octahedral complexes, but in the case of zinc also tetrahedral complexes are possible. Thus, dopamine might bind more efficient to the zinc atoms, which are more flexible with regard to coordination geometry.

To investigate the functionalisation of non-oxidic compounds, we investigated the chemisorption of thiol functionalized polystyrene on CdTe nanorods. The reduced coverage observed was 2.4 and the interchain distance 3.9 nm, which is quite similar to the values for SnO_2 (Tab. C.4). As the precursor diblock copolymer was the same in both cases the same number of reactive ester moieties was available for the reaction with the anchor units. Thus both diblock copolymers (carrying thiol anchor units for CdTe and dopamine anchor units for the oxidic nanorods) are identically in block lengths of soluble and anchor block. The fact that a similar surface coverage is found indicates that both anchor units interact with similar strength with the surfaces.

Table C.4: Adsorption characteristics of diblock copolymers **PS 90/10 dopamine/cysteamine** on various nanorods. For s and σ* see equation 2 and 3.

nanorod	chains / nanorod	nm^2 / chain	s [nm]	R_g [nm]	σ*
TiO_2[a]	28	21.4	4.6	3.4	1.7
ZnO[a]	1855	4.2	2.0	3.4	9.1
SnO_2[a]	19	14.3	3.8	3.4	2.5
CdTe[b]	201	15.4	3.9	3.4	2.4

a: functionalized by **PS 90/10 dopamine**, b: functionalized by **PS 90/10 cysteamine**

The solubility of functionalized nanorods was investigated using various experiments. In general non – or only very slowly – sedimenting solutions can be obtained from the functionalized nanorods after sonification and filtration. At first, however, the pristine nanorod powders cannot be broken up upon ultrasonification in solution. Thus highly opaque dispersions are obtained, where the strong scattering comes solely from undispersed material. This can be shown by polarizing microscopy and scanning electron microscope images (see fig. C.9). The pristine material consists of larger aggregates that can be seen in the microscope as scattering particles of around 5 µm (see fig. C.9A and C). After polymer functionalisation the aggregates are broken up during ultrasonification and dissolved nanorods are found together with some remaining aggregates. These larger aggregates can be removed by filtration (0.2 µm PTFE syringe filter) and solely dissolved nanorods are remaining (see fig. C.9B). These solutions are now clear and oriented domains can be found after evaporation of the solvent (see fig. C.9D). By dynamic and static light scattering[19,38] single nanorods are found to be individually dispersed. These solutions are stable – in the case of TiO_2 nanorods – for long times, however solutions of ZnO (ρ = 5.6 g/cm^3) and SnO_2 (ρ = 7.0 g/cm^3) tend to sediment faster due to the higher densities. The similarity of the results obtained with different block copolymers, different anchor

groups and different inorganic nanorods demonstrates that our concept for surface functionalisation of nano-objects is generally applicable.

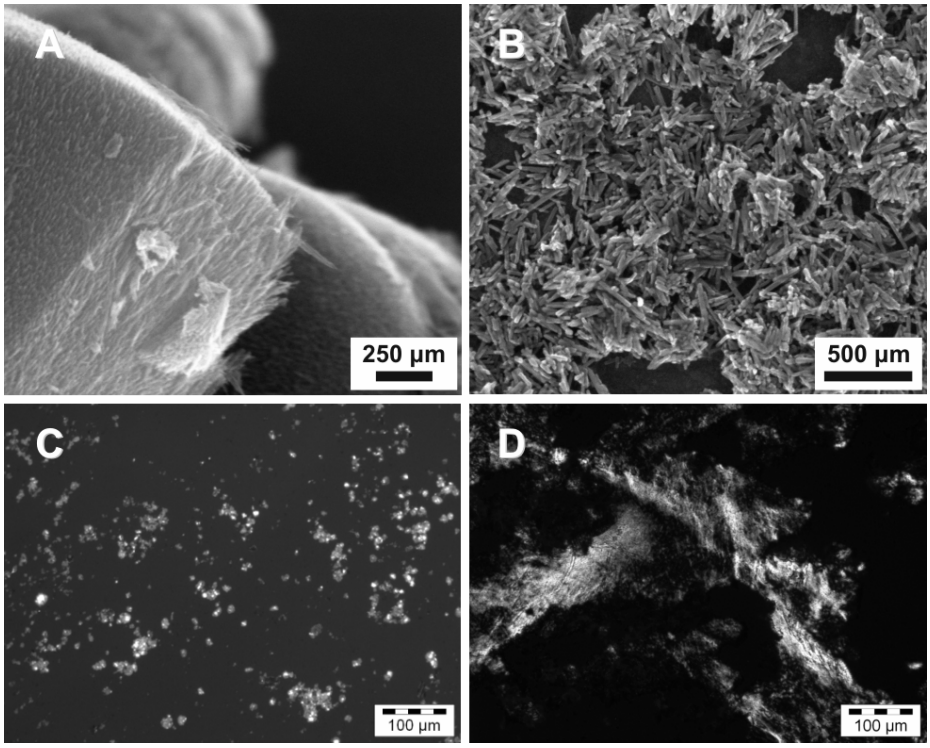

Figure C.9: ZnO nanorods: **A**: SEM image of pristine nanorods; **B**: SEM image of **PS 90/10 dopamine** functionalized nanorods; **C**: polarizing microscopy image of pristine nanorods; **D**: polarizing microscopy image of **PS 90/10 dopamine** functionalized nanorods (evaporated from 20 µl solution of 1.7 mg functionalized nanorods in 1 mL THF sheared between glass slides).

Liquid crystalline phases

Rigid rod objects are – from a theoretical point of view – able to form LC-phases as neat material.[2,3,6] This – theoretical expected – LC-phase is, however, limited to lower temperatures by either a crystalline or a disordered non equilibrium phase (a glass),[39] if the interaction between the rods is too strong to allow a reorganization (this case is realized often in the aggregates of inorganic nanorods). As the temperature to reach

the mobile LC-phase is often above the decomposition temperature, the theoretically expected neat thermotropic LC-phase cannot be observed experimentally. The "dilution" of the rigid-rod objects with a solvent leads now to a decrease of both the glass transition temperature (introduction of mobility) and the clearing temperature, and it shifts the LC-phase into an experimentally accessible temperature range (see figure C.10). These phases are then called "lyotropic" but they are also thermotropic.

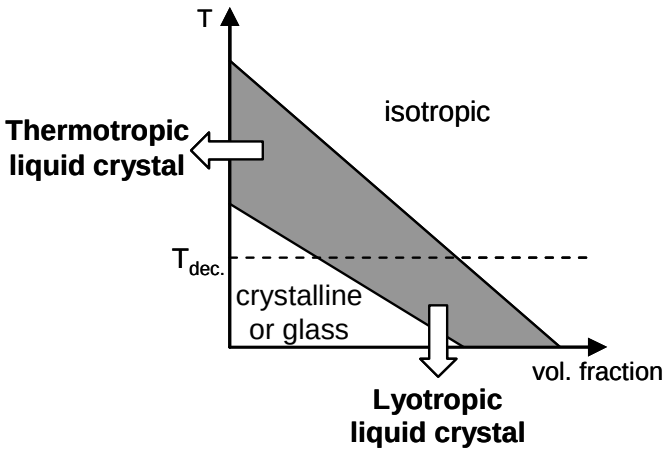

Figure C.10: Schematic presentation of the formation of thermotropic and lyotropic phases in rigid-rod systems.

The expression "lyotropic" – widely used throughout the literature – should however be used carefully. For amphiphiles, for which lyotropic phases are well known, the solvent leads to the formation of form anisotropic aggregates of the amphiphiles. These aggregates (e.g. cylinder micelles) are the constituent units of the lyotropic phase and they are only formed in the presences of solvent. The "lyotropic" phase of rigid-rod objects is however formed from the individual rods, which organize above a critical volume fraction into LC-phases.

Generally this behavior is observed for all polymer functionalized nanorods presented here. It is found e.g. in common solvents like THF, $CHCl_3$,

dichlorobenzene and DMF when a glass slide is drop coated with filtered solution. At high concentrations of the particles during evaporation of the solvent birefringent domains can be observed. Their exact volume fraction was hard to determine because of the volatility of the solvents and the small amounts of particles dissolved. The textures that can be observed after evaporation of the solvent (THF) are similar. Compared with TiO_2 for which such textures have already been described in ref. 19 the birefringent domains are smaller for LC-phases from SnO_2 nanorods, whereas the domains are slightly bigger in the case of ZnO nanorods. After evaporation of the solvent the birefringent domains cannot be sheared and a clearing temperature cannot be determined due to a lack of mobility of the functionalized rods without a liquid matrix (see figure C.9D).

In order to investigate the temperature dependence of the LC phase for lyotropic phases of differently functionalized nanorods an appropriate high boiling solvent had to be found. Oligomeric PEG (M_n = 400 g/mol) is a suitable solvent for PMMA, as both can be mixed in any composition[40] and does not evaporate even at elevated temperatures. Upon mixing PMMA functionalized TiO_2 nanorods with PEG 400, liquid crystalline phases are found in a volume fraction regime between 0.2 and 0.7 (for the hairy-rods). A typical texture can be found in figure C.11A and C.11B. They show textures common for a smectic (below 55 °C) and a nematic (between 55 and 65 °C) phase. Another way to reduce the volume fraction of the TiO_2 nanorods is to use more functionalisation polymer than needed to form a polymer matrix around the hairy-rods. This was done with the low T_g polymer (diethylene glycol monomethyl ether) methacrylate (glass transition temperature below 0 °C) which shows a waxy, honey like consistency at room temperature and is therefore mobile enough. Liquid crystalline phases are found in these mixtures (see fig. C.11C) with a pure polymeric matrix. The clearing temperature is around 90 °C and the system “freezes” around

the T_g of the polymer matrix. This principle should also be useful for other polymer matrices, as heating above the T_g should allow the self organization of embedded nanorods by a liquid crystalline phase.

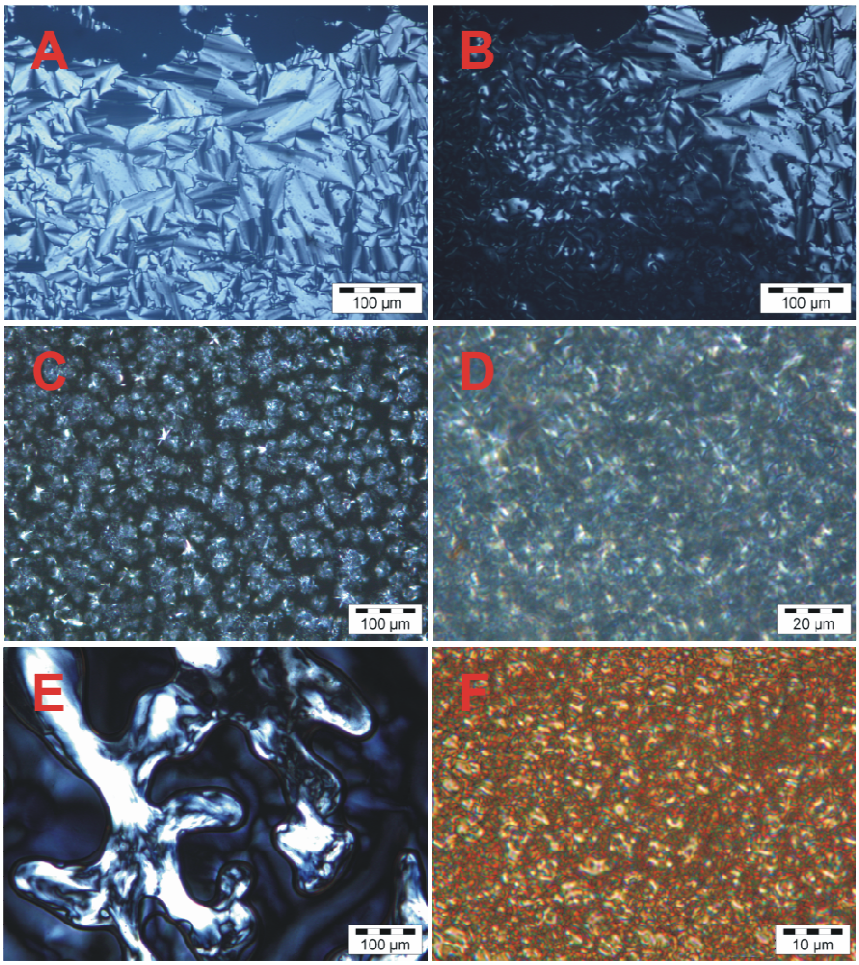

Figure C.11: Polarizing microscopy images of **A**, **B**: **PMMA 70/30 dopamine** functionalized TiO_2 nanorods (50 wt%). Smectic-nematic phase transition around 55 ℃ (**A**: 45 ℃, **B**: 55℃); **C**: **PDEGMEMA 40/30 dopamine** functionalized TiO_2 nanorods (50 wt%) in excess **PDEGMEMA 40/30 dopamine** (T = 25℃); **D**: **PS 90/10 dopamine** functionalized SnO_2 nanorods (70 wt %) in oligo-PS matrix (T = 25℃); **E**: **PS 90/10 dopamine** functionalized ZnO nanorods (70 wt%) in oligo-PS matrix (T = 25℃; **F**: **PS 90/10 cysteamine** functionalized CdTe nanorods (70 wt%) in oligo-PS matrix (T = 25℃).

In the case of the polystyrene functionalized particles it was possible to disperse them in low molecular weight polystyrene (M_n = 580 g/mol). We prepared mixtures of about 70 wt% functionalized particles and 30 wt% of the polystyrene oligomers. Although the viscosity of the mixtures was too high at room temperature, a fluent system could be found when heating to about 35 °C. With this oligomeric solvent clearing temperatures of the liquid crystalline phases can be found. For TiO_2 the clearing of the solution could be observed between 86 and 92°C and for SnO_2 birefringence disappeared between 60 and 68°C (see fig. C.11D). For ZnO a different texture was found: if a little pressure is put on the sample between two glass slides large and bright birefringent areas are observed (see fig. C.11E and C.11F). The clearing point of this phase, which is between 200 and 230 °C, is much higher than for the other phases. This may be due to the much larger dimensions of the ZnO rods, which results in less mobility. For CdTe also liquid crystalline textures could be found in polarization microscopy (see fig. C.11E). In comparison with the structures of the oxidic nanorods the textures showed a red color, due to the absorbance of CdTe nanorods. Otherwise the texture resembled styrene modified SnO_2 nanorods, which also have a comparable size. The clearing temperature was found between 60 and 69°C in polarized optical microscopy.

Conclusion

In this work, we focused on the polymer functionalisation of semi conducting nanorods in order to orient them. The chosen inorganic materials TiO_2, SnO_2, ZnO and CdTe were functionalized with PMMA, PDEGMEMA and PS block copolymers synthesized by RAFT polymerization. The synthesis of the polymers was carried out using a macro initiator approach followed by the polymerization of a reactive ester monomer. Polymer analogous reaction with an anchor unit gave anchor group

functionalized diblock copolymers of low polydispersity. The functionalized inorganic nanorods were soluble in organic solvents and formed stable dispersions. Their degree of surface coverage was investigated by TGA measurements and shows a clear dependency of the polymer architecture. A maximal coverage was found for short anchor blocks (around 20 repeat units) and soluble blocks of 40 to 100 repeat units. As expected the number of adsorbed chains decreases as the anchor block gets longer. On the other side, the length of the soluble block is also limiting the grafting as the coils hinder each other. It was possible to cover oxidic as well as chalcogenic inorganic materials sufficiently with a polymer corona by using appropriate anchor units in the diblock copolymers showing the generality of this functionalisation concept.

Liquid crystalline phases of functionalized nanorods were found and investigated in organic media. In organic solvents, liquid crystals were found in concentrated solutions and showed a clear lyotropic behavior. After evaporation of the solvents, the oriented particles are immobilized. To avoid such problems, high boiling solvents as oligomeric PEG or PS were used as organic matrix. They allow it to investigate temperature dependant phase transitions. In all cases we found liquid crystalline textures and clearing temperatures in a broad range between 60 and 230 °C. The clearing temperature depends on the particle size as well as the used matrix. The LC phases could only be found above the glass transition temperatures of the matrix as the system is otherwise frozen in a glassy state. We also investigated polymeric matrices with low glass transition temperatures and found the same behavior as for oligomeric matrices.

We were able to demonstrate the generality of the functionalisation principle by grafting different oxidic and chalcogenic nanorods with different types of polymers. Afterwards, various organic matrices were used to form liquid crystalline composites.

We were able to self organize the nanorods as liquid crystals by their property to behave as mesogens which is due to their anisotropy. Future work will be done to investigate the orientation of semi conducting materials in order to improve optoelectronic device efficiencies.

Experimental

Methyl methacrylate and styrene (from Acros) and (diethylene glycol monomethyl ether) methacrylate ((2-methoxy-ethoxy)-ethyl methacrylate, from Aldrich) were distilled before usage, benzyl dithiobenzoate (RAFT reagent),[41] pentafluorophenole acrylate[26] were synthesized as described in literature. αα'-azoisobutyronitrile (AIBN, from Fluka) was recrystalized from diethyl ether, dopamine hydrochloride (3-hydroxy tyramine hydrochloride, from Acros) was used as purchased, dioxane and tetrahydro furan (THF) was dried and distilled before usage, all other solvents were also distilled before use. Gel permeation chromatography (GPC) was carried out in THF as solvent and the detector system contained refractive index (Jasco), UV-VIS (Jasco) and light scattering (Wyatt) detectors. Thermo gravimetry was carried out in a Perkin Elmer Pyris 6 TGA under nitrogen atmosphere. NMR spectra were obtained in a Bruker AC 300. Infrared spectroscopy was done in a Bruker Vector 22, UV-Vis spectroscopy was measured in a Shimadzu UV 2102 PC UV-Vis Scanning Spectrophotometer.

The syntheses of **PMMA 70/30 dopamine** and **PDEGMEMA 40/30 dopamine** are already described in literature and all other variations of the block length were synthesized accordingly.[19]

Synthesis of TiO_2 nanorods: The synthesis of TiO_2 nanorods was carried out using the method reported in ref. 19.

Synthesis of SnO_2 nanorods: SnO_2 nanorods were synthesized by the modified method as reported by Cheng et al.[28] In a typical procedure, $SnCl_4$ x 5 H2O (0.001 mol) was dissolved in methanol (10 ml). To this was added 20 ml of tetramethyl ammonium hydroxide (25% w/w in methanol). The solution with dissolved precursor was transferred to a Teflon-lined stainless steel autoclave and heated at 150 ℃ for 24 h. A white-gray precipitate was colle cted, purified, and dried in air at ambient temperature.

Synthesis of ZnO nanorods:[29] For the synthesis of ZnO nanorods, $Zn(Ac)_2$ x $2H_2O$ (1.09 g) was dissolved in 10 mL of methanol. 20 mL of the tetra methyl ammonium hydroxide (25% w/w in methanol) was added with stirring at room temperature. The solution was transferred to a Teflon-lined stainless steel autoclave and heated at 50 ℃ for 24 h followed by a period a t elevated temperature 150 ℃ for another 24 h. The white precipitate was collected and purified by washing with water and dried in air at room temperature.

Synthesis of CdTe nanorods: The CdTe nanocrystals are synthesized in a coordinating solvent by sequential chalcogenide precursor injection similar to the procedure reported by Shien et al.[42] The cadmium precursor is prepared by degassing a mixture of 0.114 g CdO (0.89 mmol), 0.43 g n-tetradecylphosphonic acid (TDPA) (0.155 mmol) and 7 g of trioctylphosphine oxide (TOPO) at 65 ℃ for three hours. The mixture is heated slowly to 320 ℃ under argon and then cooled to the 300 ℃. Tellurium precursor is prepared by dissolvi ng 0.2 g of Te powder in 4 mL of trioctylphosphine (TOP) and stirring for 72 hours at room temperature. Rods are synthesized by injecting the Te precursor in 0.25 mL volumes four times, every 2 minutes, into the hot reaction mixture. To remove the reaction mixture, the nanorods are precipitated with isopropanol, washed by centrifugation and re-suspension in toluene (twice). Finally, the particles were dissolved in 20 mL of chloroform.

Polystyrene-*b*-dopaminacrylamide (**PS 90/10 dopamine**): To synthesize the macro initiator 6.4 mL (56 mmol, 140 eq.) styrene, 97 mg (0.4 mmol, 1 eq) of the chain transfer agent benzyl dithiobenzoate and 6.5 mg (0.04 mmol, 0.1 eq) AIBN (azoisobutyronitrile) were added all together with 3 mL tetrahydro furan in a Schlenk tube. Oxygen was exchanged by nitrogen in three freeze-pump-thaw cycles and polymerization was carried out at 65 °C for 12h. The macro initiator was purified by precipitation in methanol for three times to give 3.8 g (67 %) of the desired polymer. To synthesize the reactive block copolymer, 2 g (0.16 mmol, 1 eq) of the macro initiator was dissolved with AIBN (2.6 mg, 0.016 mmol, 0.1 eq), pentafluorophenol acrylate (760 mg, 3.2 mmol, 20 eq) and THF in a Schlenck tube and oxygen was exchanged by nitrogen in three freeze-pump-thaw cycles. The mixture was polymerized for 48 h at 65 °C and the polymer was purified by precipitating in methanol for three times to yield 1.74 g (63 %) of the reactive block copolymer. For the polymer analogous reaction 700 mg (0.06 mmol, 1 eq.) reactive diblock copolymer, dopamine hydrochloride (171 mg, 0.9 mmol, 15 eq) and triethylamine (90 mg, 0.9 mmol, 15 eq) were dissolved in 2 mL THF and stirred under nitrogen at room temperature for 5 h. Afterwards the solution was filtered and precipitated in methanol for three times to yield 520 mg (74 %) of the desired product **PS 90/10 dopamine**. M_n (GPC) = 11590 g/mol, PDI (GPC) = 1.15. ^{1}H-NMR (300MHz, $CDCl_3$/MeOD 4:1): δ[ppm]: 7.06 (m, 3H, Ph-H), 6.57 (m, 2H, Ph-H), 6.14 (m, 3H, $ArH_{dopamine}$), 3.52 (m, 2H, CONH-C*H*$_2$-CH_2-Ph), 3.39 (m, 2H, CONH-C*H*$_2$-CH_2-Ph), 2.97 (m, 1H, CH_2-C*H*-), 2.38 (m, 1H, CH-C*H*$_2$), 1.87 (m, 1H, CH-C*H*$_2$), 1.84 (m, 1H), 1.39 (m, 2H). ^{19}F-NMR (400 MHz, $CDCl_3$): no signals found. IR: v_{max}/cm^{-1}: 3374 ($OH_{dopamine}$), 3027 (CH), 2923 (CH), 1650 (CONH).

Poly(styrene-*b*-cysteamine acrylamide) (**PS 90/10 cysteamine**): To synthesize the block copolymer with thiol anchor groups the reactive diblock copolymer (700 mg,

0.06 mol, 1 eq.) and cysteamine (69.4 mg, 0.9 mmol, 15 eq.) were dissolved in 2 mL THF and stirred under nitrogen at room temperature for 5 h. Afterwards the solution was precipitated in methanol for three times to yield of the desired product **PS 90/10 cysteamine** (580 mg, 81 %). M_n (GPC) = 10570 g/mol, PDI (GPC) = 1.19. ^{1}H-NMR (300MHz, $CDCl_3$/MeOD 4:1): δ[ppm]: 6.88 (m, 3H, Ph-H), 6.43 (m, 2H, Ph-H), 3.58 (m, 2H, NH-C*H*$_2$-CH_2-SH), 3.08 (m, 2H, NH-C*H*$_2$-CH_2-SH), 3.02 (m, 1H, CH_2-C*H*-), 2.44 (m, 1H, CH-C*H*$_2$), 1.91 (m, 1H, CH-C*H*$_2$), 1.67 (m, 1H, CH-C*H*$_2$), 1.27 (m, 1H, CH-C*H*$_2$). ^{19}F-NMR (400 MHz, $CDCl_3$): no signals found. IR: v_{max}/cm^{-1}: 2561 (SH), 1667 (CONH), 697 (CS).

Preparation of polymer/nanorods hybrids: (for TiO_2, SnO_2 and ZnO) 10 mg of nanorod powder were dispersed in THF by sonification. After 10 min 5 mg of the functionalisation polymer was added and the mixture was sonificated for further 20 min, and stirred over night under N_2 atmosphere. To get rid of the excess of functionalisation polymer the solution was centrifuged (4000 rpm) and the supernatant solution was exchanged against distilled THF for three times.

CdTe nanorods were functionalized by dissolving 2 mg of **PS 90/10 cysteamine** in 1 mL solution of CdTe in chloroform (2 mg/ml). The reaction mixture was stirred for 1 d at 40 °C. The functionalized rods were purified by centrifugation (4700 rpm / 4°C) and exchanging the supernatant solution by distilled THF for three times.

Before investigations of the liquid crystalline behavior the solution were freshly filtered (0.45 µm PTFE syringe filter).

Acknowledgement

We would like to thank the “Fonds der chemischen Industrie” for having founded parts of this work (stipend for S. Meuer) as well as the “International Research Training Group: Self organized Materials for Optoelectronic Applications” (stipend for M. Zorn). SEM pictures were kindly taken by XXXXXX (Max Planck Institute for Polymer Research, Mainz).

References

1 P. G. Bolhuis, D. A. Kofke, *Phys. Rev. E*, 1996, **54**, 634
P. Bartlett, P. B. Warren, *Phys. Rev Lett.*, 1999, **82**, 1979

2 M. Stegemeyer, Guest Ed. in *Liquid crystals*, Steinkopf, Darmstadt/Germany / Springer, New York/USA, 1994; D. Demus, J. Goodby, G. W. Gray, H.-W. Spiess, V. Vill in *Handbook of liquid crystals*, Wiley-VCH, Weinheim, Germany 1998

3 M. Ballauff, *Angew. Chem*., 1989, **101**, 261

4 C. Noël, P. Navard, *Progr. Polym. Sci.*, 1991, **16**, 55

5 P. Davidson, J. C. P. Gabriel, *Curr. Opin. Colloid Interface Sci.*, 2005, **9**, 377

6 P. J. Flory, *Proc. R. Soc. London Ser. A*, 1956, **254**, 73; P. J. Flory, G. Ronca, *Mol. Cryst. Liq. Cryst.*, 1979, **54**, 289

7 G. Petekidis, D. Vlassopoulos, G. Fytas, N. Kountourakis, *Macromolecules*, 1997, **30**, 919-931

8 M.Graetzel, Inorg. Chem., 2005, **44**, 6841-6851

9 P. Suri, R.M. Mehra, *Sol. Energy Mater. Sol. Cells,* 2007, **91**, 518-524

10 W.J.E. Beek, M.M. Wienk, R.A:J. Janssen, *Adv. Mater*., 2004, **16**, 1009-1013

11 J. Sites, J. Pan, *Thin Solid Films*, 2007, **515**, 6099-6102

12 P.K. Sudeep, T. Emrick, *Polymer Reviews*, 2007, **47**, 155-167

13 W. U. Huynh, J.J. Dittmer, A.P. Alivisatos, *Science*, 2002, **295**, 2425-2427

14 H. Zocher, *Z. Anorg. Allg. Chem.*, 1925, **147**, 91

15 C. A. Brunello, C. F. O. Graeff, *J. Non-Cryst. Solids,* 2002, **304**, 265

16 F. C. Bawden, N. W. Pirie, J. D: Bernal, I. Fanhucken, *Nature*, 1936, **138**, 1051

17 A. Dessombz, D. Chiche, P. Davidson, P.Panine, C. Chanéac, J.-P. Jolivet, J. Am. Chem. Soc. 2007, 129, 5904; L. J. Michot, I. Bihannic, S. Maddi, C. Baravian, P. Levitz, P. Davidson, *Langmuir*, 2008, **24**, 3127

18 M. N. Tahir, N. Zink, M. Eberhardt, H. A. Therese, U. Kolb, P. Theato, W. Tremel, *Angew. Chem.*, 2005, **45**, 4809; M. N. Tahir, M. Eberhardt, P. Theato, S. Faiß, A. Janshoff, T. Gorelik, U. Kolb, W. Tremel, *Angew. Chem. Int. Ed.*, 2006, **45**, 908

19 S. Meuer, P. Oberle, P. Theato, W. Tremel, R. Zentel, *Adv. Mater.*, 2007, **19**,

2073-2078

20 L. Li, J. Walda, L. Manna, A. P. Alivisatos, *Nano Letters*, 2002, **2**, 557; B. J. Lemaire, P. Davidson, J. Ferre, J. Jamet, D. Petermann, P. Panine, I. Dozov, D. Stoenescu, J. Jolivet, *Faraday Discuss.*, 2005, **128**, 271

21 N. R Jana, *Chem. Comm*., 2003, **15**, 1950

22 Z. X. Zhang, J. S. van Duijneveldt, *J. Chem. Phys.*, 2006, **124**, 154910; E. S. H. Leach, A. Hopkinson, K. Franklin, J. S. van Duijneveldt, *Langmuir*, 2005, **21**, 3821

23 D. van der Beek, H. Reich, P. van der Schoot, M. Dijkstra, T. Schilling, R. Vink, M. Schmidt, R. van Roij, H. N. W. Lekkerkerker, *Phys. Rev Lett.*, 2006, **97**, 087801; M. P. B. van Bruggen, F. M. van der Kooij, H. N. W. Lekkerkerker, *J. Phys.: Condens. Matter*, 1996, **8**, 9451

24 S. Meuer, L. Braun, R. Zentel, *Chem. Comm.*, 2008, in press; X. Lou, R. Daussin, S. Cuenot, A.-S. Duwez, C. Pagnoulle, C. Detrembleur, C. Bailly, R. Jérôme, *Chem. Mater*., 2004, **16**, 4005 4011; G. J. Bahun, C. Wang, A. Adronov, *J. Polym. Sci., Part A: Polym. Chem.*, 2006, **44**, 1941

25 M. Zorn, R. Zentel, *Macromol. Rapid Comm.*, 2008, in press

26 M. Eberhardt, P. Theato, *Macromol. Rapid Commun.,* 2005, **26**, 1488; M. Eberhardt, R. Mruk, R. Zentel, P. Theato, *Eur. Polym. J.*, 2005, **41**, 1569-1575

27 X.-L. Li, Q. Peng, J.-X. Yi, X. Wang, Y. Li, *Chem. Eur. J.*, 2006, **12**, 2383 – 2391

28 B. Cheng, J.M. Russell, W, Shi, L. Zhang, E.T. Samulski, *J. Am. Chem. Soc.*, 2004, **126**, 5972-5973

29 B. Cheng, W. Shi, J.M. Russell-Tanner, L. Zhang, E.T. Samulski*, Inorg. Chem*., 2006, **45**, 1208-1214

30 C. Barner-Kowollik, T. P. Davis, J. P. A. Heuts, M. H. Stenzel, P. Vana, M. Whittaker, *J. Polym. Sci. Part A: Polym. Chem.*, 2003, **41**, 365-375

31 P.Z Araujo, P.J. Morando, M.A. Blesa, *Langmuir*, 2005, **21**, 3470

32 C. Xu, K. Xu, H. Gu, R.heng, H. Liu, X. Zhang, Z. Guo, B. Xu, *J. Am. Chem. Soc.*, 2004, **126**, 9938

33 T. Rajh, L. X. Chen, K. Lukas, T. Liu, M. C. Thurnauer, D. M. Tiede, *J. Phys. Chem. B*, 2002, **106**, 10543; L. de la Garza, Z. V. Saponjic, N. M. Dimitrijevic, M. C. Thurnauer, T. Rajh, *J. Phys. Chem. B*, 2006, **110**, 680

34 A. G. Koutsioubas, N. Spiliopoulos, D. Anastassopoulos, A. A. Vradis, G. D. Priftis, *J. Polym. Sci., Part B: Polym. Phys.*, 2007, **45**, 2060-2070

35 *Polymer Handbook*, ed. J. Brandrup, E. H. Immergut, E. A. Grulke, A. Abe, D. R. Bloch, 4th edn., 2005, ch. VII / E, pp. 232ff.

36 R. Baranowski, M. P. Whitmore, *J. Chem. Phys.*, 1995, **103**, 2343-2353

37 A. C. Costa, M. Geoghegan, P. Vlček, R. J. Composto, *Macromolecules*, 2003, **36**, 9897-9904

38 S. Meuer, Ph.D. Thesis University of Mainz, 2008, in prep.

39 R. Zentel in *Liquid Crystals* (Eds: H. Stegemeyer), Steinkopf, Darmstadt/Germany

/ Springer, New York/USA, 1994, p. 103 - 140

40 H. Ito, T. P. Russell, G. D. Wignall, *Macromolecules*, 1987, **20**, 2213

41 Y.K. Chong, J. Krstina, T.P.T. Le, G. Moad, A. Postma, E. Rizzardo, S.H. Thang, *Marcomolecules*, 2003, **36**, 2256

42 F. Shien, A.E. Saunders, B.A.Korgel, *J. Phys. Chem. B*, 2005, **109**, 8538-8542

C.2.2 Mesogen Characterization and Lyotropic Phase Behavior

After the positive primary results we asked ourselves: How are the nanorods dispersed in solution? Are they really dispersed as single nanorods or rather as small aggregates, as it is usually found for the original “hairy rods”: stiff main chain polymers? To answer this question we used light scattering as ensemble characterization method and AFM for the visualization of single objects.

Light scattering was performed for both PMMA functionalized nanorods in THF as well as PDEGMEMA functionalized nanorods in water. The first system was investigated by dynamic as well as static light scattering and the resulting radii were in the vicinity of the average length found by TEM and SEM. This result was not expected, as the radii should be much smaller for uniform cylinders. But the TiO_2 nanorods are not uniform in length as assumed by the simple equations, but polydisperse. Therefore, we implanted a distribution function into the calculations and found now also theoretically a similar hydrodynamic radius and radius of gyration as the length average of the rods. This proves that the nanorods are dispersed as single rods and not as aggregates. The other system (PDEGMEMA functionalized nanorods in water) was investigated by dynamic light scattering at various temperatures. As PDEGMEMA has a lower critical solution temperature (LCST) around 25 °C, the polymer corona should collapse resulting in an unstable dispersion. We found that the hydrodynamic radius (determined by dynamic light scattering) shrinks when approaching the LCST and the dispersions get macroscopically unstable (by turbidity measurements). The temperature upon which instability was observed was usually 2 °C below the LCST and was molecular weight dependent. Thus, we showed that it is possible to use stimuli responsive polymers for the functionalization of nanoparticles and that the response has a direct impact on dispersion stability.

AFM is very useful to visualize the polymer corona around the nanorods, when using the tapping mode and a low T_g polymer corona (PDEGMEMA). The phase contrast, which is sensitive for the viscoelastic behavior of the substrate, should differ significantly for the hard core and the low T_g polymer corona. Investigation of the polymer corona is also necessary to understand the thermal behavior of the lyotropic LC phases found before. From theoretical considerations, a lyotropic liquid crystal should be independent of temperature. But we found that the LC phase of polymer functionalized nanorods in solution possesses a clearing temperature indicating a strong influence of temperature. We believe that this effect is due to the soft polymer corona introducing a different potential than a hard rod potential. A hard rod interaction potential implies only the assumption that the rods cannot penetrate each other and is therefore strongly simplified. Introducing a soft polymer shell around the nanorods results in a different potential, as the polymer coronas can either interact with themselves or the solvent, but can also penetrate each other. Therefore polymer-polymer interaction terms need to be considered as well as polymer-solvent interaction terms leading to an understandable thermal impact upon the interaction potential. Thus, the lyotropic phase diagram of PMMA functionalized nanorods in PEG 400 was investigated. PEG 400 is a very useful solvent for PMMA since it does not evaporate and has a high viscosity preventing sedimentation. The samples were analyzed by differential scanning calorimetry (DSC) and polarizing microscopy equipped with a heating stage. All samples clearly show a reversible temperature dependent phase transition. This is a consequence of the polymer corona. In addition, the clearing temperature rises as the polymer coated nanorods pack closer and their interaction increases. This stabilizes the liquid crystalline phase.

C.2.2.1 Publication in Macromolecules 2008, accepted

Liquid crystals from polymer functionalized TiO_2 nanorod mesogens

S. Meuer, K. Fischer, I. Mey, A. Janshoff, M. Schmidt, R. Zentel

Abstract

In this work, we functionalized TiO_2 nanorods with dopamine functionalized diblock copolymers. After functionalization they are well dispersible in organic solvents. Light scattering proves that the nanorods are dispersed as single objects and we could use AFM (tapping mode) to visualize the homogeneous polymer shell around the nanorods. When using a LCST polymer like poly(diethylene glycol monomethyl ether) methacrylate (PDEGMEMA), the functionalized nanorods showed a temperature dependent dispersion stability. The dispersions became microscopically (light scattering) and macroscopically (turbidity measurement) unstable when reaching the LCST of PDEGMEMA. After investigation of the nanorod mesogens, we investigated their liquid crystalline behavior. The phase diagram of PMMA functionalized nanorods in PEG 400 as the mobile matrix was explored and we found a rising clearing temperature with increasing volume fractions of nanorods. On the other hand we investigated PDEGMEMA functionalized nanorods in excess PDEGMEMA polymer as the matrix and found again liquid crystalline phases.

Introduction

The use of nano-objects in the real macroscopic world also requires their macroscopic organization which can be realized in lyotropic liquid crystals (LC)[1]. Generally the formation of lyotropic liquid crystals[2,3,4] from rigid-rod objects as result of form-anisotropy is well understood[5,6] and such phases offer the potential to orient anisotropic nanoparticles. In this respect the orientation of functional semi conducting nanoparticles is interesting for materials science and especially for photovoltaics.[7,8,9,10] As an example, oriented semi conducting materials might improve the device performance in solar cells by alignment of electron-carrying nanorods perpendicular to the electrode.[11] Following this concept it was shown by Alivisatos and co-workers that the efficiency of nanoparticle solar cells could be enhanced, if rod-shaped particles are chosen.[12] Research in this direction is, so far, limited by the solubility of functional nanoparticles, which is needed to obtain the LC-phase at high concentration.

Historically lyotropic LC-phases in water have been observed for various rigid-rod objects like V_2O_5 ribbons,[13,14] tobacco mosaic viruses[15] and TiO_2 nanorods[16] but the charges used to stabilize these systems disable any electronic use. Therefore ion free mineral liquid crystals from uncharged anisotropic nanoparticles in organic solvents are needed. This requires the “solubilisation” of the nano-objects in organic solvents. For this purpose the particles have to be surface functionalized with a soluble corona to overcome the strong adhesion forces among them.[17,18] The concept of “hairy rods”, which was originally developed for stiff main chain liquid crystalline polymers, is very promising for such inorganic nano-objects too.[2] In that concept, a stiff insoluble core is solubilised by linking long chains (the hairs) on its surface. Alkyl chains are often used[19,20] to stabilize nanoparticles of sphere- or rod-like shape and they are also used for delaminated clay fragments.[21] In some cases

they allow the preparation of highly concentrated solutions, which give rise to a liquid crystalline ordering, if anisotropic nanoparticles are used.

Polymeric surfactants[18,21,22] offer advantages here for the solubilisation of inorganic nano-objects: polymers themselves are objects of nanometer dimensions. Therefore polymer coated surface are stabilized sterically up to distance of nanometers and not just for angstroms as with alkyl chains. In addition, new polymers designed for surface functionalisation have multiple anchor units for surface attachment. Therefore adsorption-desorption equilibria reactions are avoided, and a robust fixation of the multi-dentate polymer ligand to the surface can be achieved.

In general both approaches using small molecules and polymers for the stabilization of nanoparticles lead to soluble and highly mobile systems.[19-23] Liquid crystalline phases of both surfactant and polymer stabilized nanorods have been found so far, but polymers offer two major advantages compared to small molecular surfactants: Polymers can be prepared with additional complex functions as stimuli responsive behavior or conductive properties. On the other hand, polymer functionalized nanoparticles can be incorporated into polymer matrices, which is not possible for surfactant stabilized systems as they are usually expelled from the polymer matrix. This has been shown e.g. for TiO_2 nanorods functionalized by random P(MMA-co-MA) copolymers. They could be incorporated homogeneously into PMMA films that showed interesting optical properties.[23]

We wanted to focus on the functionalization with well defined block copolymers where all anchor units are localized in one block. Thus polymer driven cross-linking and aggregation of nanorods can be avoided and the soluble block is fully unfolded into the surrounding solvent enhancing the steric stabilization. Using this concept we recently demonstrated the formation of liquid crystalline phases in highly concentrated solutions of TiO_2 nanorods.[18] This concept could also be applied

successfully to carbon nanotubes.[24] In addition we were able to solubilise and organize TiO_2 nanorods in an organic hole conducting matrix.[25] While – so far – the self assembly is known, little is known about the individual solubilised nanoparticles (the mesogens) and the details of the formation of the LC-phase.

In this work we focus on the detailed investigation of the individual TiO_2 nanorods functionalized with polymethyl methacrylate (PMMA) and "stimuli responsive" poly(diethylene glycol monomethyl ether) methacrylate (PDEGMEMA) block copolymers. We characterized the functionalized nanorods by light scattering methods and AFM. In addition, we were interested in the origin of the thermotropic phase behavior found before[18] which cannot be explained by a simple hard rod interaction and investigated the phase diagram of PMMA functionalized nanorods in PEG 400.

Synthesis

Polymer synthesis

The polymers used in this work were prepared via RAFT polymerization. This controlled radical polymerization technique allows the sequential build up of diblock copolymers with rather narrow polydispersities.[26,27] We used methyl methacrylate as well as (diethylene glycol monomethyl ether) methacrylate as soluble block. Polymers made from these monomers are well soluble in THF, chloroform and dioxane. Poly (diethylene glycol monomethyl ether) methacrylate (PDEGMEMA) is also soluble in polar solvents like alcohols and has a lower critical solution temperature in water around 25 °C. For the interaction with the nanorod surface we used the well investigated anchor unit dopamine. It is found highly exposed in natural adhesion proteins from mussels and binds very strongly to oxidic surfaces.[28] In order to incorporate this unit into the polymer, we used a reactive ester monomer, that is

stable during polymerization and can be reacted with a primary amine polymer-analogous (see figure C.12).[27] The amide is formed quantitatively and all side products can be removed by repeated precipitation of the polymer solution.

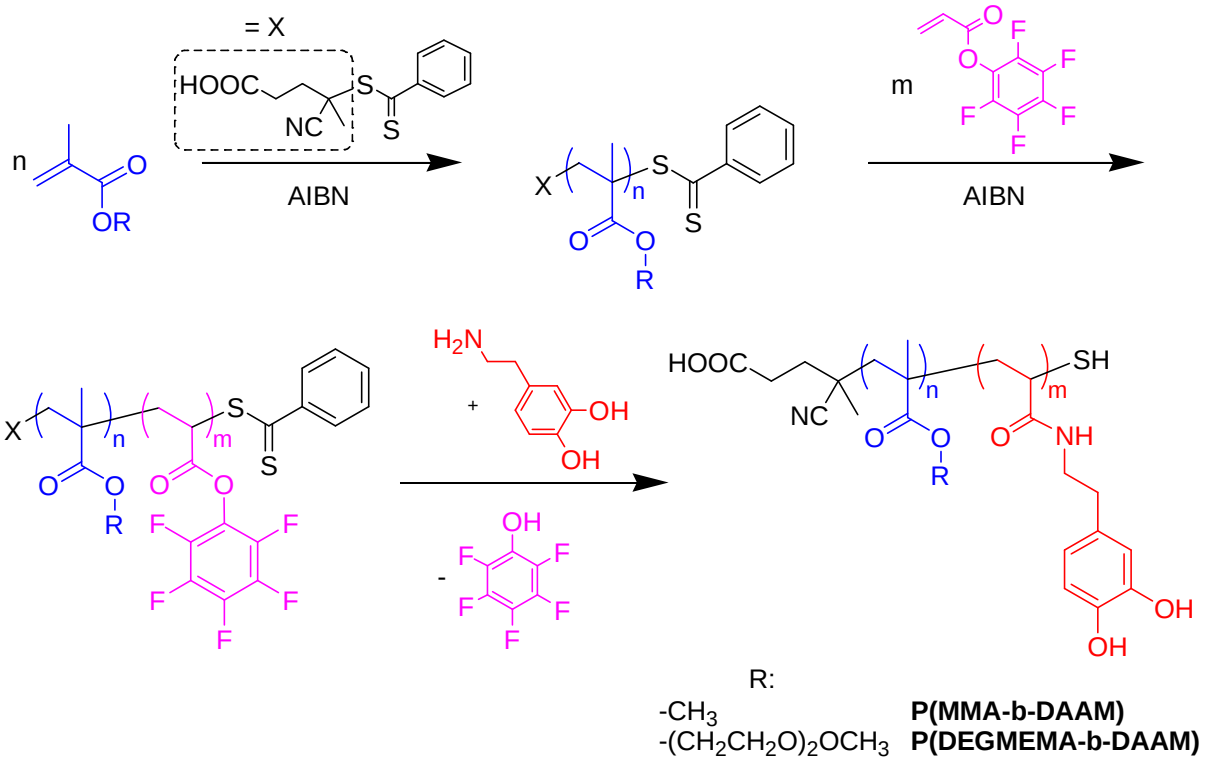

Figure C.12: Diblock copolymer synthesis.

The resulting diblock copolymers poly (methyl methacrylate-*b*-dopamine acryl amide) (**P(MMA-b-DAAM)**) and poly ((diethylene glycol monomethyl ether) methacrylate-*b*-dopamine acryl amide) (**P(DEGMEMA-b-DAAM)**) could be prepared with molecular weights and polydispersities (PDI) reported in table C.5. The PDIs for the polymer-analogously modified diblock copolymers **P(MMA-b-DAAM)** and **P(DEGMEMA-b-DAAM) 1** were around 1.2, which is fairly low. The PDI for **P(DEGMEMA-b-DAAM) 2** is larger with 1.5 which might be due to diethylene glycol dimethacrylate impurities from the monomer synthesis, which act as cross linker. This is especially critical if larger blocks are prepared as the probability for inter polymer cross-linking (by

incorporation of the same cross-linking monomer in two growing polymer chains) increases dramatically with the block length.

Table C.5: Polymer characterization and adsorption behavior.

Name	M_n / g mol^{-1} [a]	PDI[a]	soluble units	anchor units	N_{chains} [b]	A_{chain} / nm^2 [b]
P(MMA-b-DAAM)	12,800	1.17	66	30	85	13
P(DEGMEMA-b-DAAM) 1	14,500	1.21	44	30	90	12
P(DEGMEMA-b-DAAM) 2	47,500	1.53	186	60	9	127

a: determined by GPC (THF), b: calculated from TGA experiments

TiO_2 nanorods

The TiO_2 nanorods used in this work were synthesized with a hydrothermal method which was published before[18] and were used without further modification. Their aspect ratio is stable around 5.5 but their absolute length is rather polydisperse with an average length $<L_n>$ of 71 nm and $<L_w>$ of 90 nm resulting in a polydispersity index ($<L_w>/<L_n>$) of 1.3. To obtain this distribution, we analyzed 350 rods from SEM and TEM images and used the distribution to calculate the average surface per nanorod to be 3800 nm^2 and their average volume to be 15000 nm^3. With these values and the known density of rutile (4260 kg/m^3) one can calculate the surface and the number of rods present per mg powder to $<s>_{1mg}$ = 9.6*10^{16} nm^2 and $<N>_{1mg}$ = 8.8*10^{13}.

Polymer functionalized nanorods

The functionalization (grafting-to) is done in dilute solution (both polymer and nanorods, see Experimental) to prevent inter-particle cross linking. As we start from a dried powder of nanorods, sonification is necessary to break the aggregates. This is unfortunately incomplete, so that filtration (0.2 µm, syringe filter) is necessary to

remove unbroken aggregates (around 10 weight-%). Bidentate ligands containing enediol moieties such as dopamine serve as robust anchor groups to many metal oxides[29] and it has been proven spectroscopically that such ligands convert the under-coordinated surface sites back to a bulk-like lattice structure, which results in a really robust binding.[30] Unbound polymer was removed by repeated washing with fresh solvent and the amount of bound polymer was measured using thermo gravimetry (TGA). The samples were heated up to 800 °C under a nitrogen atmosphere and the weight loss was measured as a function of temperature. As TiO_2 withstands these temperatures, the weight loss is only due to the decomposition of the polymer (usually by depolymerisation). With known molecular weight (see table C.5) and nanorod surface (see section "TiO_2 nanorods") it is possible to calculate roughly the number of polymer chains that bound per nanorod and the corresponding surface area per chain (see table C.5). The values for **P(MMA-b-DAAM)** and **P(DEGMEMA-b-DAAM) 1** are quite similar with roughly 90 chains per nanorod and an area of 12 nm^2 per polymer chain. The coverage of **P(DEGMEMA-b-DAAM) 2** is much smaller and only about 9 polymer chains are bound to the surface corresponding to an area of approximately 130 nm^2. The lower grafting density of **P(DEGMEMA-b-DAAM) 2** results – most probably – from two effects. First the larger soluble block makes it more difficult to approach the nanorods and second the larger anchor block occupies a larger part of the nanorod surface. Both effects reduce the ability of this diblock copolymer **P(DEGMEMA-b-DAAM) 2** to bind to the nanorods surface. For **P(MMA-b-DAAM)** and **P(DEGMEMA-b-DAAM) 1** both the length of the soluble and anchor block are more efficient and the surface area per chain is much smaller than pi times R_g^2 (around 41 nm^2 for **P(MMA-b-DAAM)** and around 26 nm^2 for **P(DEGMEMA-b-DAAM) 1**). This can be explained by the formation of a brush like orientation of the polymers on the nanoparticle surface. **P(DEGMEMA-b-DAAM) 2**

does not form a brush like layer on the nanorods, but more a dense packing of random coils (also called mushroom like layer) as the surface area per chain (127 nm^2) is almost the same as pi times R_g^2 which is 110 nm^2 in this case. In all cases, the surface is covered with a dense polymer layer leading to good solution stability in suitable solvents for the soluble block.

Characterization of the functionalized nanorods

PMMA functionalized TiO_2 nanorods

The **P(MMA-b-DAAM)** functionalized TiO_2 nanorods were investigated by dynamic and static light scattering in order to determine the microscopic dimensions which provide information on the stability and aggregation of the dispersed nanorods. Since TiO_2 has an extremely large refractive index increment, a highly diluted dispersion of $c = 4.5*10^{-5}$ g/L in THF containing 10^{-3} M LiBr was utilized. The results are shown in figure C.13, yielding a hydrodynamic radius $\langle 1/R_h \rangle_z^{-1}$ = 68 nm and a radius of gyration $\langle R_g^2 \rangle_z^{1/2}$ = 88 nm. It is to be noted that due to the large scattering contrast of TiO_2 the radius of gyration resembles the pure TiO_2 dimension (i.e. the contribution of the anchored polymer chains can be neglected). In contrast, the hydrodynamic radius also contains significant contributions of the anchored polymer chains which increase the hydrodynamic friction although being optically invisible.

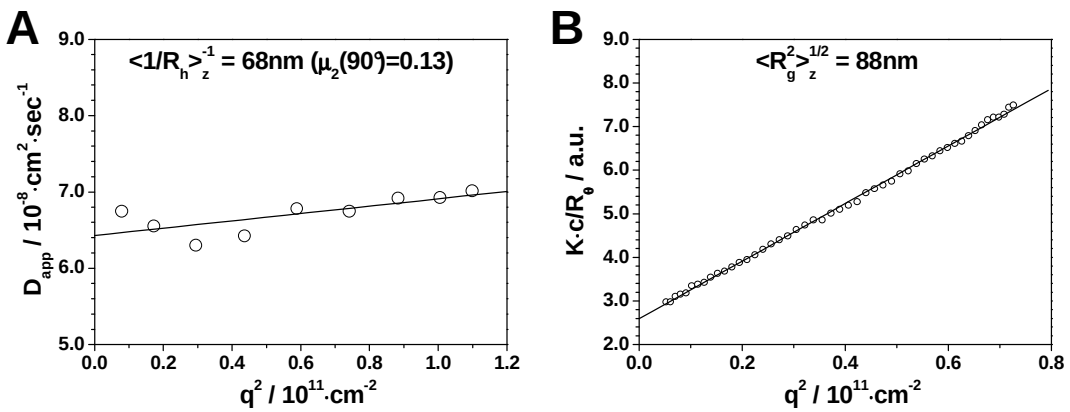

Figure C.13: **A**: dynamic and **B**: static light scattering of **P(MMA-b-DAAM)** functionalized TiO_2 nanorods.

Both radii (68 and 88 nm) are in the vicinity of the number average length of the rods (L_n = 70 nm). However, the ratio between both radii and L_n is not as expected from theory, as e.g. for monodisperse rods $\boldsymbol{R_g} = 1/\sqrt{12} \cdot \boldsymbol{L}$ ($R_{g,\ theory}$ = 20 nm). As the nanorods used are highly polydisperse, this must be taken into account: We modified the known equations of the z-averaged radius of gyration and hydrodynamic radius and implanted a Schulz-Flory or Schulz-Zimm distribution function.[31] Although there is no particular justification to assume a Schulz-Flory or Schulz-Zimm length distribution, it is well known that for a given polydispersity the shape of the distribution function has little influence (usually less than experimental error) on the relation between z-averaged and number averaged quantities.[32] Therefore the distribution utilized should demonstrate that principally the results can be explained by a certain length distribution. Furthermore we modified the equation for our nanorod problem: The mass of a nanorod scales with length times width squared which can be simplified for stable aspect ratios (length / width; in our case around 5.5) to length cubed. These equations can be solved for these simple distribution functions (see Supporting Information) and show the following: the proportionality

factor between $\langle R_g^2 \rangle_z^{1/2}$ and $\langle L_n \rangle$ becomes significantly larger, i.e. 1.1 for a Schulz-Flory (L_w/L_n = 2) and 0.8 for a Schulz-Zimm (L_w/L_n = 1.5) distribution. The experimentally observed value of 1.2 suggests that the length distribution in solution is significantly broader as compared to the TEM analysis. For the quantitative analysis of the hydrodynamic radius the contribution of the polymer shell to the length as well as to the effective hydrodynamic cross-section of the cylinders has to be known. Estimating the hydrodynamic contribution of the soluble PMMA chains to be in the order of the end to end distance $\langle R^2 \rangle^{1/2}$ = 5 nm the hydrodynamic radius may be calculated as

Equation C.4 $$\langle 1/R_h \rangle_z^{-1} = F(L_n + 2\langle R^2 \rangle^{1/2})/(2 \ln((L_n + 2\langle R^2 \rangle^{1/2})/(d + 2\langle R^2 \rangle^{1/2}) + \gamma)$$

with $\langle 1/R_h \rangle_z^{-1}$ the z-average of the hydrodynamic radius, F a factor resembling the impact of the length distribution function with F = 3 for a Schulz-Flory and F = 7/3 for a Schulz-Zimm distribution (see supplementary information), L_n the number average of the nanorod length, $\langle R^2 \rangle^{1/2}$ the average end to end distance of a polymer coil, d the average width of the nanorods and γ a numerical correction factor.

Since L/d does not change with L the logarithmic term is not independent of L anymore. However, since the variation of the aspect ratio introduces a logarithmic correction, only, the value for the aspect ratio $(L_n + 2\langle R^2 \rangle^{1/2})/(d + 2\langle R^2 \rangle^{1/2})$ is fixed to 3.5. Utilizing γ = 0.38 (Lit. 33) the experimental R_h-value of 68 nm is slightly smaller than calculated for a Schulz-Flory distribution (R_h = 73.5 nm) but significantly larger than calculated for a Schulz-Zimm distribution (R_h = 57 nm; see Supporting Information).

It should be mentioned that the value of the second cumulant μ_2 = 0.13 (determined at 90° scattering angle) also indicates a larger polydispersity of the

particles in solution as compared to the TEM analysis. Nevertheless the results from the scattering experiments show that the polymer functionalized rods are dispersed as individual objects, indicating a successful stabilization of the TiO_2 nanorods by the block copolymer.

PDEGMEMA functionalized TiO_2 nanorods

PDEGMEMA is a polymer with interesting properties: it has a low glass transition temperature around 0 °C and is a honey-like viscous fluid at room temperature. In addition it offers solubility not only in THF, chloroform, etc. but also in alcohols and water. In the latter solvent a lower critical solution temperature (LCST) is found around 20 to 25 °C (depending on the molecular weig ht).[34] Below that temperature, the polymer is completely soluble, but rapidly starts to precipitate when raising the temperature above the LCST. We used this phenomenon later to switch the dispersions.

But in a first experiment, we used the low T_g-value of PDEGMEMA to visualize the hard TiO_2 core in the soft polymer matrix by AFM "tapping mode" imaging. In this method, the AFM tip is vibrating while scanning the surface. Thus one can record additionally to the height of the sample the phase shift in the tip frequency, which is dependent on the viscoelastic behavior of the sample. Thus the soft polymeric **P(DEGMEMA-b-DAAM)** shell around the nanorods should give a nice contrast in the phase image, whereas the height image should show no difference between core and shell. Figure C.14 shows the AFM images of **P(DEGMEMA-b-DAAM) 1** functionalized nanorods in tapping mode. Line scans along on of the nanorods are also shown for the height and phase close-up image.

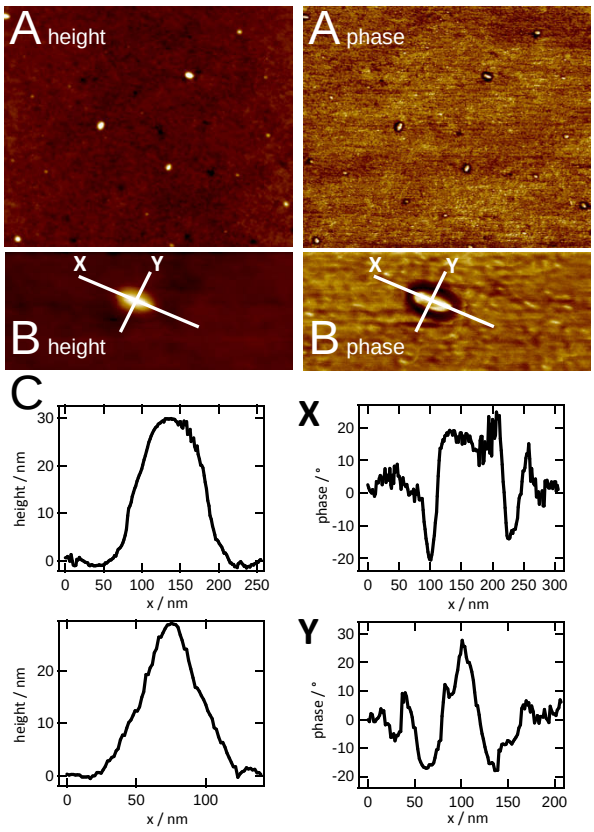

Figure C.14: AFM images taken in tapping mode. Height and phase image of **A**: several **P(DEGMEM-b-DAAM)** functionalized nanorods, **B**: a single several **P(DEGMEM-b-DAAM)** functionalized nanorod. **C**: Line scans along the axes X and Y marked in figure C.14B.

Figure C.14 shows AFM images of TiO_2 nanoparticles on SiO_2 surface obtained in tapping mode at air. Figure C.14A show several nanoparticles on the surface and a close-up of a single nanorod is shown in figure C.14B. In the phase image a halo around the particle is visualized contributing to energy loss due to increased contact area of the cantilever and to the viscoelastic properties of the polymer coating of the nanoparticles. The available aspect ratio is lower than expected (around 3, expected 5.5 from the starting material), which might be due to sample-tip interactions resulting in a broadening of the nanorod width and length. This effect is usually in the range of nanometers as the tip diameter is around 7 to 10 nm. The length (e.g. 70 nm) is

therefore not effected too much, but the width (e.g. 13 nm) is almost doubled leading to a much smaller observable aspect ratio.

In order to investigate the LCST switching behavior of **P(DEGMEMA-b-DAAM)** functionalized TiO_2 nanorods in water, we combined two experiments. First, we prepared a concentrated dispersion (5 mg/ml), which is opaque and measured the turbidity as a function of temperature. As we start from an opaque dispersion, the measured transmission of light is poor and increases as the dispersion is broken at the LCST followed by sedimentation of the very heavy (d_{TiO2} = 4.2 g/cm^3) aggregates. Second, we measure dynamic light scattering from highly dilute dispersions (0.02 mg/ml, 10^{-3} M NaCl in water, PTFE/LG filtered) at various temperatures. The hydrodynamic radius ($<1/R_h>_z^{-1}$) is calculated for each temperature and should get smaller when approaching the LCST. As this is accompanied by precipitation, the measurements were carried out below the LCST to avoid the much stronger scattering of aggregates. The overlaid results of both experiments are shown in figure C.15. We made both experiments for **P(DEGMEMA-b-DAAM) 1** and **2** functionalized TiO_2 nanorods to investigate the effect of different grafting densities.

The experiments show three zone: the first zone well below the LCST, the second zone starts around 19 ℃ for **P(DEGMEMA-b-DAAM) 1** and around 20 ℃ for **P(DEGMEMA-b-DAAM) 2** and the third zone well above the first two zones. In the first zone the dispersions are stable macroscopically and dynamic light scattering shows nicely dispersed single nanorods with a maximal hydrodynamic radius. This indicates that the nanorods are well stabilized on the microscopic scale. In the second zone the interaction of the polymer with the solvent gets poorer. In dynamic light scattering the hydrodynamic radius of the individual nanorods starts to decrease, and the first aggregates are formed. Thus the auto correlation function had to be baseline corrected. At the same time the concentrated solution becomes less

scattering, because the heavy aggregates (d_{TiO2} = 4.2 g/cm^3) starts to sediment. In the third zone the dispersions are broken macroscopically (complete sedimentation of large aggregates leading to clear supernatant liquor).

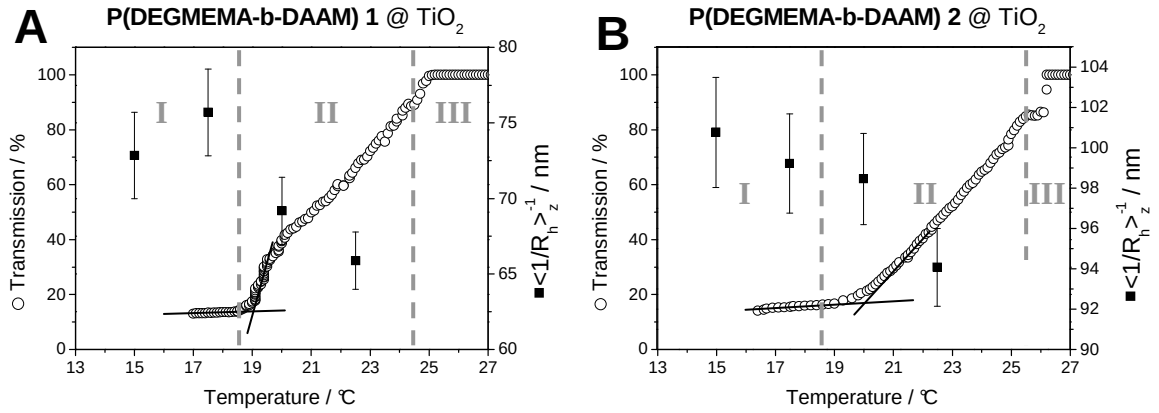

Figure C.15: Overlaid turbidity measurement (open spheres, left coordinate) and measured $<1/R_h>_z^{-1}$ (solid cubes, right coordinate, determined by dynamic light scattering) of **A**: **P(DEGMEMA-b-DAAM) 1** and **B**: **P(DEGMEMA-b-DAAM) 2** functionalized TiO_2 nanorods.

The effect of grafting density and molecular weight of the soluble block can be seen in figure C.15. The position of the second zone (the onset of dispersion instability) shifts from 19 ℃ **P(DEGMEMA-b-DAAM) 1** to 20 ℃ for **P(DEGMEMA-b-DAAM) 2**. This effect can be explained by the molecular weight difference of the two polymers.[34] The difference in the hydrodynamic radius can be rationalized by the difference in the molecular weight between **P(DEGMEMA-b-DAAM) 1** and **2** in combination with the lower grafting density of **P(DEGMEMA-b-DAAM) 2**: In cold water it is around 75 nm for **P(DEGMEMA-b-DAAM) 1** and 100 nm for **P(DEGMEMA-b-DAAM) 2**.

Liquid crystalline phases

PMMA functionalized TiO_2 nanorods in PEG 400

We had previously observed thermotropic phases from polymer functionalized TiO_2 nanorods,[18] whereas only lyotropic (i.e. concentration dependent) phase formation is expected due to hard-core interactions. Thus we wanted to investigate this effect. We focused on **P(MMA-b-DAAM)** and **P(DEGMEMA-b-DAAM) 1** stabilized nanorods, which have similar hydrodynamic radii, for the investigation of their liquid crystalline self-organization. For a thermal investigation of the liquid crystalline behavior of PMMA functionalized nanorods, a high boiling organic solvent is needed. It must – of course – be a suitable solvent for the polymer shell and should withstand more than 150 °C. PEG 400 (oligomers with approx. 10 repeat units) and PMMA are well miscible[35] and in first experiments a liquid crystalline phase could be found.[18] Here we investigated the concentration dependency on the clearing temperature by differential scanning calorimetry (DSC) and polarized optical microscopy. We prepared a set with a constant amount of TiO_2 nanorods and a various amount of PEG 400 in THF solution. The samples were then filtered and concentrated in a DSC pan. In addition, we used this solution to fill glass capillaries and allowed the THF to evaporate. Thus we can analyze the samples in DSC as well as in polarizing microscopy (equipped with a heating stage). The temperatures found match well and the results are shown in figure C.16A (The temperature error bars resemble the typical broadness of the transition (around 10 °C). The concentration error bar is due to the fact that filtration loss is occurring). A typical image of a filled glass capillary is shown in figure C.16B. The texture looks smectic like and in a former work[18] we used TiO_2 nanorods of a broader size distribution where we found a narrow nematic and broad smectic phases. The batch of nanoparticles used this time had less very large rods. Obviously this leads to disappearance of the nematic phase.

At first all samples show clearly a reversible temperature dependent phase transition. This is a consequence of the polymer corona, which creates a soft interaction potential due to steric stabilization. In addition, the clearing temperature from liquid crystalline to isotropic shows a clear concentration dependency: With increasing volume fraction of the nanorods, the clearing temperature rises. As the polymer coated nanorods pack closer their interaction increases, which stabilizes the liquid crystalline phase. The boundaries of this phase diagram are a volume fraction of 0.77 (cubic dense packing of cylinders with half sphere end caps and aspect ratio of 5.5) which corresponds to a dense packing of the rods and a volume fraction of 0.2 below which we could not observe a liquid crystalline phase below.

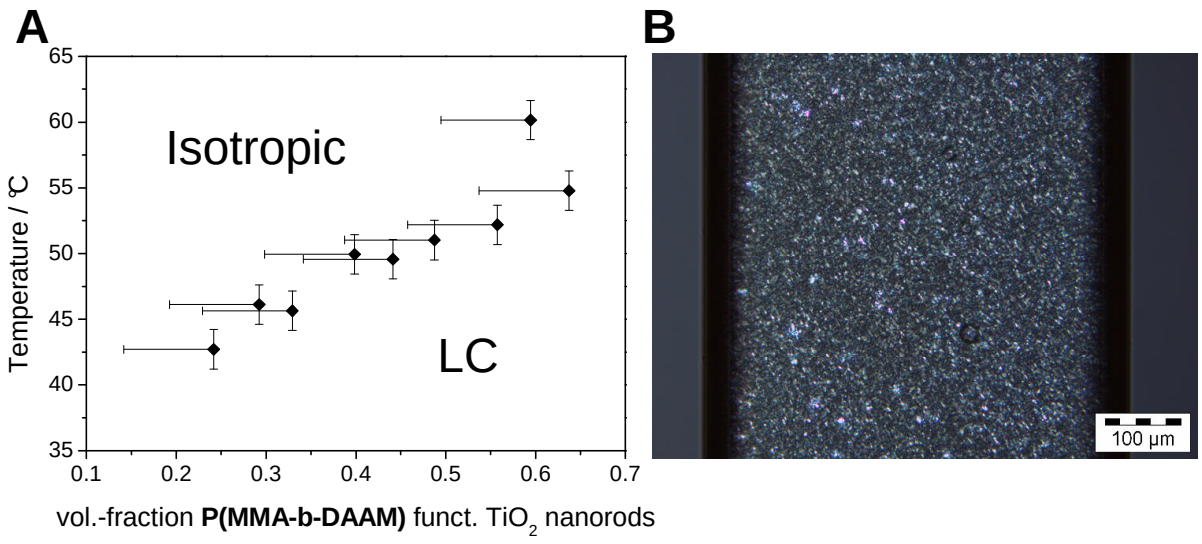

Figure C.16: **A**: Phase diagram of **P(MMA-DAAM)** functionalized TiO_2 nanorods in PEG 400; **B**: Liquid crystal phase of 0.65 vol. fraction **P(MMA-DAAM)** functionalized nanorods in PEG 400; capillary at 25 °C.

PDEGMEMA functionalized TiO_2 nanorods in excess PDEGMEMA

As PDEGMEMA is a polymer with a low T_g and is therefore mobile at room temperature, we prepared samples with excess **P(DEGMEMA-b-DAAM) 1** as

"solvent" and investigated their liquid crystalline behavior. We prepared two samples with 20 and 50 volume percent of functionalized nanorods in THF solution. The samples were then filtered, the THF removed and investigated by DSC as well as by polarizing microscopy. We found again liquid crystalline phases for both and the observed transition temperatures were 80 and 95 °C. With this example we could show, that the principle of using excess polymer as solvent to form a liquid crystalline phase works. In figure C.17, the liquid crystalline phase of **P(DEGMEMA-b-DAAM) 1** functionalized nanorods in excess **P(DEGMEMA-b-DAAM) 1** is shown.

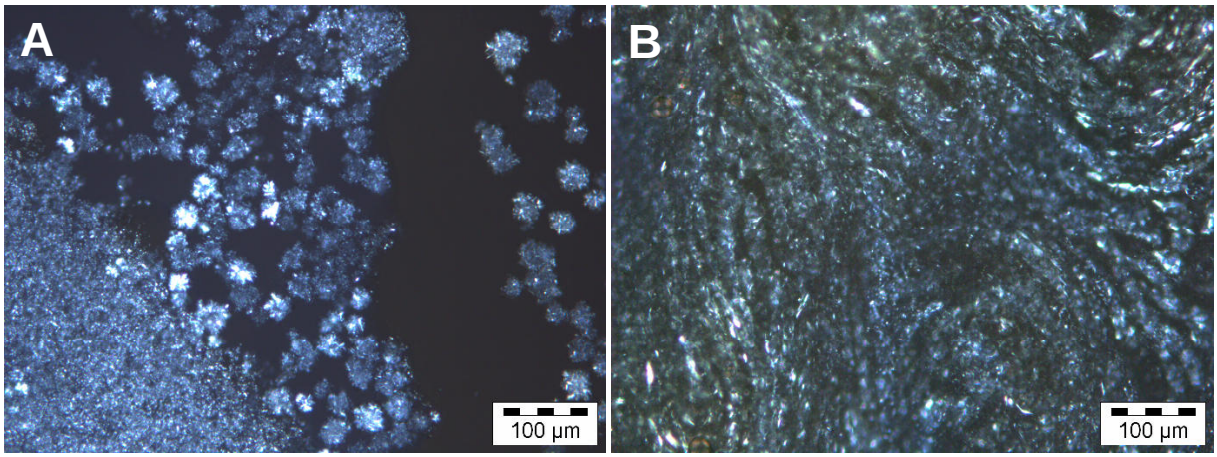

Figure C.17: Liquid crystalline phase of **P(DEGMEMA-b-DAAM) 1** functionalized TiO_2 nanorods in excess **P(DEGMEMA-b-DAAM) 1**; **A**: 0.2, **B**: 0.5 vol. fraction of nanorods.

Figure C.17A shows a sample (20 volume percent nanorods) that demixes upon heating into a nanorod rich phase (lower left corner) and a nanorod poor phase (upper right corner). This biphasic demixing is well known for dispersed rigid-rod objects and shows nicely the concentration dependency of the lyotropic liquid crystal. A liquid crystalline phase with the larger volume percent of nanorods (50) is shown in figure C.17B.

Conclusion

We were able to show, that it is possible to functionalize TiO_2 nanorods with dopamine functionalized diblock copolymers. After functionalization it is possible to stably disperse the nanorods successfully in organic solvents. Light scattering proved that the nanorods were dispersed as single objects and we could use AFM (tapping mode) to visualize the homogeneous polymer shell around the nanorods. The PDEGMEMA functionalized nanorods showed a temperature dependent dispersion stability. The dispersions became microscopically (light scattering) and macroscopically (turbidity measurement) unstable when reaching the LCST of PDEGMEMA.

After careful investigations of the nanorod mesogens, we investigated the liquid crystalline phase. The phase diagram of PMMA functionalized nanorods in PEG 400 was explored and we found – as one would expect – a rising clearing temperature with increasing volume fraction of nanorods. On the other hand we investigated PDEGMEMA functionalized nanorods in excess PDEGMEMA polymer as “solvent” and found again liquid crystalline phases.

Experimental

Methyl methacrylate and styrene (from Acros) and (diethylene glycol monomethyl ether) methacrylate ((2-methoxy-ethoxy)-ethyl methacrylate, from Aldrich) were distilled before usage. Benzyl dithiobenzoate (RAFT reagent)[36] and pentafluorophenol acrylate[27] were synthesized as described in literature. αα'-azoisobutyronitrile (AIBN, from Fluka) was recrystalized from diethyl ether. Dopamine hydrochloride (3-hydroxy tyramine hydrochloride, from Acros) was used as purchased. Dioxane and tetrahydro furan (THF) was dried and distilled before usage. All other solvents were also distilled before use. Gel permeation chromatography

(GPC) was carried out in THF as solvent and the detector system contained refractive index (Jasco), UV-VIS (Jasco) and light scattering (Wyatt) detectors. Thermo gravimetry was carried out in a Perkin Elmer Pyris 6 TGA under nitrogen atmosphere. NMR spectra were obtained in a Bruker AC 300. AFM images were taken with a Multimode (Nanscope 2a Controller, Veeca St. Barbara) employing an AC 160 Cantilever (Olympus, Germany).

Static light scattering (SLS) measurements were performed with an ALV-SP86 goniometer, an ALV-3000 correlator, a Uniphase HeNe Laser (25 mW output power at λ = 632.8 nm wavelength) and ALV/High QE APD avalanche diode fiber optic detection system. For dynamic light scattering (DLS) an ALV-SP125 goniometer, an ALV-5000 correlator and a Spectra Physics 2060 Argon ion laser (500 mW output power at λ = 514.5 nm wavelength) were utilized. The scattered intensity was divided by a beam splitter (approximately 50:50), each portion of which was detected by a photomultiplier. The two signals were cross-correlated in order to eliminate non random electronic noise.

The complex solutions were typically measured from 30°-150° in steps of 5° (SLS) or in steps of 10° (DLS). The static scattering intensities were analyzed according to standard procedures in order to yield the weight average molar mass, M_w, and the mean square radius of gyration, $R_g = \sqrt{\left\langle R_g^2 \right\rangle_z}$. The correlation functions showed a monomodal decay and were fitted by a sum of two exponentials, from which the first cumulant Γ was calculated. The z-average diffusion coefficient D_z was obtained by extrapolation of Γ/q^2 for to q = 0 leading to the inverse z-average hydrodynamic radius $R_h = \left\langle R_h^{-1} \right\rangle_z^{-1}$ by formal application of Stokes law. Prior to mixing the homopolymer solutions were filtered through 0.2 µm pore size Dimex filters (Millipore LG) into 20 mm diameter quartz cuvettes (Hellma).

Synthesis of TiO_2 nanorods: The synthesis of TiO_2 nanorods was carried out using the method reported in ref. 18.

Synthesis of **P(MMA-b-DAAM)**: First, the macro chain transfer agent (macro-CTA) was synthesized as follows: 2g (20mmol) of methyl methacrylate, 112mg (0.4mmol) (4-cyanopentanoic acid)-4-dithiobenzoate and 8mg ($5*10^{-5}$mol) AIBN were added in a schlenk-tube and oxygen was exchanged by nitrogen by five freeze-pump-thaw cycles. Polymerization was carried out at 90℃ for 14h. The macro-CTA was purified by dissolving in THF and precipitating in methanol for three times to yield 1.25g (62%). M_n (MALDI-TOF) = 8500g/mol, PDI (MALDI-TOF) = 1.07. Second, the reactive diblock copolymer was synthesized: 0.5g ($5.9*10^{-5}$mol) of the macro-CTA, 0.5g (2mmol) pentafluorophenole acrylate and 1mg ($6*10^{-6}$mol) AIBN were added to 2ml dioxane in a schlenk-tube. Oxygen was exchanged by nitrogen by five freeze-pump-thaw cycles and polymerization was carried out at 90℃ for 16h. The diblock copolymer was purified by dissolving in THF and precipitating in hexane three times to yield 0.55g. Third, the reactive diblock copolymer was transformed to the polymerligand **P(MMA-b-DAAM)**: 0.55g ($4*10^{-5}$mol) reactive diblock copolymer, 0.25g (1.2mmol) dopamine hydrochloride and 0.12g (1.2mmol) triethylamine were dissolved in 2ml THF and stirred at room temperature over night. The solution was filtered to remove the triethylamine hydrochloride and precipitated in hexane to yield 0.33g (67%) **P(MMA-b-DAAM)**. M_n (GPC) = 12800g/mol, PDI (GPC) = 1.17. ^{1}H-NMR (300MHz, 4:1 d-acetone:d-methanol): δ[ppm]: 6.7-6.3 (m, 3H, Ph-*H*), 3.59 (s, 3H, O-C*H*$_3$), 2.2-1.7 (m, 5H, [-C*H*$_2$-C*H*R-]$_n$ and [-C*H*$_2$-CRMe-]$_n$), 1.6-0.6 (m, 3H, [-CH$_2$-CR(C*H*$_3$)-]$_n$).

Synthesis of **P(DEGMEMA-b-DAAM) 1 & 2**: The procedure is the same as for **P(MMA-b-DAAM)**: For the first step of a.) **PDEGMEMA 1**: 2g (10.6mmol) (2-methoxy-ethoxy)-ethyl methacrylate, 0.6g ($1.1*10^{-4}$mol) (4-cyanopentanoic acid)-4-

dithiobenzoate and 14,5mg ($9*10^{-5}$mol) AIBN and b.) **PDEGMEMA 2**: 2g (10.6mmol) (2-methoxy-ethoxy)-ethyl methacrylate, 0.3g ($5.4*10^{-5}$mol) (4-cyanopentanoic acid)-4-dithiobenzoate and 2.2mg ($1.4*10^{-5}$mol) AIBN polymerized at 90℃ for 5.5h. Purification by dissolving in ethyl acetate and precipitating in petrol ether (three times) to yield a.) **PDEGMEMA 1**: 1.1g (55%). M_n (GPC) = 8100g/mol, PDI (GPC) = 1.15. b.) **PDEGMEMA 2**: 1.3g (65%). M_n (GPC) = 35000g/mol, PDI (GPC) = 1.28. ^{1}H-NMR (300MHz, $CDCl_3$): δ[ppm]: 4.4-3.2 (m, 11H, -C*H*$_2$-C*H*$_2$-O-C*H*$_2$-C*H*$_2$-O-C*H*$_3$), 2.0-1.6 (m, 2H, [-C*H*$_2$-CRMe-]$_n$), 1.3-0.7 (m, 3H, [-CH$_2$-CR(C*H*$_3$)-]$_n$). For the second step a.) **P(DEGMEMA-b-DAAM) 1**: 1.1g ($1.3*10^{-4}$mol) of the macro-CTA were added to 0.58g (2.4mmol) pentafluorophenole acrylate and 1mg ($6*10^{-6}$mol) AIBN in 2ml dioxane b.) **P(DEGMEMA-b-DAAM) 2**: 0.5g ($1.3*10^{-4}$mol) of the macro-CTA were added to 0.21g ($8.8*10^{-4}$mol) pentafluorophenole acrylate and 0.6mg ($4*10^{-6}$mol) AIBN in 2ml dioxane. Polymerization was carried out at 70℃ for 17h. For the third step, the reactive diblock copolymers were directly reacted with 10 fold excess dopamine hydrochloride and triethylamine (1 : 1) in 2ml THF. After filtration, the polymer solution was precipitated in petrol ether to yield a.) **P(DEGMEMA-b-DAAM) 1**: 0.97g (58%), M_n (GPC) = 7900 g/mol, PDI (GPC) = 1.25. b.) **P(DEGMEMA-b-DAAM) 2**: 0.44g (62%), M_n (GPC) = 47500 g/mol, PDI (GPC) = 1.53. ^{1}H-NMR (300MHz, $CDCl_3$): δ[ppm]: 6.7-6.3 (m, 3H, Ph-*H*), 4.4-3.2 (m, 11H, -C*H*$_2$-C*H*$_2$-O-C*H*$_2$-C*H*$_2$-O-C*H*$_3$), 2.9-2.5 (m, 4H, -NH-C*H*$_2$-C*H*$_2$-Ph(OH)$_2$), 2.0-1.5 (m, 5H, [-C*H*$_2$-CRMe-]$_n$ and [-C*H*$_2$-C*H*R-]$_n$), 1.3-0.7 (m, 3H, [-CH$_2$-CR(C*H*$_3$)-]$_n$).

Acknowledgements

We would like to thank the “Fonds der chemischen Industrie” and the “Graduate school of excellence: Materials Science in Mainz” for having funded this work (stipend for S. Meuer). TiO_2 nanorods were synthesized and kindly donated by XXXX

working for XXXXXX (Institute for inorganic and analytical chemistry at the University of Mainz).

Supporting Information

Supporting information includes calculations used for the light scattering of polydisperse nanorods relating the $\langle R_g^2 \rangle_z^{1/2}$ and $\langle 1/R_h \rangle_z^{-1}$ to $\langle L_n \rangle$.

A: Relation of $\langle R_g^2 \rangle_z$ to L_n

The z-average of the radius of gyration is defined as:

$$\left\langle R_g^2 \right\rangle_z = \frac{\sum_i n_i M_i^2 \left\langle R_g^2 \right\rangle}{\sum_i n_i M_i^2} = \frac{\int_0^\infty N(L) L^6 \left\langle R_g^2 \right\rangle dL}{\int_0^\infty N(L) L^6 dL}$$

and can be rewritten for nanorods with constant aspect ratio $M \propto L \cdot d^2 \propto L^3$, $for\ L/d = const.$, the distribution function $N(L) = \frac{L^{m-1}}{m!} y^{m+1} \cdot e^{-yL}$, $y = \frac{m+1}{L_n}$, and $\left\langle R_g^2 \right\rangle = L^2/12$ to:

$$= \frac{\int_0^\infty L^6 \frac{L^{m-1}}{m!} y^{m+1} e^{-yL} L^2/12 \, dL}{\int_0^\infty L^6 \frac{L^{m-1}}{m!} y^{m+1} e^{-yL} dL}$$

$$= 1/12 \frac{\int_0^\infty L^{8+m-1} e^{-yL} dL}{\int_0^\infty L^{6+m-1} e^{-yL} dL} \qquad \text{with } \int_0^\infty x^n e^{-ax} dx = \frac{n!}{a^{n+1}},\ for\ n \in N$$

$$= 1/12 \frac{(7+m)!}{(5+m)!} \cdot \frac{1}{y^2}$$

$$= \frac{(7+m)(6+m)}{12} \cdot \frac{L_n^2}{(m+1)^2}$$

$$= \frac{7}{6} L_n^2 \;\Rightarrow\; \sqrt{\langle R_g^2 \rangle_z} = 1.08\; L_n \;,\; \textit{for}\; m = 1 \;(\textit{Schulz} - \textit{Flory})$$

$$= \frac{2}{3} L_n^2 \;\Rightarrow\; \sqrt{\langle R_g^2 \rangle_z} = 0.82\; L_n \;,\; \textit{for}\; m = 2 \;(\textit{Schulz} - \textit{Zimm})$$

B: Relation of $(\langle R_h^{-1} \rangle_z)^{-1}$ to L_n

The z-average of the hydrodynamic radius is defined as:

$$\left(\frac{1}{R_h}\right)_z = \frac{\sum_i n_i M_i^2 R_h^{-1}}{\sum_i n_i M_i^2} = \frac{\int_0^\infty N(L) L^6 R_h^{-1} dL}{\int_0^\infty N(L) L^6 dL}$$

and can be rewritten for nanorods with stable aspect ratio $M \propto L \cdot d^2 \propto L^3$, $da\; L/d = const.$, the distribution function $N(L) = \frac{W(L)}{L} = \frac{L^{m-1}}{m!} y^{m+1} e^{-yL}$, $y = \frac{m+1}{L_n}$ and $R_h^{-1} = \frac{2(\ln(p) + \gamma)}{L}$

to:

$$= \frac{\int_0^\infty \frac{L^{m-1}}{m!} y^{m+1} e^{-yL} L^6 \cdot \frac{2(\ln(p) - \gamma)}{L} dL}{\int_0^\infty \frac{L^{m-1}}{m!} y^{m+1} e^{-yL} L^6 dL}$$

$$= 2(\ln(p) - \gamma) \frac{\int_0^\infty \frac{L^{5+m-1}}{m!} y^{m+1} e^{-yL} dL}{\int_0^\infty \frac{L^{6+m-1}}{m!} y^{m+1} e^{-yL} dL}$$

$$= 2(\ln(p) - \gamma) \frac{\int_0^\infty L^{4+m} e^{-yL} dL}{\int_0^\infty L^{5+m} e^{-yL} dL} \qquad \text{with} \int_0^\infty x^n e^{-ax} dx = \frac{n!}{a^{n+1}},\; \textit{for}\; n \in N$$

$$= 2(\ln(p) - \gamma) \cdot \frac{\frac{(m+4)!}{y^{4+m+1}}}{\frac{(m+5)!}{y^{5+m+1}}}$$

$$= 2(\ln(p) - \gamma) \cdot \frac{(m+4)!}{(m+5)!} \cdot y$$

$$= \frac{m+1}{m+5} \cdot \frac{2(\ln(p) - \gamma)}{L_n}$$

$$\left(\frac{1}{R_h}\right)_z^{-1} = \frac{m+5}{m+1} \cdot \frac{L_n}{2(\ln(p) - \gamma)} \qquad = 3 \cdot \frac{L_n}{2(\ln(p) - \gamma)} \text{ , for } m = 1 \text{ (Schulz – Flory)}$$

$$= 2\tfrac{1}{3} \cdot \frac{L_n}{2(\ln(p) - \gamma)} \text{ , for } m = 2 \text{ (Schulz – Zimm)}$$

References

1 Stegemeyer, M., Guest Ed. in *Liquid crystals*, Steinkopf, Darmstadt/Germany / Springer, New York/USA, 1994; Demus, D., Goodby, J., Gray, G. W., Spiess, H.-W., Vill, V. in *Handbook of liquid crystals*, Wiley-VCH, Weinheim, Germany ,1998.

2 Ballauff, M. *Angew. Chem*. **1989**, *101*, 261.

3 Noël, C.; Navard, P. *Progr. Polym. Sci.* **1991**, *16*, 55.

4 Davidson, P.; Gabriel, J. C. P. *Curr. Opin. Colloid Interface Sci.* **2005**, *9*, 377.

5 Flory, P. J. *Proc. R. Soc. London Ser. A* **1956**, *254*, 73; Flory, P. J.; Ronca, G. *Mol. Cryst. Liq. Cryst.* **1979**, *54*, 289.

6 Petekidis, G.; Vlassopoulos, D.; Fytas, G.; Kountourakis, N. *Macromolecules*, **1997**, *30*, 919-931.

7 Graetzel, M. *Inorg. Chem.* **2005**, *44*, 6841-6851.

8 Suri, P.; Mehra, R.M. *Sol. Energy Mater. Sol. Cells* **2007**, *91*, 518-524.

9 Beek, W. J. E.; Wienk, M. M.; Janssen, R. A. J. *Adv. Mater*. **2004**, *16*, 1009-1013.

10 Sites, J.; Pan, J. *Thin Solid Films* **2007**, *515*, 6099-6102.

11 Sudeep, P. K.; Emrick, T. *Polymer Reviews* **2007**, *47*, 155-167.

12 Huynh, W. U.; Dittmer, J. J.; Alivisatos, A. P. *Science* **2002**, *295*, 2425-2427.

13 Zocher, H. *Z. Anorg. Allg. Chem.* **1925**, *147*, 91.

14 Brunello, C. A.; Graeff, C. F. O. *J. Non-Cryst. Solids* **2002**, *304*, 265.

15 Bawden, F. C.; Pirie, N. W.; Bernal, J. D.; Fanhucken, I. *Nature* **1936**, *138*, 1051.

16 Dessombz, A.; Chiche, D.; Davidson, P.; Panine, P.; Chanéac, C.; Jolivet, J.-P. *J. Am. Chem. Soc.* **2007**, *129*, 5904; Michot, L. J.; Bihannic, I.; Maddi, S.; Baravian, C.; Levitz, P.; Davidson, P. *Langmuir* **2008**, *24*, 3127.

17 Tahir, M. N.; Zink, N.; Eberhardt, M.; Therese, H. A.; Kolb, U.; Theato, P.; Tremel, W. *Angew. Chem.* **2005**, *45*, 4809; Tahir, M. N.; Eberhardt, M.; Theato, P.; Faiß, S.; Janshoff, A.; Gorelik, T.; Kolb, U.; Tremel, W. *Angew. Chem. Int. Ed.* **2006**, *45*, 908.

18 Meuer, S.; Oberle, P.; Theato, P.; Tremel, W.; Zentel, R. *Adv. Mater.* **2007**, *19*, 2073-2078; Zorn, M.; Meuer, S.; Tahir, M. N.; Khalavka, Y.; Sönnichsen, C.; Tremel, W.; Zentel, R. *J. Mat. Chem.* **2008**, *18*, 3050 – 3058.

19 Li, L.; Walda, J.; Manna, L.; Alivisatos, A. P. *Nano Letters* **2002**, *2*, 557; Lemaire, B. J.; Davidson, P.; Ferre, J.; Jamet, J.; Petermann, D.; Panine, P.; Dozov, I.; Stoenescu, D.; Jolivet, J. *Faraday Discuss.* **2005**, *128*, 271.

20 He, J.; Zhang, Q.; Gupta, S.; Emrick, T.; Russell, T. P.; Thiyagarajan P. *Small* **2007**, 3, 1214-1217; Jana, N. R. *Chem. Comm*. **2003**, *15*, 1950.

21 Zhang, Z. X.; van Duijneveldt, J. S. *J. Chem. Phys.* **2006**, *124*, 154910; Leach, E. S. H.; Hopkinson, A.; Franklin, K.; van Duijneveldt, J. S. *Langmuir* **2005**, *21*, 3821.

22 van der Beek, D.; Reich, H.; van der Schoot, P.; Dijkstra, M.; Schilling, T.; Vink, R.; Schmidt, M.; van Roij, R.; Lekkerkerker, H. N. W. *Phys. Rev Lett.* **2006**, *97*, 087801; van Bruggen, M. P. B.; van der Kooij, F. M.; Lekkerkerker, H. N. W. *J. Phys.: Condens. Matter* **1996**, *8*, 9451.

23 Sciancalepore, C.; Cassano, T.; Curri, M. L.; Mecerreyes, D.; Valentini, A.; Agostiano, A.; Tommasi, R.; Striccoli, M. *Nanotechnology* **2008**, *19*, 205705; Convertino, A.; Leo, G.; Tamborra, M.; Sciancalepore, C.; Striccoli, M.; Curri, M. L.; Agostiano, A. *Sensors and Actuators B* **2007**, *126*, 138–143.

24 Meuer, S.; Braun, L.; Zentel, R.; *Chem. Comm.* **2008**, DOI: 10.1039/b803099e; Lou, X.; Daussin, R.; Cuenot, S.; Duwez, A.-S.; Pagnoulle, C.; Detrembleur, C.; Bailly, C.; Jérôme, R. *Chem. Mater*. **2004**, *16*, 4005 4011; Bahun, G. J.; Wang, C.; Adronov, A. *J. Polym. Sci., Part A: Polym. Chem.* **2006**, *44*, 1941.

25 Zorn, M.; Zentel, R. *Macromol. Rapid Comm.* **2008**, DOI: 10.1002/marc.200800165.

26 Moad, G.; Rizzardo, E.; Thang, S. H. *Aust. J. Chem.* **2005**, *58*, 379-410.

27 Eberhardt, M.; Theato, P. *Macromol. Rapid Commun.* **2005**, *26*, 1488;
Eberhardt, M.; Mruk, R.; Zentel, R.; Theato, P. *Eur. Polym. J.* **2005**, *41*, 1569-1575.

28 Lee, H.; Lee, B. P.; Messersmith, P. B. *Nature* **2007**, *448*, 338-342.

29 Xu, C.; Xu, K.; Gu, H.; Heng, R.; Liu, H.; Zhang, X.; Guo, Z.; Xu, B. *J. Am. Chem. Soc.* **2004**, *126*, 9938.

30 Rajh, T.; Chen, L. X.; Lukas, K.; Liu, T.; Thurnauer, M. C.; Tiede, D. M. *J. Phys. Chem. B* **2002**, *106*, 10543; de la Garza, L.; Saponjic, Z. V.; Dimitrijevic, N. M.; Thurnauer, M. C.; Rajh, T. *J. Phys. Chem. B* **2006**, *110*, 680.

31 Schmidt, M. *Macromolecules* **1984**, *17*, 553-560; Oberthuer, R. C*. Makromol. Chem.* **1978**, *179*, 2693-2706.

32 Stickler, M. *Die Angewandte Makromolekulare Chemie* **1984**, *123/124*, 85-117; Sutter, W.; Kuppel, A. *Die Makromolekulare Chemie* **1971**, *149*, 271-289

33 Broersma, S. *J. Chem. Phys.* **1960**, *32*, 1632

34 Han, S.; Hagiwara, M.; Ishizone, T. *Macromolecules* **2003**, *36*, 8312-8319.

35 Ito, H.; Russell, T. P.; Wignall, G. D. *Macromolecules* **1987**, *20*, 2213-2220.

36 Chong, Y. K.; Krstina, J.; Le, T. P. T.; Moad, G.; Postma, A.; Rizzardo, E.; Thang, S. H. *Marcomolecules* **2003**, *36*, 2256.

C.2.3 Thermotropic Phase Behavior and Macroscopic Orientation

After the detailed investigations of the mesogens and the lyotropic phase behavior the thermotropic phase behavior was investigated in more detail. It was again analyzed in PEG 400 as “solvent” as it is a suitable solvent for PMMA that does not evaporate (decomposition around 200 ℃) and has a h oney-like viscosity preventing sedimentation. We took a deeper look on a 50 wt% / 21 vol% mixture of PMMA functionalized TiO_2 nanorods in PEG 400, which was prepared by dissolving both in THF followed by evaporation of the auxiliary solvent. Thus, a very homogeneous mixture can be obtained. It was then analyzed by polarizing microscopy equipped with a heating stage and DSC and the following phase sequence was found: isotropic 63℃ nematic 52℃ smectic A 42℃ higher ordered sme ctic. The phases were identified according to their texture in polarizing microscopy. As we were working with polydisperse nanorods, we were not expecting phases other than nematic. In a nematic phase it is not a problem having short and long rods mixed, as they can easily pack without losing the orientation (see figure C.18). The smectic phase is harder to imagine, as the layered structure cannot be realized that easily.

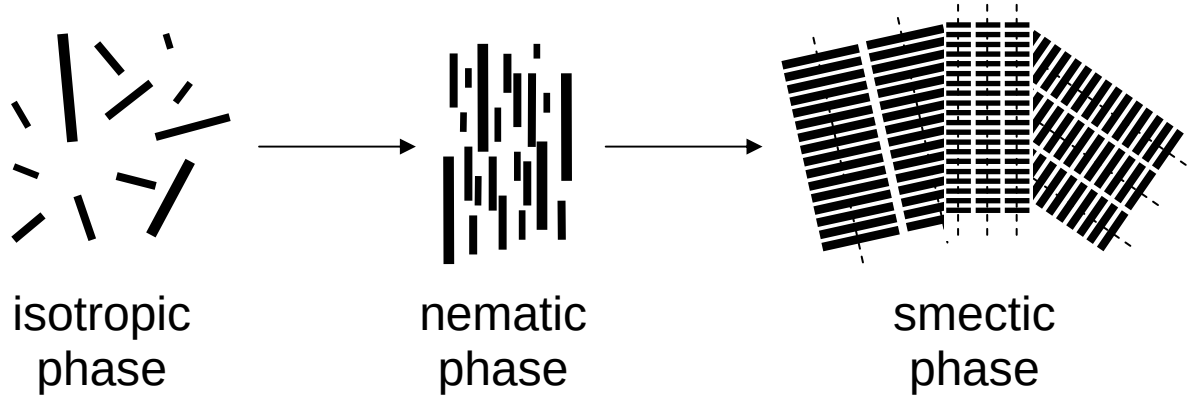

Figure C.18: Schematic packing of polydisperse rods in LC phases.

Figure C.18 shows one of the possibilities to form a smectic phase from polydisperse rods, a size separated form. The other way to incorporate long rods into a shorter layered smectic would be by a transversal migration to form a tapered lamellae. In our experiments, we found size separation and broad transition ranges between the phases (partially still smectic and partially already nematic) strongly indicating size separation. Additionally, we found smectic reflections in small angle X-ray scattering with a layer distance around the length of the nanorods proving the smectic phase.

The formation of a lyotropic LC phase can be used to orient the nanorods. We found oriented nematic structures from dried dispersions in THF, indicating that the orientation of nanorods is possible. We tried to form an aligned sample using the following method: A structured substrate was drawn out of a diluted stable dispersion of PDEGMEMA functionalized nanorods in methanol. This has to be done very slowly (200 nm/s) to ensure a stable meniscus at the air-dispersion boundary on the substrate. Lyotropic phases are formed in the meniscus on the substrate during evaporation of the solvent. For this experimental setup, a sufficient wetting of the substrate by the solvent is important. We used a hydrophilic silicon wafer with parallel etched line structures of about 100 µm width. Within the channels a stable meniscus is formed which ensures a homogeneous ordering. The resulting ordered structures were analyzed by an image software and each rod was sized by hand. The image was tiled and the order parameter was calculated for each tile. The resulting vector map was calculated and showed an average order parameter of 0.7, a reasonable value for a well-ordered nematic phase.

C.2.3.1 Publication in Advanced Materials 2007, 19, 2073-2078

Liquid crystalline phases from polymer functionalized TiO_2 nanorods

Stefan Meuer, Patrick Oberle, Patrick Theato, Wolfgang Tremel, Rudolf Zentel

Introduction

The successful use of nano-objects in the real macroscopic world requires, besides the preparation of nano-objects, also their macroscopic organization and orientation. The organization of nanometer sized objects – both of organic or inorganic nature – is a topic of (i) colloidal science and realized in colloidal crystals,[1] (ii) of liquid crystals (LC)[2] and (iii) block-copolymers.[3] These two topics overlap in the area of lyotropic liquid crystals.[4,5,6] An additional benefit of liquid crystals (LC) is to allow an orientation of anisotropic nano-objects.

The formation of LC-phases is experimentally and theoretically well investigated for rigid-rod objects.[7,8,9] Theory predicts that a nematic phase forms spontaneously above a certain threshold concentration, which depends on the shape anisotropy. The experimental observation of the lyotropic phase requires mobility of the nano-objects at high concentration. Thus a neat material of highly anisotropic nano-objects usually does not form LC-phases due to lack of mobility, but LC-phases are formed, if highly concentrated solutions can be obtained. This requires the "solubilisation" of the nano-objects – to be discussed later – and the choice of a suitable solvent.

Mineral liquid crystals were first observed by Zocher[10] in 1925, and since then many reports appeared on LC-phases with embedded nano-objects such as charged V_2O_5 assemblies[11] or tobacco mosaic viruses[12] in water. They give rise to a nematic phase and it is possible to orient them macroscopically by external fields (e.g. magnetic fields or shear forces). But these systems are restricted to aqueous solutions usually in a very narrow pH range. To overcome these restrictions and to obtain a better understanding of these systems, mineral liquid crystals from uncharged anisotropic nanoparticles in organic solvents are of big interest. TiO_2 nanoparticles e.g. are semi-conducting, have a high refractive index[13] and show interesting optical properties, which makes them useful in modern solar cell concepts.[14] Since they can be prepared with a high aspect ratio (length/width), the formation of liquid crystalline phases may be anticipated, if a good mobility and solubility[15,16] can be achieved.

In order to realize LC-phases in organic solvents, the particles have to be surface functionalized to overcome the strong adhesion forces among them and to disperse them well.[17] Therefore the concept of “hairy rods”, which was originally developed for stiff main chain liquid crystals, is promising.[4] In that concept, a stiff insoluble core is solubilised by long alkyl chains (the hairs) on its surface. The applicability of the concept has already been demonstrated for anisotropic nanoparticles. An-isotropic CdSe nanorods were functionalized with triphenylphosphine oxide as well as with tetradodecyl phosphoric acid to give liquid crystalline phases in cyclohexane.[18,19]

First experiments with polymeric surfactants were reported by the group of Lekkerkerker, who employed an amine functionalized polyisobutylene to stabilize boehmite rod-like particles and gibbsite platelets sterically.[20,21] These systems showed an isotropic-nematic phase transition in toluene. Replacing the short alkyl chains by polymeric side chains considerably enhances the chemical variability as

the polymeric side chains ensure a good solubility in organic solvents and simultaneously allow to implant interesting properties such as stimuli responsive behavior or conducting properties.[14] By using diblock copolymers with multiple anchor groups instead of a single anchor unit adsorption-desorption equilibria reactions as they are known for molecular surfactants are avoided, and a robust fixation of the multidentate polymer ligand to the surface can be achieved by the simultaneous complexation of surface cations.

Results and Discussion

For the build-up of defined functional polymers, controlled radical polymerization is the most suitable polymerization method. It is highly compatible with most functional groups and allows the controlled synthesis of block copolymers. In this study the radical addition fragmentation transfer polymerization (RAFT) was chosen. The synthesis was carried out following a macro initiator approach. First a monomer for the soluble block (methyl methacrylate for **PL1** or (2-methoxy-ethoxy)-ethyl methacrylate for **PL2**) was polymerized. The two different monomers give rise to different glass transition temperatures (T_g-values) in the resulting polymers. Due to its low T_g-value PL2 will also show mobility in the neat (solvent free) state. The reactive diblock copolymer was synthesized by reinitiation of the macro initiator to polymerize a reactive ester monomer (pentafluorophenole acrylate) to form a second block. After the polymerization of the reactive ester monomers it is possible to introduce the anchor groups polymer-analogously by an amide formation.[22] The properties of the resulting block-copolymers are collected in table C.6 and in the experimental part. Since the length of the individual anchor blocks is rather short, both blocks are probably miscible.[23] The appropriate anchor group for a each solid state compound is dictated by the concepts of coordination chemistry, which are used extensively in the

classic scheme of qualitative inorganic analysis with organic dyes.[24,25] For Ti^{4+} catechole groups are known to preferentially bind to the reactive edges of oxide nanocrystals.[26]

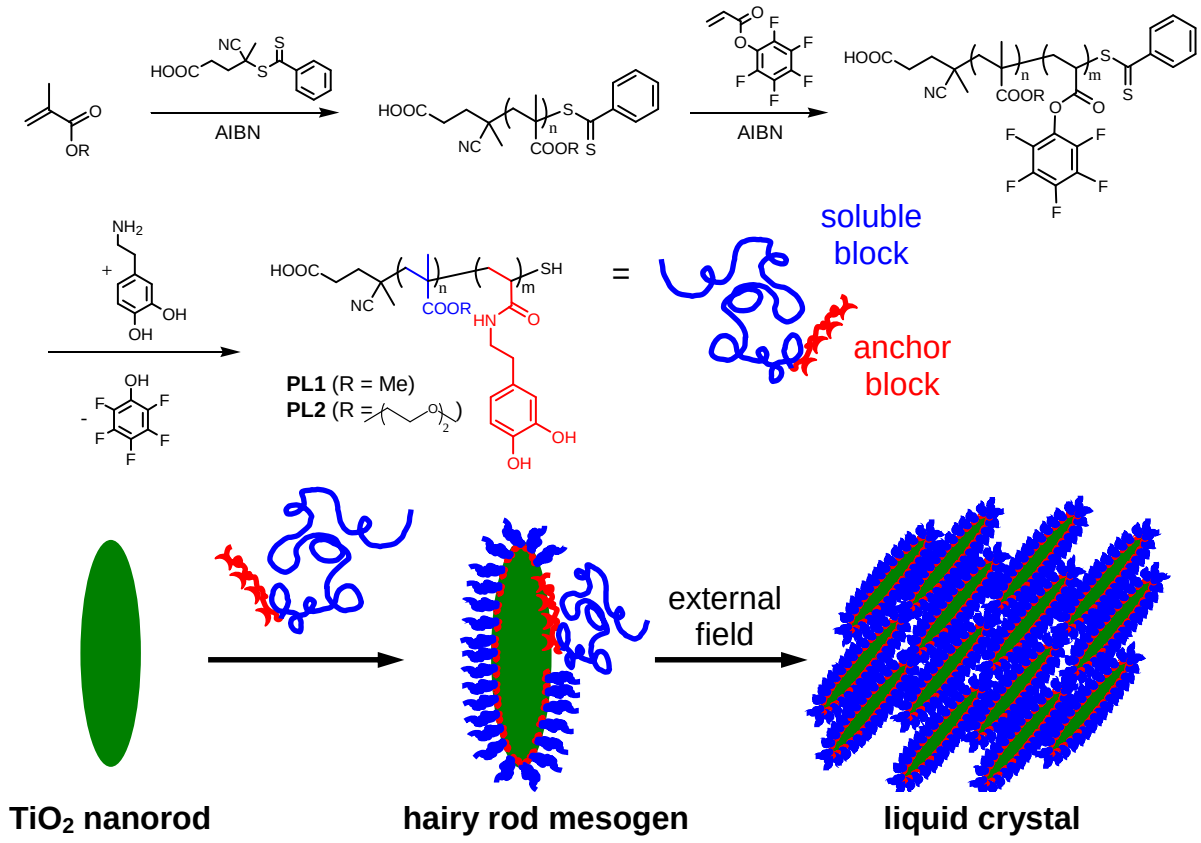

Figure C.19: Build-up of defined diblock copolymers with an anchor and a soluble block for the functionalization of TiO_2 nanorods to form the hairy rod mesogen.

Table C.6: Properties of polymer ligands.

	M_n/g*mol^{-1}	PDI	n : m	T_g/℃	suitable solvents
PL1	14.600	1.17	10.6 : 1	115	benzene[a], $CHCl_3$[a], dioxane[a], THF[a], toluene[a], PEG[b]
PL2	7.900	1.25	21.1 : 1	-34	acetone[a], $CHCl_3$[a], dioxane[a], ethyl acetate[a], ethylene glycol[a], methanol[a], THF[a]

[a]own experiments, [b]ref. 28

The introduction of catechole anchor groups can be achieved by reaction of dopamine (4-(2-amino-ethyl)-benzene-1,2-diol) with the pentafluorophenole acrylate block to give the polymer ligands **PL1** and **PL2** (fig. C.19 and tab. C.6). Polymers with these anchor groups can be used to functionalize anisotropic TiO_2 nanorods[17] whose properties will be discussed later (fig. C.23A) in more detail. The connection of catecholes onto TiO_2 surfaces can be monitored spectroscopically, because of an orange colored surface complex,[27] and this effect can be seen when a solution of **PL1** or **PL2** in an organic solvent is added to TiO_2 nanorods.

In order to accelerate the dispersion process, the mixture was sonicated and a stable dispersion was formed. To determine the amount of block-copolymer strongly bound to the TiO_2 nano-rods the following process was applied: An excess of the block copolymer is added to the TiO_2 nano-rod dispersion. Then the nano-rods are sedimented by centrifugation, the clear upper solution is decanted and the nano-rods are redispersed in new solvent (see experimental part). Finally the amount of strongly bound block copolymer is determined by thermo gravimetry. In this way it is found that about 0.16 mg of block-copolymer binds per mg of TiO_2. For the solubilisation of the nano-rods 0.2 mg of block-copolymer per mg of TiO_2 are used. Thus there is a small amount of weakly bound or free block-copolymer available.

These dispersions can be produced in organic solvents like chloroform or any other solvent that is suitable for the soluble block. Dispersions with up to 0.5 wt% are normally stable for days. In more concentrated solutions, however, sedimentation occurs over time. The precipitate can be redispersed by shaking, and even after a complete evaporation of the solvent, the particles can be redispersed easily in any suitable solvent for the soluble block (PMMA (**PL1**) or poly(2-methoxy-ethoxy)-ethyl methacrylate) (**PL2**)).

The used TiO_2 nanorods were polydisperse. The smallest nanorods had a length / width of 50 / 8nm whereas the largest were 150 / 25nm big. The average length of the nanorods was 70.5 ± 39.6nm (standard deviation), with an aspect ratio around 5.5. The polydispersity can be given either by the ratio of number and weight average length $<L_w>/<L_n>$ = 1.3, or as percentage value: 56%. Dilute solutions of **PL1** functionalized nanorods (2 mg/ml in THF) were investigated by dynamic and static light scattering. The resulting hydrodynamic radius and radius of gyration were in the order of single nanorods ($<1/R_h>_z^{-1}$ = 68 nm, $<R^2_g>_z^{1/2}$ = 88 nm). The ratio of both radii is smaller than expected for nanorods with an aspect ratio of 5.5. This can be explained by the fact that the polymeric shell effects the hydrodynamic radius but not the radius of gyration. It is remarkable that the dilute solution consists of the individual rod-like particles, because hairy-rod structures often forms aggregates even in dilute solution.[9]

First experiments with the dispersions showed, that birefringent domains (probably nematic) appear during solvent evaporation (increase of concentration), which can be oriented by shearing forces. Such birefringent regions are typical for lyotropic phases of rod-like particles,[4,5] which phase separate into an LC-phase rich in anisotropic objects and an isotropic phase poor in the anisotropic objects.[8] The evaporation speed of the solvents (THF or $CHCl_3$) did, however, not allow a more quantitative characterization of the phase behavior. A polarizing microscope image of a sheared and afterwards dried dispersion is shown in Figure C.20A. The small droplet-like birefringent areas possess a radial director configuration, while the elongated domains are oriented along the shearing direction. The appearance of a lyotropic nematic phase on increasing concentration was proven in a sedimentation experiment in a capillary and is presented in figure C.20B.

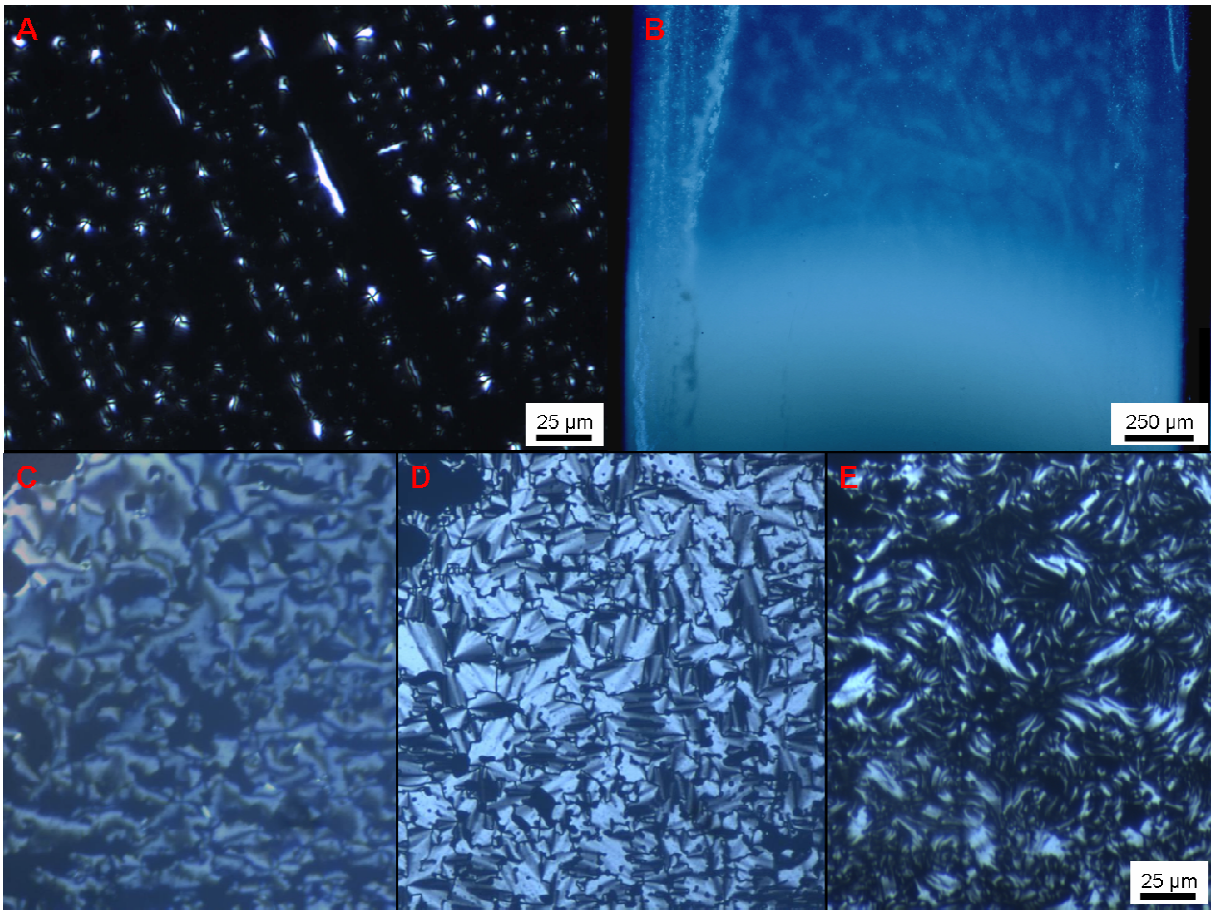

Figure C.20: Polarizing microscope images of sheared dispersion of **PL1** covered TiO_2 nanorods in (i) THF: **A**: nematic droplets formed in an isotropic environment; **B**: sedimented LC phase in a capillary; (ii) PEG 400 at 68℃: **C**: nematic schlieren texture; **D** in PEG 400 at 45℃: smectic fan shaped texture; in **E**: in PEG 400 at 25℃: striated texture.

To investigate the formation of LC phases in more detail, a model system with polyethylene glycol (PEG) 400 as solvent was chosen. PEG is a solvent that does not evaporate even at high temperatures, but dissolves **PL1**. PEG is close to a theta solvent for PMMA.[28] Both polymers are miscible in any ratio and neutron scattering has proved (ref. 28) that PMMA has an unperturbed chain conformation in PEG. For this system a much higher concentration of TiO_2 nanorods was employed (50 wt% / 21 vol%). Such mixtures of **PL 1** covered nanorods in PEG 400 have a highly viscous

waxy consistence. Thus it is not possible to determine the formation of a lyotropic phase during sedimentation. On the contrary the thermotropic phase behavior gets accessible. It can be investigated in thin layers by polarizing microscopy. Several different phases are found: (1) an isotropic phase at high temperatures, (2) as expected a nematic phase, extending at this concentration through the whole volume, but also (3) two additional phases at lower temperatures (Figure C.20C-E). The observed textures for the nematic phase was a schlieren texture (Figure C.20C). For the first additional phase it is a fan-shaped texture (Figure C.20D) and for the second additional phase a striated texture (Figure C.20E). Thus the first additional phase at higher temperature is probably a smectic A phase. The assignment of the second phase will require more detailed investigations including X-ray diffraction, light scattering and rheological experiments.

Unpublished Insertion

Small angle X-ray scattering was used to take a deeper look onto the phases found in figure C.20. The experiments were done on a Bruker Nanostar with a sample-detector distance of 106.9 cm in collaboration with Prof. F. Giesselmann and C. Hägele (Institute for Physical Chemistry, University of Stuttgart/Germany). The investigation of the phases was very difficult as the expected reflexes have very small angles very close to the beam stopper. We did only get a nice scattering image of the first smectic phase which is shown in figure C.21. The peak corresponds to a smectic layer distance of 55 nm, which is in the range of the shorter nanorods from the polydisperse sample. As we expected a distribution of layer distances, the broadness of the reflection is reasonable and proves that the phase is smectic. In order to detect the very small angle reflections, we measured at a very large sample-

detector distance of 106.9 cm which limits the accessible angle to small angles. The corresponding wide angle reflexes are out of the accessible angular range.

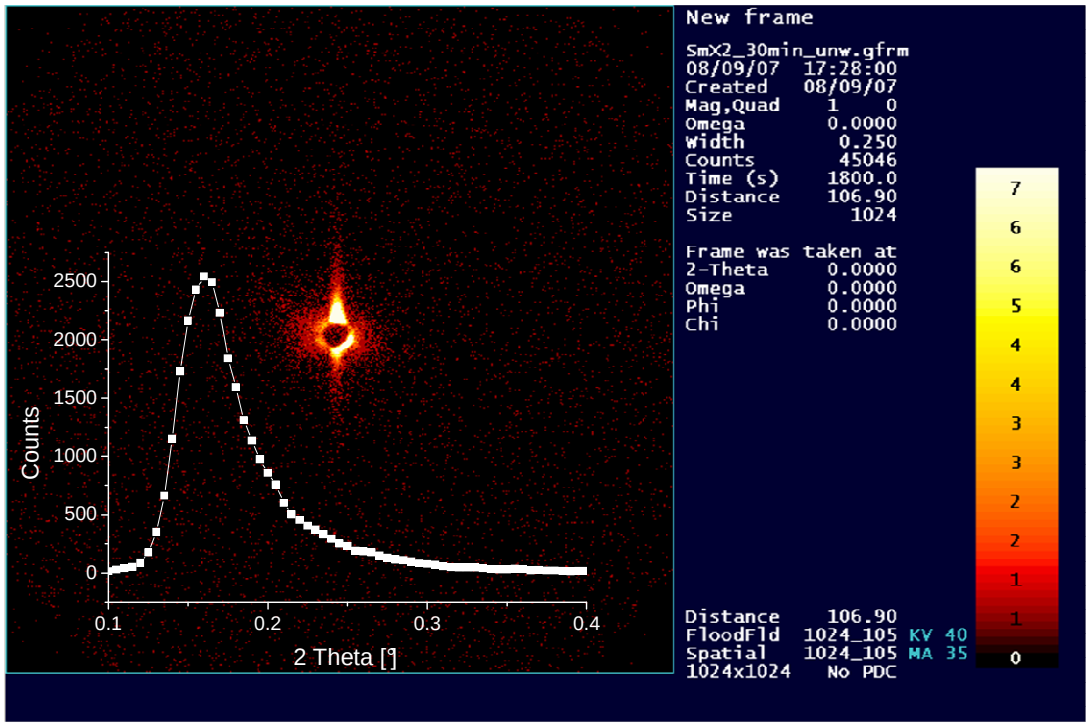

Figure C.21: Small angle X-ray scattering of the smectic phase shown in figure C.20.

The phase transition temperatures determined by optical microscopy with a heating stage could be verified by differential scanning calorimetry (DSC) to be the following: I 63℃ N 52℃ S_A 42℃ LC. Because of the rod-like structure of the TiO_2 nanorods a nematic phase was expected. A nematic phase is also compatible with the polydispersity of the TiO_2 nanorods used (56%; L_w/L_n = 1.3). In nematic phases polydisperse nanorods can still pack and a broadening of the biphasic region to the isotropic phase is expected, which arises from the distribution between short rods (isotropic phase) and long rods (nematic phase). It is, however, difficult to understand, how smectic phases can be formed, because it is difficult to orient the centers of gravity of differently sized nanorods in layered structures.[29] Just recently the formation of smectic structures from polydisperse rods has been described,[30] and

it was speculated that it might result from a segregation of nanorods according to their size. Such a segregation was observed for rigid rod LC-polymers.[31] Another explanation might be the formation of a layered structure, where each layer is formed by particles of the same length or by a transversal migration to form a tapered lamellae.[31]

Unpublished Insertion

After publication, we found another strong indication that size separation occurs. We found a region that demixed from left to right on chance, leaving the very small rods on the left and the very large ones on the right side (indicated by an arrow in figure C.22). The region is unfortunately unordered, but as this happens already in the isotropic phase, it should also happen in the liquid crystalline phase.

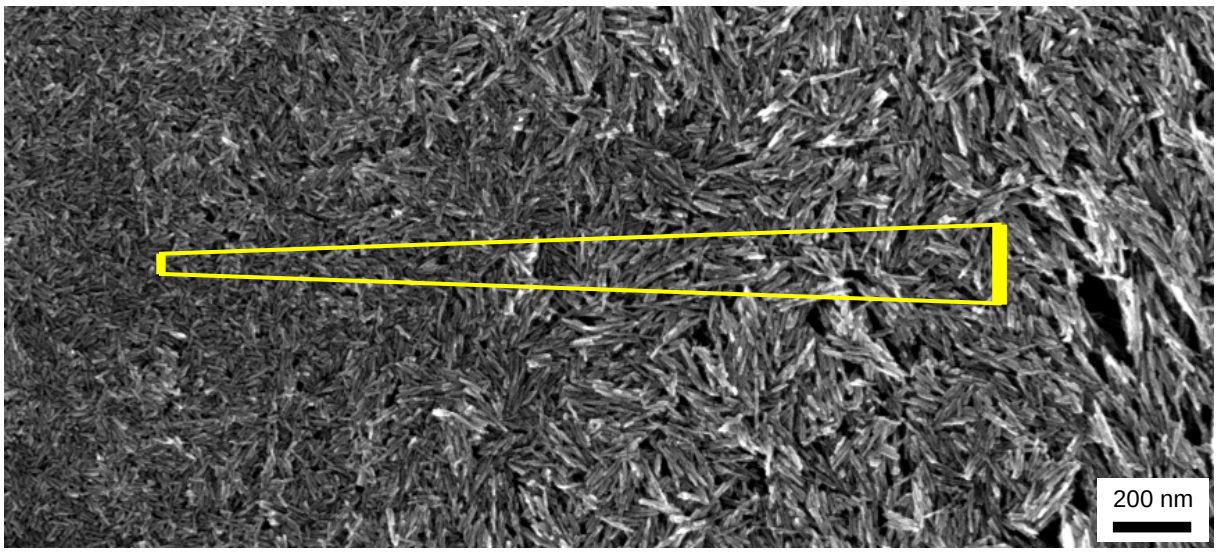

Figure C.22: SEM image of an isotropic nanorod phase showing size separation.

The nature of the inorganic mesogens enables a more detailed investigation of the ordering of the nano-rods (mesogens) within the LC-phase by electron microscopy methods. By SEM it is possible to visualize the single mesogens (fig. C.23) after evaporating the solvent of the lyotropic phase (i.e. not applicable to the thermotropic

phases in the mixtures with PEG, fig. C.20) and to investigate their orientation in the liquid crystal. These measurements do not only allow to assign the LC-phase (nematic) formed during drying, but also to study the individual order of the anisotropic nano-objects with respect to the macroscopic order parameter S of the LC-phase. Such a possibility to study both the macroscopic order parameter and the individual mesogens was -so far- only known from lyotropic phases of virus particles.[32] For comparison, crude TiO_2 nanorods are shown in Figure C.23A and, as already mentioned, their size distribution is polydisperse. After their modification with **PL1** or **PL2** the individual TiO_2 nanorods can be dissolved at low concentration, as proven by dynamic and static light scattering.

Information about packing is obtained from diluted isotropic solutions (0.2 mg polymerligand per mg nanorod; 0.2 wt% nanorods in solution) deposited onto silicon wafers. In this case the lyotropic phase is formed during the evaporation of the solvent. At the beginning the concentration of nanorods is too small for the formation of a LC phase and an isotropic phase can be found on the substrate (fig. C.23B). Later the concentration is high enough and a lyotropic phase can be seen (fig. C.23C) after complete drying. The dried lyotropic phase has a nematic ordering with the rods being oriented along the director but with no ordering of the centers of mass.

In additional we checked if it is possible to orient the lyotropic phase by pulling a substrate out of the dispersion. This is done very slow (200 nm/s) to ensure a stable meniscus at the air-dispersion boundary on the substrate. Lyotropic phases are formed in the meniscus on the substrate during evaporation of the solvent. For this experimental setup, a sufficient wetting of the substrate by the solvent is important. We used a hydrophilic silicon wafer with parallel etched line structures of about 100 µm width and a dispersion of **PL2** covered nanorods in methanol. The scanning electron microscope images are shown in Figure C.23D-F.

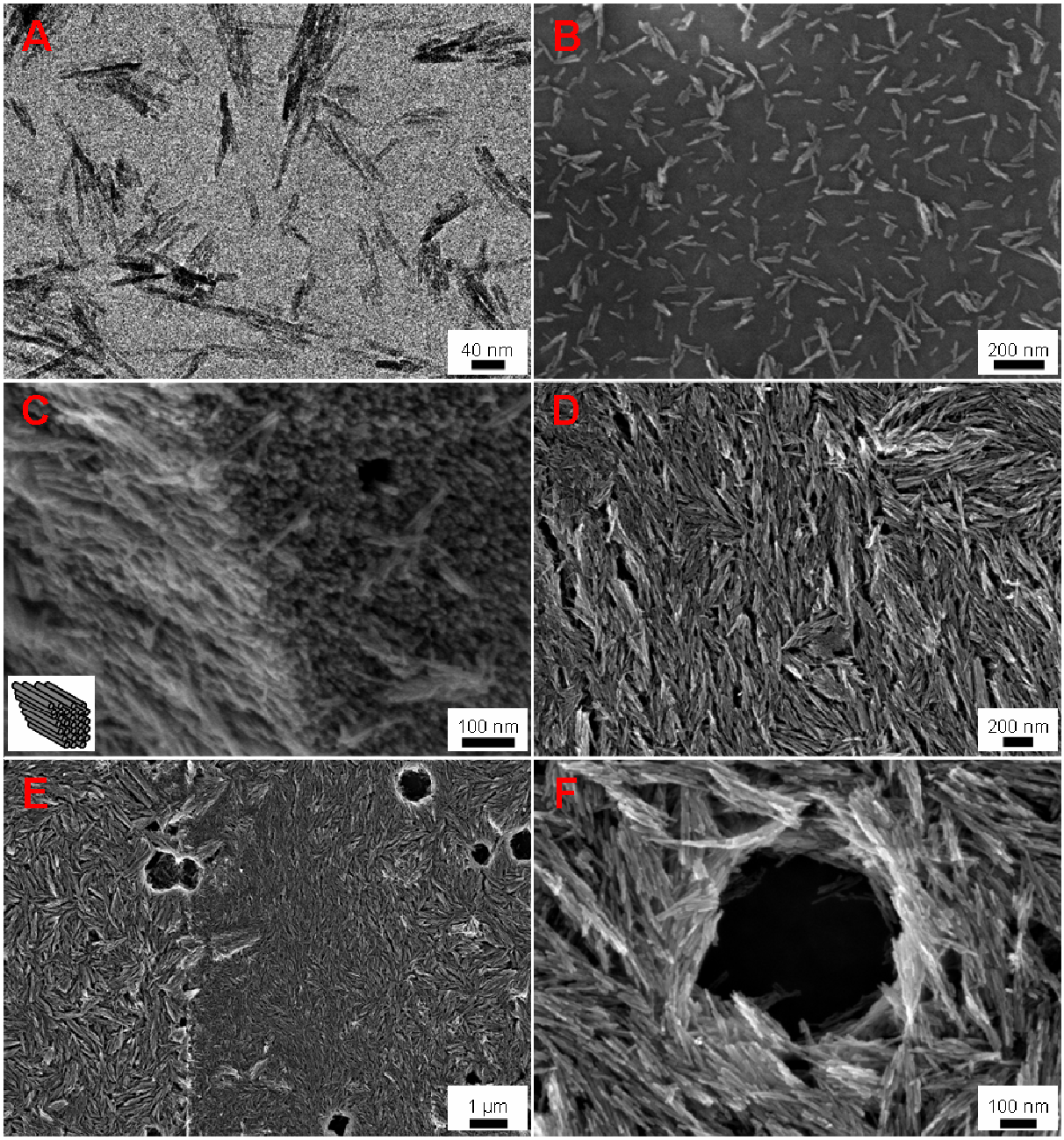

Figure C.23: **A**: TEM image of unmodified TiO_2 nanorods; SEM images: **B**,**C**: **PL1** covered nanorods from THF dispersion: isotropic phase (B) and dried LC phase (C); **D**-**F**: silicon substrate drawn out of methanol dispersions of **PL2** covered nanorods: nematic phase (D), size separated nematic phases (E), defect ordering around an air bubble (F).

The drawing direction in the images is always towards the upper side. Therefore the meniscus forces draw the nanoparticles upward and this orientation is mostly

conserved after the methanol evaporated. Figure C.23D and E show that the TiO_2 nanorods orient preferably in the drawing direction. Figure C.23E also shows a lateral demixing of nano-rods of different size to form two nematic phases in coexistence with each other. On the left side, large nanorods ordered and collapsed to bundles upon evaporation of the solvent. On the right side of Figure C.23E small nanorods were oriented with high accuracy and some air bubbles were captured within the phase. A close-up image of a defect is shown in Figure C.23F. Such a demixing can explain the formation of smectic phases from nano-rods of different size. Smectic ordering was, however, not observed for the systems under investigation.

Unpublished insertion

After submission of the manuscript, the order parameter was calculated for the image shown in figure C.23D. The angular distribution of the nanorods was measured using an image software by sizing each nanorod per hand. The order parameter was then calculated according to the equation A.1 given in the introduction. The image was tiled and the director of each tile indicated by an arrow (the length corresponds to the order parameter, the direction to the director) resulting in a vector map (see figure C.24). The order parameter over the entire area of 3600 times 2600 nm ($9.4*10^6$ nm^2) was calculated to 0.7, a value usually found for well-ordered nematic phases. As the order parameter can also be analyzed on a more local level, it is found that it fluctuates from 0.1 to 0.95. One can distinctly see the gradual changes in the director field over space reminding of some wind or water flow fields.

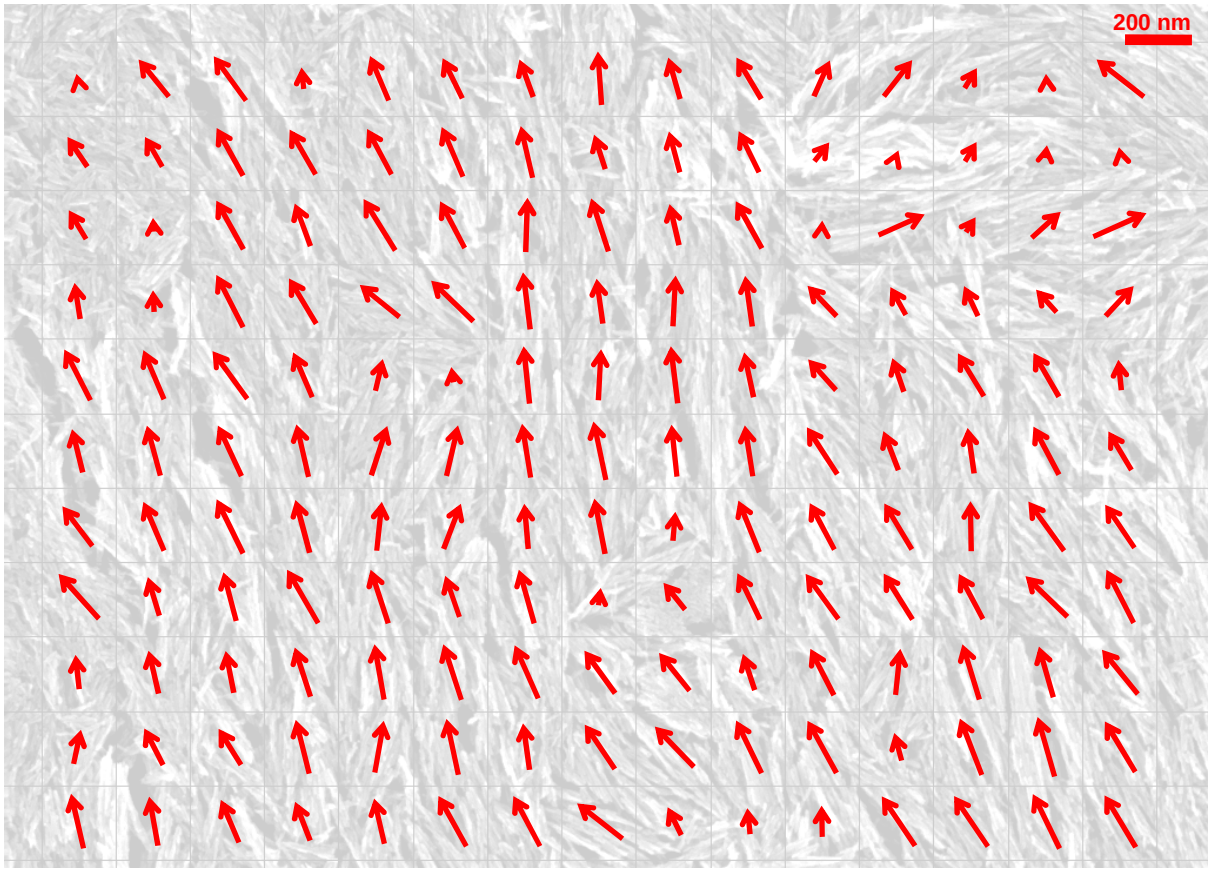

Figure C.24: Vector map of the image shown in figure C.23D. The local order parameter is indicated by the length of the arrow, the director by the direction.

These results show that the size-polydisperse TiO_2 nanorod mesogens can -in fact- phase separate as predicted by theory,[33,34,35,36] and the phase separation can be monitored by electron microscopy. The existence of smectic phases, seen by polarizing microscopy of thermotropic systems (Figure C.23C and D), cannot be rationalized from steric reasons only. One must assume another ordering force that aligns the centers of mass like an induced dipole moment. Considering such an additional interaction, theory predicts that smectic phases are more favorable than nematic phases.[37] Based on the calculations from ref. 35 and 36 we assume that a polydispersity in length favors the formation of nematic phases whereas for a polydispersity in width the smectic phase is preferred. In the present case the aspect ratio is rather stable around 5.5, i.e. the polydispersity of the particle length is always

correlated to that of the width, and therefore both theoretical concepts do not properly describe the system. We assume that attractive forces lead to the preferred formation of a smectic phase.

Conclusion

As conclusion we could show, that it is possible to modify TiO_2 nanorods with a diblock copolymer. The polymer was built up by RAFT polymerization using a macro initiator approach and possessed an anchor block and a soluble block. After functionalization it is possible to disperse the individual nanorods successfully in organic solvents to give stable dispersions. By raising the concentration of these dispersions it is possible to form anisotropic aggregates that contain nematically ordered nanorods. A nematic and a smectic phases could be observed as thermotropic phases in PEG 400 as solvent. Considering the size polydispersity of the TiO_2 nanorods it was unexpected to find smectic phases, but the effect can be explained by theoretic calculations/simulations. They predict that a size separation can occur and that smectic phases can be more favorable than nematic phases, when there is an interaction between the nanorods. In our case induced dipole moments may be the explanation for the existence of smectic phases.

Macroscopic ordering of the mesogens was accomplished by sheering and by meniscus forces. In the latter case we draw a substrate out of a nanorod dispersion and showed that meniscus forces can be used to orient the nanoparticles in the direction of the pulling force. Ordered nematic phases are obtained by that approach and a size separation of the mesogens occurred in line with the theoretical predictions.

Additional investigations are in progress to understand the size separation processes of the liquid crystal phases. Further modifications of the block-polymer

side chains will lead to interesting hybrid systems with stimuli responsive[38] or hole-conducting[39] components.

Experimental

Methyl methacrylate (from Acros) and (2-methoxy-ethoxy)-ethyl methacrylate (from Aldrich) were distilled before usage, (4-cyanopentanoic acid)-4-dithiobenzoate (RAFT reagent) and pentafluorophenole acrylate was synthesized as described in ref. 22, α,α'-azoisobutyronitrile (AIBN) (from Fluka) was recrystalized from diethyl ether, dopamine hydrochloride (3-Hydroxy tyramine hydrochloride) (from Acros) was used as purchased, dioxane and THF was dried and distilled before usage, all other solvents were used without further purification.

Gel permeation chromatography (GPC) was carried out in THF as solvent and the detector system contained refractive index (Jasco), UV-VIS (Jasco) and light scattering (Wyatt) detectors.

TiO_2 nanorods: 35 ml of concentrated nitric acid were refluxed using an oil bath at 140℃. 20 ml of a 3 M aqueous solution of $TiCl_4$ were added slowly under vigorous stirring. After a violent evolution of NOx a white precipitate formed within 2 minutes. To complete the reaction, the mixture was refluxed for 13 h and allowed to cool to room temperature. The precipitate was removed by suction filtration using a Büchner funnel and a blue ribbon filter (for ultra-fine particles). The product was washed sequentially with H_2O and ethanol to remove traces of nitric acid and finally dried for 12 h at 120℃. Characterization by X-ray powder diffraction and transmission electron microscopy showed to product to be TiO_2 nanorods (rutile polymorph) with particle lengths ranging from 50- 150 nm.

Poly(methyl methacrylate-b-dopamine acryl amide) (**PL1**): First, the macro initiator was synthesized as followed: 2g (20mmol) of methyl methacrylate, 112mg

(0.4mmol) (4-cyanopentanoic acid)-4-dithiobenzoate and 8mg ($5*10^{-5}$mol) AIBN were added in a schlenk-tube and oxygen was exchanged by nitrogen by five freeze-pump-thaw cycles. Polymerization was carried out at 90℃ for 14h. The macro initiator was purified by dissolving in THF and precipitating in methanol for three times to yield 1,25g (62%). M_n (MALDI-TOF) = 8500g/mol, PDI (MALDI-TOF) = 1.07. Second, the reactive diblock copolymer was synthesized: 0.5g ($5.9*10^{-5}$mol) of the macro initiator, 0.5g (2mmol) pentafluorophenole acrylate and 1mg ($6*10^{-6}$mol) AIBN were added to 2ml dioxane in a schlenk-tube. Oxygen was exchanged by nitrogen by five freeze-pump-thaw cycles and polymerization was carried out at 90℃ for 16h. The diblock copolymer was purified by dissolving in THF and precipitating in hexane for three times to yield 0.55g. Third, the reactive diblock copolymer was transformed to the polymerligand **PL1**: 0.55g ($4*10^{-5}$mol) reactive diblock copolymer, 0.25g (1.2mmol) dopamine hydrochloride and 0.12g (1.2mmol) triethylamine were dissolved in 2ml THF and stirred at room temperature over night. The solution was filtered to remove the triethylamine hydrochloride and precipitated in hexane to yield 0.33g (67%) **PL1**. M_n (GPC) = 14600g/mol, PDI (GPC) = 1.17. ^{1}H-NMR (300MHz, 4:1 d-acetone:d-methanol): δ[ppm]: 6.7-6.3 (m, 3H, Ph-*H*), 3.59 (s, 3H, O-C*H*$_3$), 2.2-1.7 (m, 5H, [-C*H*$_2$-C*H*R-]$_n$ and [-C*H*$_2$-CRMe-]$_n$), 1.6-0.6 (m, 3H, [-CH$_2$-CR(C*H*$_3$)-]$_n$). Block length ratio calculated by ^{1}H-NMR is 10.6:1 (methyl methacrylate:dopamine acryl amide).

Poly((2-methoxy-ethoxy)-ethyl methacrylate-b-dopamine acryl amide) (**PL2**): The procedure is the same as for **PL1**: For the first step: 2g (10.6mmol) (2-methoxy-ethoxy)-ethyl methacrylate, 0.2g ($7*10^{-4}$mol) (4-cyanopentanoic acid)-4-dithiobenzoate and 14,5mg ($9*10^{-5}$mol) AIBN polymerized at 90℃ for 5.5h. Purification by dissolving in ethyl acetate and precipitating in petrol ether (three times) to yield 1.1g (55%). M_n (GPC) = 8100g/mol, PDI (GPC) = 1.15, ^{1}H-NMR

(300MHz, $CDCl_3$): δ[ppm]: 4.4-3.2 (m, 11H, -C*H*$_2$-C*H*$_2$-O-C*H*$_2$-C*H*$_2$-O-C*H*$_3$), 2.0-1.6 (m, 2H, [-C*H*$_2$-CRMe-]$_n$), 1.3-0.7 (m, 3H, [-CH_2-CR(C*H*$_3$)-]$_n$). For the second step: 1.1g ($1.3*10^{-4}$mol) of the macro initiator, 0.58g (2.4mmol) pentafluorophenole acrylate and 1mg ($6*10^{-6}$mol) AIBN in 2ml dioxane. Polymerization at 70℃ fo r 17h. For the third step, the reactive diblock copolymer was directly reacted with 0.70g (3.7mmol) dopamine hydrochloride and 0.37mg (3.7mmol) triethylamine in 2ml THF. After filtration, the polymer solution was precipitated in petrol ether to yield 0.97g (88%) **PL2**. M_n (GPC) = 7900 g/mol, PDI (GPC) = 1.25. ^{1}H-NMR (300MHz, $CDCl_3$): δ[ppm]: 6.7-6.3 (m, 3H, Ph-*H*), 4.4-3.2 (m, 11H, -C*H*$_2$-C*H*$_2$-O-C*H*$_2$-C*H*$_2$-O-C*H*$_3$), 2.9-2.5 (m, 4H, -NH-C*H*$_2$-C*H*$_2$-Ph(OH)$_2$), 2.0-1.5 (m, 5H, [-C*H*$_2$-CRMe-]$_n$ and [-C*H*$_2$-C*H*R-]$_n$), 1.3-0.7 (m, 3H, [-CH_2-CR(C*H*$_3$)-]$_n$). Block length ratio calculated by ^{1}H-NMR is 21.1:1 ((2-methoxy-ethoxy)-ethyl methacrylate:dopamine acryl amide).

Thermo gravimetric analysis of the surface coverage: 10mg TiO_2 nanorods were dispersed together with 10mg **PL1** in 10 ml THF. The dispersion was centrifuged after one hour and the THF decanted. The dispersion was recovered with 10ml of fresh THF. This procedure was repeated three times and the TiO_2 nanorods dried in vacuum. In the thermo gravimetry the **PL1** functionalized TiO_2 nanorods were heated to 500℃ and the weight loss determined to 0 .16mg per mg **PL1** covered TiO_2 nanorods.

Acknowledgements

We would like to thank the “Fonds der chemischen Industrie” for having funded this work (stipend for S.M.) and XXXXX from the Max Planck Institute for polymer research (MPI-P, Germany, Mainz) for SEM measurements. We also thank XXXXX from the “Elektronenmikroskopie Zentrum Mainz” (EMZM, Germany, Mainz) for TEM measurements and fruitful discussions. Dynamic and static light scattering were

carried out by XXXXX from the group of XXXXX (Institut für physikalische Chemie, Universität Mainz). We would like to thank both for the measurements and discussions.

References

1 a) P. G. Bolhuis, D. A. Kofke, *Phys. Rev. E* **1996**, *54*, 634. b) P. Bartlett, P. B. Warren, *Phys. Rev Lett.* **1999**, *82*, 1979.

2 a) M. Stegemeyer, Guest Ed., *Liquid crystals*, Steinkopf, Darmstadt, Germany/ Springer, New York, USA **1994**. b) D. Demus, J. Goodby, G. W. Gray, H.-W. Spiess, V. Vill, *Handbook of liquid crystals*, Wiley-VCH, Weinheim, Germany **1998**.

3 N. Hadjichristidis, S. Pispas, *Adv. Polym. Sci.* **2006**, *200*, 37.

4 M. Ballauff, *Angew. Chem*. **1989**, *101*, 261.

5 C. Noël, P. Navard, *Progr. Polym. Sci.* **1991**, *16*, 55.

6 P. Davidson, J. C. P. Gabriel, *Curr. Opin. Colloid Interface Sci.* **2005**, *9*, 377.

7 a) P. J. Flory, *Proc. R. Soc. London Ser. A* **1956**, *254*, 73. b) P. J. Flory, G. Ronca, *Mol. Cryst. Liq. Cryst.* **1979**, *54*, 289.

8 Theory and experiments predict the following scenario depending on the concentration of the anisotropic objects[3,4]. At high dilution an isotropic solution is formed. In an ideal case it consists of the individual rod-like objects, but in reality aggregate formation is already often observed in diluted solution[9] far inside the isotropic phase. On increasing the concentration a biphasic region is reached composed of a highly concentrated solution of the nano-rods, which form the lyotropic phase and of an isotropic phase, which consists of diluted nano-objects. At significant higher concentrations the isotropic phase disappears and the system becomes a single phase again. The phase transitions (e.g. onset of the lyotropic phase) depends on the anisotropy of the nano-objects. The width of the biphasic region can be very broad for polydisperse samples. Thereby: aggregation plays an important part in any lyotropic phase from rod-like objects. It is present in two ways: (i) as a possible aggregation of individual objects in the isotropic phase; (ii) as a highly concentrated lyotropic phase in equilibrium with an isotropic phase in the biphasic region.

9 G. Petekidis, D. Vlassopoulos, G. Fytas, N. Kountourakis, *Macromolecules* **1997**, *30*, 919.

10 H. Zocher, *Z. Anorg. Allg. Chem.* **1925**, *147*, 91.

11 C. A. Brunello, C. F. O. Graeff, *Journal of Non-Crystalline Solids* **2002**, *304*, 265.

12 F. C. Bawden, N. W. Pirie, J. D: Bernal, I. Fanhucken, *Nature* **1936**, *138*, 1051.

13 J. Lee, J. Choi, J. Lee, S. K. Choi, H. D. Chun, *Nanotechnology* **2005**, *16*, 1449.

14 P. M. Sommeling, M. Späth, J. Kroon, R. Kinderman, J. van Roosmalen, *European Photovoltaic Solar Energy Conference, Proceedings of the International Conference, 16th, Glasgow, United Kingdom* **2000**, *1*, 67.

15 L. Onsager, *Ann. NY Acad. Sci* **1949**, *51*, 627.

16 H. Ringsdorf, I. Voigt-Martin, J. Wendorff, R. Wüstefeld, R. Zentel, „*Molecular Engineering of Liquid Crystalline Polymers"* in: *Chemistry and Physics of Macromolecules* (Eds: E. W. Fischer, R. C. Schulz, H. Sillescu), VCH, Weinheim, Germany **1991**, 21.

17 M. N. Tahir, N. Zink, M. Eberhardt, H. A. Therese, U. Kolb, P. Theato, W. Tremel, *Angew. Chemie* **2005**, *45*, 4809.

18 L. Li, J. Walda, L. Manna, A. P. Alivisatos, *Nano Lett.* **2002**, *2*, 557.

19 B. J. Lemaire, P. Davidson, J. Ferre´, J. Jamet, D. Petermann, P. Panine, I. Dozov, D. Stoenescu, J. Jolivet, *Faraday Discuss.* **2005**, *128*, 271.

20 D. van der Beek, H. Reich, P. van der Schoot, M. Dijkstra, T. Schilling, R. Vink, M. Schmidt, R. van Roij, H. N. W. Lekkerkerker, *Phys. Rev Lett.* **2006**, *97*, 087801.

21 M. P. B. van Bruggen, F. M. van der Kooij, H. N. W. Lekkerkerker, *J. Phys.: Condens. Matter* **1996**, *8*, 9451.

22 M. Eberhardt, P. Theato, *Macromol. Rapid Commun.* **2005**, *26*, 1488.

23 M. W. Matsen, F. S. Bates, *Macromolecules* **1996**, *29*, 1091.

24 G. Jander, E. Blasius, Lehrbuch der analytischen und präparativen anorganischen Chemie, Hirzel, Stuttgart **1970**.

25 G. Ebner, D. Schelz, *Textilfärberei und Farbstoffe*, Springer, Berlin, **1988**.

26 P. Z. Araujo, P. J. Morando, M. A. Blesa, *Langmuir* **2005**, *21*, 3470.

27 T. Rajh, L. X. Chen, K. Lukas, T. Liu, M. C. Thurnauer, D. M. Tiede, *J. Phys. Chem. B* **2002**, *106*, 10543.

28 H. Ito, T. P. Russell, G. D. Wignall, *Macromolecules* **1987**, *20*, 2213.

29 M. A. Bates, D. Frenkel, *J. Chem. Phys.* **1998**, *109*, 6193.

30 G. J. Vroege, D. M. E. Thies-Weesie, A. V. Petukhov, B. J. Lemaire, P. Davidson, *Adv. Mat.* **2006**, *18*, 2565.

31 a) H. Witteler, G. Lieser, G. Wegner, M. Schulze, *Makromol. Chem. Rapid Commun.* **1993**, *14*, 471. b) W. Wang, G. Lieser, G. Wegner, *Macromolecules* **1994**, *27*, 1027.

32 A. Nedoluzhko, T. Douglas, *Journal of Inorganic Biochemistry* **2001**, *84*, 233.

33 P. J. Flory, A. Abe, *Macromolecules* **1978**, *11*, 1119.

34 R. van Roij, B. Mulder, *Phys. Rev. E* **1996**, *54*, 6430

35 A. Speranza, P. Sollich, *J. Chem. Phys.* **2002**, *117*, 5421

36 S. Varga, K. Purdy, A. Galindo, S. Fraden, G. Jackson, *Phys. Rev. E* **2005**, *72*, 051704.

37 P. G. Bolhuis, A. Stroobants, D. Frenkel, H. N. W. Lekkerkerker, *J. Chem. Phys.* **1997**, *107*, 1551.

38 a) N. Metz, P. Theato, *Polymer Preprints* **2006**, *47*, 716. b) P. Theato, R. Zentel, *J. Coll. & Interface Sci* **2003**, *268*, 278.

39 M. Behl, R. Zentel, *Macromolecular Chemistry and Physics* **2004**, *205*, 1633.

C.3 Polymer Functionalized Carbon Nanotubes

The functionalization techniques used for carbon nanorods are multifarious. The simplest approach uses strong oxidizing acids which partially oxidize the CNT surface to carboxylic acids. Thus treated CNTs are water soluble and electrostatic repulsion of the tubes leads to the desired disentanglement. The price is a highly undefined surface leading to unpredictable electronic properties, as sp^3 centers are created in the charge carrying outer tube. These carboxylic units can also be addressed by normal organic chemistry leading to various shells. A more gentle approach uses the adsorption of molecules or polymers on the surface. This can be done with various groups: charged surfactants like sodium dodecylsulfate, polyelectrolytes as DNA, polymer that wrap around the CNTs as poly(4-vinylpyridine), non-wrapping adsorption with partially collapsed block copolymers like block copolymers from ethylene oxide and propylene oxide and complexation by π-π interactions like pyrene units. Large aromatic systems like pyrene are electronically very similar to graphite as pyrene can be seen as cut piece from a graphite sheet.

This chapter focuses mainly on pyrene functionalized polymers as they combine a mild and electronically non-destructive CNT functionalization with a steric stabilization by a polymer corona. These systems are then – depending on the polymer used – soluble in organic as well as aqueous solvents. In general detergents have been found to be rather effective for dispersing CNTs in water. However, this does not open the possibility to incorporate CNTs into polymer films as demonstrated in the last part of this chapter.

Pyrene does not interfere with radical reactions and can therefore be used for both approaches presented in figure C.3: an alpha pyrene functionalized polymer as well as pyrene anchor block copolymers.

C.3.1 Impact of Polymer Architecture on the Adsorption Behavior

As mentioned before, both alpha pyrene functionalized as well as pyrene containing block copolymers are accessible. The alpha functionalized systems require the synthesis of a pyrene functionalized RAFT agent as shown in figure C.3, but allow a very easy way to various alpha pyrene functionalized polymers. Especially the effects of the soluble block length can be investigated rather easy, as suitable polymers can be produced by just changing the RAFT agent to monomer feed ratio. The impact on adsorption stability can be investigated and, as expected, the adsorption drops rather fast with increasing soluble block length. On the other hand, the system offers the advantage of having exactly the same anchor when comparing different soluble blocks.

The synthesis of pyrene containing diblock copolymers can be done according to the second approach of figure C.3. First, a soluble block is synthesized by RAFT polymerization. Second, a reactive ester monomer is polymerized upon that macro-RAFT agent. The block length of the second block has been varied in this case to investigate the impact of anchor block length for a given soluble block (see figure C.2). The reactive ester diblock copolymers are then reacted with amine functionalized pyrene derivatives to form the pyrene diblock copolymer. We varied the pyrene component by varying the spacer length between pyrene moiety and amine to investigate the impact of pyrene mobility when attached to the polymer backbone. The anchor block length was varied from 5 to 20 repeat units and methyl and butyl spaced pyrene units were used to investigate the impact of anchor mobility. For comparison, also a block copolymer poly(methyl methacrylate-*block*-4-vinyl pyridine) was synthesized, as pyridine is also known to bind well on CNTs.

The polymers were then dissolved and CNTs added. The CNTs were then washed from unbound polymers and analyzed by thermo gravimetry (TGA) to

determine the amount of bound polymer (CNTs are thermally stable up to 800 °C). For the block copolymers depending on the spacer length 13 (methyl spaced) or 20 units (butyl spaced) were found to be optimal for the adsorption. When comparing the different polymers one can say that anchor block copolymers are more efficient than alpha functionalized polymers and that for block copolymers longer spacers enhance the adsorption. The spacer length is critical for a decoupling of the pyrene unit from the backbone, as the pyrene units bind parallel to the CNT surface whereas the backbone is also parallel. Thus, the pyrene units have to twist parallel to the backbone which is easier for longer spacers.

A very efficient butyl spaced pyrene diblock copolymer was then chosen to investigate optimal conditions for the formation of CNT dispersions in THF. We varied the CNT concentrations from 20 to 0.4 mg/ml and polymer concentrations from 11 to 0.1 mg/ml and always found black dispersion after ultrasound treatment. The dispersions were centrifuged afterwards to reveal the amount of undispersed material and we found no precipitate. Stable dispersions without precipitate after centrifugation were found for CNT concentrations smaller than 2.5 mg/ml and polymer feed concentrations between 0.1 and 2.4 mg/ml. Within that concentration window, the dispersions prepared with less polymer than 1.5 mg/ml are only stable up to a CNT concentration of 1.3 mg/ml. The reasons for instability are adsorption / desorption equilibria on one side and depletion phenomena on the other side. The first effect can be removed by raising the polymer concentration, pushing the equilibrium to the adsorbed state, but this enhances depletion (This effect is known from theoretical considerations for mixtures of rods (CNTs) and spheres (polymer coils). In a very simple, purely entropic model the spheres entropically mediate an effective attraction between the rods. See next chapter.). Thus, stable dispersions are only found up to a polymer concentration of 2.4 mg/ml.

C.3.1.1 Publication for Macromolecules, in preparation

Pyrene containing polymers for the functionalization of carbon nanotubes

S. Meuer, L. Braun, R. Zentel

Abstract

Pyrene containing diblock copolymers based on polymethyl methacrylate were synthesized and investigated regarding their adsorption on carbon nanotubes (CNT). The pyrene units were introduced using a reactive ester monomer for the build up of the second block which was afterwards reacted polymer analogously with amine functionalized pyrene derivatives. As we started from the same reactive ester intermediate, full block length identity is given. We varied the length of the anchor block to find an optimal block length and used pyren-1-yl-methylamine as well as 4-pyren-1-yl-butylamine as anchor units. For both anchor units a maximal adsorption was found for 13 respective 20 anchor units. The absolute adsorption was best for the 4-pyren-1-yl-butylamine anchor units as the longer spacer enhances the mobility of the anchor unit. The phase diagram of CNTs and diblock copolymer in terms of dispersion stability was investigated and a stable dispersion of 2.5 mg/ml CNTs in THF was found.

Introduction

Carbon nanotubes (CNTs) have mechanical, electrical, thermal and optical properties that make them highly interesting for applications in materials science.[1,2] “Raw”

nanotubes, however, are usually produced in the form of a disordered powder, in which the individual CNTs are highly entangled. In order to use them in technical applications, it is thus necessary to disperse them in a solvent. Once they are dispersed, they can be mixed with other substances to form composites, incorporated into fibers or deposited as a film on a substrate. Dispersing nanotubes is, however, not easy, as they strongly attract each other via van der Waals-forces. A variety of methods for chemical functionalization as well as physical methods have been used to disperse carbon nanotubes. The different strategies include chemical modification,[3,4] covalent attachment of monomers, oligomers and polymers,[5] adsorption of charged surfactants and polyelectrolytes,[6,7] wrapping with polymers,[8-11] non-wrapping adsorption of partially collapsed block copolymers[12] and complexation by π-π interactions.[13-15] A major drawback of the chemically functionalized and covalently modified CNTs is the change in their electronic structure by creating sp^3 centers (needed for both methods).[3-5] Detergents have been found to be rather effective for dispersing CNTs in water.[16-18] However this does not open the possibility to incorporate CNTs into polymer films.

Large aromatic systems like pyrene are electronically very similar to graphite as pyrene can be seen as cut piece from a graphite sheet. In these systems the interaction between two CNTs or different layers of a multi walled carbon nanotube (MWCNT) and between pyrene and CNT is quite similar. Various polymers with pyrene anchor units have been investigated by Jérôme et al.[19] and Andronov et al.[20] concerning their potential to disperse carbon nanotubes in organic solvents. Andronov et al. compared block copolymers and random copolymers and found that block copolymers are more efficient in dispersing CNTs.

In order to investigate this phenomenon we synthesized block copolymers with pyrene anchor units and a polymethyl methacrylate (PMMA) block as the soluble

block. By using a reactive ester monomer as intermediate for the second block, we can directly compare different anchoring systems with exactly the same block lengths and distributions. This very variable concept is based on a polymer analogous reaction of the corresponding amine functionalized anchor unit with the reactive ester moieties. We varied the length of the anchor block from one (α-pyrene functionalized PMMA[21]) up to 20 units and varied the spacer between polymer backbone and anchor unit. In addition we synthesized a poly(methyl methacrylate-*block*-4-vinyl pyridine) block copolymer to investigate the performance for pyridine anchor units.

Synthesis

We synthesized four different systems by the RAFT polymerization process: The first class are α-pyrene functionalized PMMA polymers (**pyrene-PMMA**), the second are block copolymers of poly(methyl methacrylate-*block*-pyren-1-yl-methyl methacrylamide) (**P(MMA-b-C1 pyrene)**), the third are block copolymers of poly(methyl methacrylate-*block*-4-pyren-1-yl-butyl methacrylamide) (**P(MMA-b-C4 pyrene)**) and the last are poly(methyl methacrylate-*block*-4-vinyl pyridine) (**P(MMA-b-4VP)**) block copolymers (see fig. C.25).

Pyrene-PMMA polymers were synthesized as already described in our former publication[21] and we included this data for comparison to the pyrene containing block copolymers. The block copolymers **P(MMA-b-C1 pyrene)** and **P(MMA-b-C4 pyrene)** were synthesized as follows: First methyl methacrylate was polymerized under RAFT conditions with (4-cyano-pentanoic acid)-4-dithiobenzoate (chain transfer agent (CTA)).[22] The resulting macromolecular chain transfer agent (macro-CTA) was purified, analyzed and reactivated in the presence of pentafluoro-phenyl methacrylate (PFPMA), a reactive ester monomer.

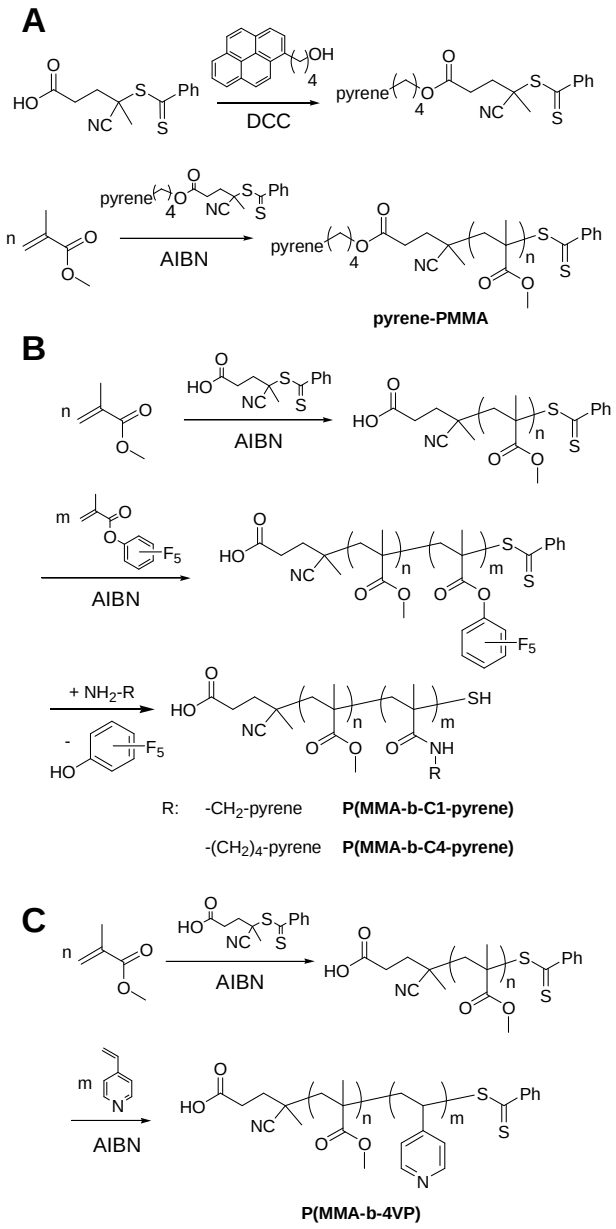

Fig. C.25: Synthesis of A: **pyrene-PMMA**, B: **P(MMA-b-C1 pyrene)** and **P(MMA-b-C4 pyrene)**, C: **P(MMA-b-4VP)**.

This monomer can be polymerized without loosing the reactive ester moiety and reacts quantitatively with primary amines.[23] After polymerization and purification, the polymer analogous reaction was carried out with pyren-1-yl-methyl amine or 4-pyren-1-yl-butyl amine to give **P(MMA-b-C1 pyrene)** or **P(MMA-b-C4 pyrene)**. The length of the anchor unit block was controlled by the amount of reactive ester monomer added to form the diblock copolymer. The last block copolymer **P(MMA-b-4VP)** was

synthesized following the same approach as before but instead of a reactive ester monomer, 4-vinyl pyridine was polymerized as second monomer. The molecular weights and polydispersities of the block copolymers as well as the block lengths can be found in table C.7.

Table C.7: Analysis of the block copolymers.

Name	MMA units[a]	feed 2nd monomer	anchor units	M_n /g mol^{-1} [a]	M_w /g mol^{-1} [a]	PDI[a]
pyrene-PMMA 90	90	-	1[b]	8,900	10,500	1.18
pyrene-PMMA 180	180	-	1[b]	18,100	23,700	1.31
pyrene-PMMA 270	270	-	1[b]	27,200	36,700	1.35
P(MMA-b-C1 pyrene) 20	140	20	4[c]	15,300	16,400	1.07
P(MMA-b-C1 pyrene) 40	140	40	13[c]	18,400	19,900	1.08
P(MMA-b-C1 pyrene) 60	140	60	18[c]	20,100	21,500	1.07
P(MMA-b-C4 pyrene) 20	140	20	5[c]	15,700	17,600	1.12
P(MMA-b-C4 pyrene) 40	140	40	16[c]	19,400	22,500	1.16
P(MMA-b-C4 pyrene) 60	140	60	20[c]	20,800	28,300	1.36
P(MMA-b-4VP)	170	100	37[c]	26,400	30,200	1.15

a: determined by GPC in THF, b: by design of the RAFT agent, c: determined by ^{1}H-NMR after polymer analogous reaction

The resulting polymers were analyzed on all steps by gel permeation chromatography (GPC) in THF as solvent. A set of elugrams is show in figure C.26: The GPC curves of the macro-CTA PMMA 140, the intermediate P(MMA-b-PFPMA) X and the resulting **P(MMA-b-C4 pyrene) X** polymers are overlaid. The elution volume of a polymer is a function of molecular weight and smaller elution volumes correspond to larger molecular weights. The macro-CTA shows the largest elution volume / smallest molecular weight as one would expect it. The reactive ester diblock copolymers have an increased molecular weight due to the second block (open symbols) and the final polymers **P(MMA-b-C4 pyrene) X** (full symbols) elute at even smaller volumes. This is due to the polymer analogous reaction that replaces the pentafluoro phenyl ester versus a 4-pyren-1-yl-butyl amide, resulting in an increase in molecular weight of roughly 90 g/mol per repeat unit. ^{1}H-NMR analysis was used to

measure the final length of the anchor blocks and similar lengths were found for both **P(MMA-b-C1-pyrene)** and **P(MMA-b-C4-pyrene)** polymers as they were made from the same intermediate reactive ester polymers.

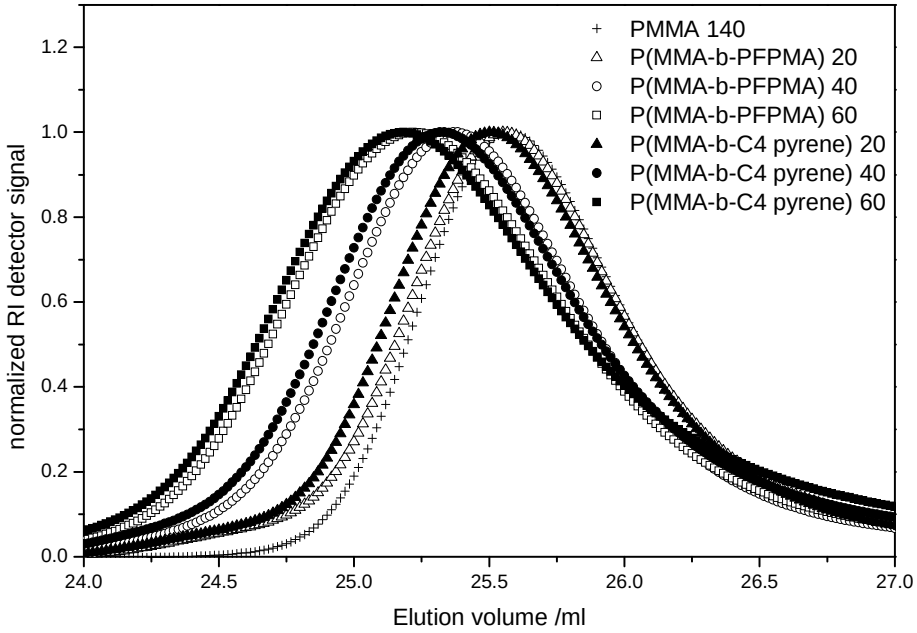

Fig. C.26: GPC elugrams of the macro-CTA PMMA 140, the intermediate reactive ester diblock copolymers P(MMA-b-PFPMA) X and final diblock copolymers **P(MMA-b-C4 pyrene) X**.

CNT Functionalization

The CNTs were kindly donated by Bayer Material Science (Multi walled carbon nanotubes, Baytubes C 150 P) and were on average 14.5 nm wide and 1 to 10 mm long and were used as received. In order to investigate the amount of adsorbed polymer chains, the pristine CNTs (10 mg) were added to a polymer solution in THF (2 mg in 2 ml) and stirred over night. The CNTs were separated by centrifugation and redispersed in fresh THF to remove unbound polymer chains. The procedure was repeated three times. The CNTs were then dried and investigated by thermo

gravimetry (TGA, under nitrogen atmosphere, see Fig. C.27). The polymers decompose between 300–450 °C and the weight loss is measured. Out of this mass, the number of chains that adsorbed per CNT can be calculated (see Table C.8). For the calculations we assumed an average surface per CNT of around 2.3 10^5 nm^2 (assuming an average length of 5 µm and width of 14.5 nm). The number of CNTs is estimated to be 8.6 10^{11} mg^{-1} (assuming a density of 1400 kg m^{-3} and a volume of 8.3 10^5 nm^3 per CNT). The interpolymer distance ***s*** between adsorbed polymers can be calculated as the square root of the surface area per polymer chain.[24]

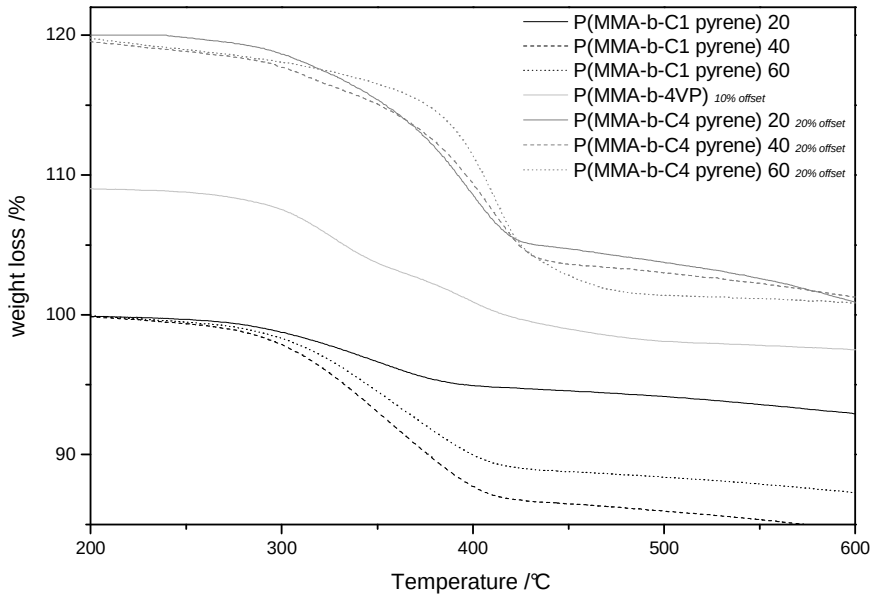

Fig. C.27: TGA analysis of the diblock copolymers **P(MMA-b-C1 pyrene) X**, **P(MMA-b-4VP)** (10% offset) and **P(MMA-b-C4 pyrene) X** (20% offset).

The TGA plots of the different polymers show the differences in adsorption. The largest weight loss is found for the **P(MMA-b-C4 pyrene) X** followed by the **P(MMA-b-4VP)** and the **P(MMA-b-C1 pyrene) X** polymer covered CNTs. The results for the pyrene-PMMA polymers (published in lit. 21) are in the range of the **P(MMA-b-C1**

pyrene) X polymers. The weight loss corresponds to numbers of adsorbed chains per CNT and inter polymer distances reported in table C.8.

Table C.8: Adsorption behavior of the diblock copolymers.

Name	MMA units[a]	anchor units	Weight loss /%[d]	chains / CNT[d]	s /nm[d]
pyrene-PMMA 90	90	1[b]	3.8	3,000	8.5
pyrene-PMMA 180	180	1[b]	4.1	1,550	12
pyrene-PMMA 270	270	1[b]	1.8	500	22
P(MMA-b-C1 pyrene) 20	140	4[c]	3.9	1,900	11
P(MMA-b-C1 pyrene) 40	140	13	10.9	4,600	7
P(MMA-b-C1 pyrene) 60	140	18	10.2	4,000	7.5
P(MMA-b-C4 pyrene) 20	140	5[c]	11.4	5,700	6.5
P(MMA-b-C4 pyrene) 40	140	16[c]	15.9	6,700	6
P(MMA-b-C4 pyrene) 60	140	20[c]	19.0	7,800	5.5
P(MMA-b-4VP)	170	37[c]	8.4	2,400	10

a: determined by GPC in THF, b: by design of the RAFT agent, c: determined by ^{1}H-NMR, d: calculated from the TGA analysis results.

The results show three trends. First of all, when looking on the results of the **pyrene-PMMA** polymers, the length of the soluble block play an important role on the adsorption and the adsorption got best for the shortest soluble block. The second trend is that for both block copolymer sets **P(MMA-b-C4 pyrene) X** and **P(MMA-b-C1 pyrene) X** the amount of adsorbed polymer increases with increasing anchor block length and reaches a maximum in the case of **P(MMA-b-C4 pyrene) 60**. And the third trend is that enlarging the spacing of the pyrene from the polymer backbone enhances the adsorption by a factor of 1.5 to 3.

The first trend can be explained by the following arguments: The larger the soluble block gets, the smaller is usually the available grafting density, as functionalization is done with polymer coils coming from solution. The coil radius limits the access to the surface and reduces the grafting density respective the number of chains bound to a single CNT. On the other hand, desorption phenomenon are more likely to happen for longer soluble blocks, as the binding

energy of a single anchor unit can be overruled by the entropy win of a free polymer chain in solution.

Secondly using an anchor block enables a multidentate binding of the anchor groups which can increase the binding especially for short anchor blocks as their entropy loss to fit the surface requirements as a result of the deformation of a three dimensional polymer coil is not too strong. For rather long anchor blocks the penalty in entropy will dominate this behavior and corresponds to the observations made by Andronov et al. that increasing the block length decreased the adsorption.[20] Thus our observations that the adsorption increases in our series of short C4 spaced anchor blocks (from 5 to 20) and reaches a plateau in our C1 spaced series is understandable.

The difference between C1 and the C4 spaced series is also related to the entropy cost to place the pyrene units with respect to the CNT surface. The short spacer forces the anchor block to an elongated conformation as the steric demand of the anchor unit cannot fulfilled otherwise. With increasing amount of anchor units, the block gets more anisotropic leading to an inefficient coverage of the CNT surface. This explains both the smaller overall adsorption and the difference in the block length dependence.

These arguments might also be the explanation for the relatively small adsorption of the **P(MMA-b-4VP)** block copolymer. Despite the fact, that pyridine might be different in efficiency for binding to CNTs, the pyridine anchor unit is very strongly bound to the backbone. The observed adsorption is weaker as the butyl spaced pyrene system even though the anchor block is longer.

CNT dispersions in THF

As the **P(MMA-b-C4 pyrene) X** polymers showed the best adsorption, we tested the performance of **P(MMA-b-C4 pyrene) 40** for the dispersion of the CNTs in tetrahydro furan (THF). Therefore we prepared samples with various concentrations of CNTs and **P(MMA-b-C4 pyrene) 40** in THF and sonified them with a tip ultrasound generator (10 W for 15 minutes, see figure C.28). The resulting dispersions were all totally black in the experimental window of CNT concentrations from 20 to 0.4 mg/ml and polymer concentrations from 11 to 0.1 mg/ml and no direct precipitation occurred. Only after centrifugation precipitation was found for some samples (grey triangles), while other dispersions (block squares) remained homogeneous afterwards. The precipitate free stable dispersion with highest CNT content was found for concentrations of CNTs of 2.5 mg/ml and of **P(MMA-b-C4 pyrene) 40** of 2.3 mg/ml. This is very different from our former investigations on **pyrene-PMMA** stabilized CNT dispersions where the polymers are bound only via a single anchor group. In that case either black and stable or totally clear and precipitated dispersions were found in a comparable small window depending on the concentrations.[25]

The stable dispersions without precipitate after centrifugation are found for CNT concentrations smaller than 2.5 mg/ml and polymer feed concentrations smaller than 2.4 mg/ml. Within that concentration window, the dispersions prepared with less polymer than 1.5 mg/ml are only stable up to a CNT concentration of 1.3 mg/ml. The phase diagram shows that increasing the polymer concentration increases the solubility of the CNTs as precipitate formation upon centrifugation is prohibited. We believe that increasing the polymer concentration is accompanied by an increased adsorption on the CNT surface leading to increased dispersion stability.

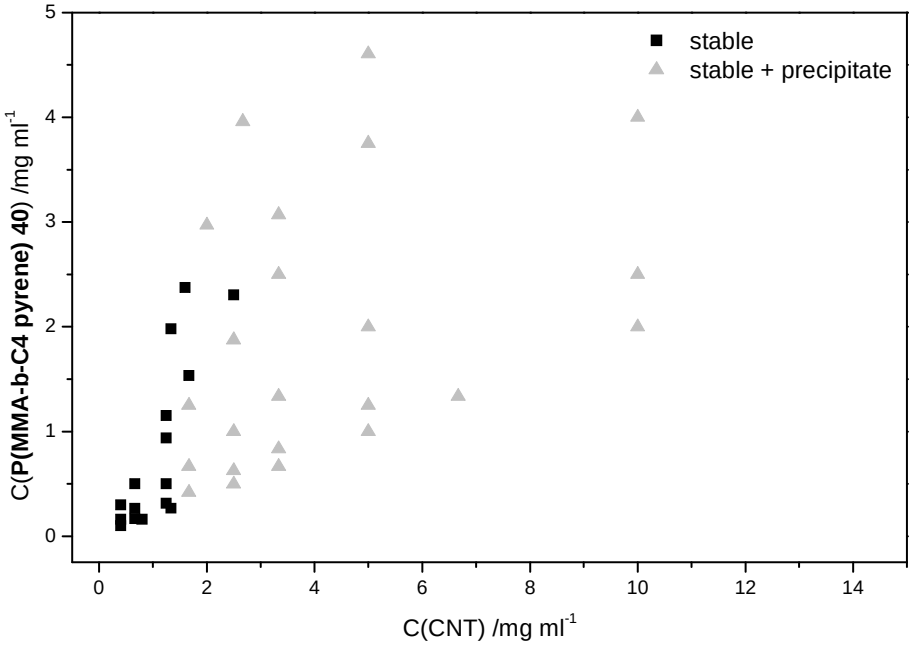

Fig. C.28: Phase diagram of **P(MMA-b-C4 pyrene) 40** stabilized CNTs in THF.

This is only true up to a polymer concentration of 2.4 mg/ml. Adding more polymer results in depletion: This effect is known from theoretical considerations for mixtures of rods (CNTs) and spheres (polymer coils). In a very simple, purely entropic model that is based on the Asakura-Oosawa model,[26] the spheres entropically mediate an effective attraction between the rods. This effect plays a very important role in all polymer stabilized colloidal systems and was also investigated for CNT dispersions.[27] The quintessence of this phenomenon is that adding more stabilizing polymer than needed is counterproductive and results in poor or even unstable dispersions. (For recent results on the phase behavior of such mixtures see e.g. Ref. 28). In contrast to our former publication of **pyrene-PMMA** stabilized polymers[25] none of the dispersion prepared were totally unstable.

Solubilities known from literature on polymer stabilized CNTs in organic solvents are as high as 0.65 mg/l and as low as 0.005 mg/l.[19,20] The solubility of these polymer

stabilized dispersions was so far achieved with ratios of polymer to CNTs around 1-2.[19,20] We were able to achieve a solubility of 2.5 mg/l with a functionalization ratio less than 1 (2.3 mg **P(MMA-b-C4 pyrene) 40** were sufficient to stabilize 2.5 mg CNTs). For comparison, literature known solubilities of surfactant stabilized CNTs in water reached solubilities of 20 mg/ml[16-18] with functionalization ratios of surfactant to CNT of 10. But theses systems are unfortunately useless for the incorporation of CNTs into polymer films as the surfactant stabilized CNTs can only be dispersed efficiently in water and as surfactants cannot mediate well to a polymer matrix.

Conclusion

We showed that the molecular design of pyrene containing polymers is very important to tune the performance of the polymers. The amount of pyrene units present per polymer chain was varied from 1 to 20 and found a maximal binding to the CNT for 13 or 20 pyrene units depending on the spacer length to the polymer backbone. This experimentally found length seems to be the optimum between two opposing effects: increasing the anchor block length starting from a single anchor unit enhances the binding to the surface, but increasing it too much leads to reduction of the grafting density and thus dispersion stability. The dispersion diagram of a pyrene containing diblock copolymers showed also two opposing effects: first increasing the polymer concentration starting from low polymer concentration enhances the CNT dispersion stability but secondly, depletion sets in for larger polymer concentrations. Thus it is not possible to work with a large excess of stabilizing polymer as it is usually used for surfactant stabilized dispersions (functionalization ratios of surfactant to CNT of 10 : 1 by weight).[16-18]

Pyrene functionalized polymers were shown to be effective for the stabilization of CNTs in organic solvents. Although polymers are not yet that efficient to disperse

CNTs as surfactant are, they offer the possibility to disperse CNTs not only in water, but also in organic media. This media includes pure organic solvents but also polymeric matrices and enables the use of polymer functionalized CNTs as fillers for polymer films. This is highly desirable as predicted mechanical and electrical properties should drive the performance of CNT reinforced polymers significantly.

Experimental

The CNTs were kindly donated by Bayer Material Science (Baytubes C 150 P) and used as received. All solvents were dried and distilled before use. Methyl methacrylate (from Acros) was distilled before usage, αα'-azoisobutyronitrile (AIBN, from Fluka) was recrystalized from diethyl ether, 1-pyrenemethylamine hydrochloride and 1-pyrenebutyric acid was used as received from Aldrich, dioxane and tetrahydro furan (THF) were dried and distilled before usage, all other solvents were used without further purification. Gel permeation chromatography (GPC) was carried out in THF as solvent and the detector system contained refractive index (Jasco RI 1570), UV-Vis (Jasco UV 1575) and light scattering (Wyatt miniDAWN) detectors. Thermo gravimetry (TGA) was carried out in a Perkin Elmer Pyris 6 TGA under nitrogen atmosphere and analyzed by the Pyris software.

Synthesis of 4-pyren-1-yl-butylamine: 1 g (3.47 mmol) of 1-pyrenebutyric acid was dispersed in 10ml dichloromethane and a drop of dimethyl formamide was added. 1.82 ml (3.64 mmol) were dissolved in dichloromethane (2M solution) and added slowly to the dispersion under gas evolution. The mixture was then refluxed for 20 minutes. The acid chloride was reacted with dry ammonia bubbling through the reaction mixture. The reaction mixture was added to 200 ml ethyl acetate and the ammonia hydrochloride extracted with water twice. The organic phase was dried with $MgSO_4$ and the solvent evaporated. 600 mg (2.11 mmol) 1-pyrenebutyric amide were

collected (61% yield). This intermediate was dissolved in diethyl ether and added slowly to a suspension of 88 mg (2.33 mmol) $LiAlH_4$ in diethyl ether. After complete addition the mixture was refluxed for 1 hour. Residual hydride was carefully destroyed by the controlled addition of water and the organic phase extracted with dichloromethane twice. The 1-pyrenebutylamine was reacted to the hydrochloride by the addition of HCl gas and collected by filtration. The 1-pyrenebutylamine hydrochloride (400 mg, 1.3 mmol, 62% yield) was a light brown solid. δ_H(100 MHz; d-DMSO): 8.4 – 7.8 (9H. m. pyrene-H), 3.35 (2H, t, pyrene-C*H*$_2$-), 2.81 (2H, sextet, NH_3^+-C*H*$_2$-), 1.83 (2H, quintet, -C*H*$_2$-CH_2-), 1.69 (2H, quintet, -C*H*$_2$-CH_2-).

Synthesis of ***P(MMA-b-C1 pyrene) X*** *and* ***P(MMA-b-C4 pyrene) X****:* For the first block, 4 g (0.04 mol) methyl methacrylate, 84 mg ($2.3*10^{-4}$ mol) RAFT agent (4-cyano-4-methyl-4-thiobenzoylsulfanyl-butyric acid, synthesized according to lit. 22) and 6.2 mg ($3.78*10^{-5}$ mol) AIBN (αα'-azoisobutyronitrile) were dissolved in 6 ml dioxane. Oxygen was exchanged by nitrogen by five freeze-pump-thaw cycles. Polymerization was carried out at 70°C for 21 h. The polymer was purified by dissolving in THF and precipitating in hexane for three times. 2.76 g of rose polymer was collected (69% yield). M_n(GPC) = 13980 g/mol, PDI = 1.15. δ_H(100 MHz; $CDCl_3$; Me_4Si) 3.54 (3H. s. O-CH_3), 1.84 (2H, m, CH_2), 0.96 (1H, s, CH), 0.80 (3H, m, CH_3).

For the second block, 500 mg ($3.58*10^{-5}$ mol) of the polymer 1 mg ($5.4*10^{-6}$ mol) AIBN and pentafluoro-phenyl methacrylate (synthesized according to lit. 23): 182 mg ($7.25*10^{-4}$ mol) for P(MMA-b-PFPMA) 20, 364 mg ($1.44*10^{-3}$ mol) for P(MMA-b-PFPMA) 40 and 542 mg ($2.15*10^{-3}$ mol) for P(MMA-b-PFPMA) 60 were dissolved in 4 ml dioxane. Oxygen was exchanged by nitrogen by five freeze-pump-thaw cycles. Polymerization was carried out at 70°C for 40 h. The polymers were purified by dissolving in THF and precipitating in petrol ether for three times. 456 mg

of P(MMA-b-PFPMA) 20, 554 mg of P(MMA-b-PFPMA) 40 and 690 mg of P(MMA-b-PFPMA) 60 was collected.

For the polymer analogous reaction, 50 mg of the corresponding P(MMA-b-PFPMA) X was reacted with 2-fold excess (to the pentfluoro-phenyl ester) of 1-pyrenemethylamine hydrochloride or 1-pyrenebutylamine hydrochloride and 3-fold excess of triethylamine in 2ml of THF. The reaction was carried out at 45℃ for 12 hours under nitrogen atmosphere. Precipitated side products were removed by centrifugation and decantation. The polymers were purified by precipitation in petrol ether for three times. δ_H(100 MHz; $CDCl_3$; Me_4Si): 8.4 - 7.3 (9H, broad m, pyrene-H) 3.54 (3H. s. O-CH_3), 1.84 (2H, m, CH_2), 0.96 (1H, s, CH), 0.80 (3H, m, CH_3). Molecular weights and block lengths can be found in table C.7.

Synthesis of ***P(MMA-b-4VP)****:* For the first block, 2 g (0.02 mol) methyl methacrylate, 23 mg ($8.2*10^{-5}$ mol) RAFT agent (4-cyano-4-methyl-4-thiobenzoylsulfanyl-butyric acid, synthesized according to lit. 22) and 1.6 mg ($1.01*10^{-5}$ mol) AIBN (αα'-azoisobutyronitrile) were dissolved in 3 ml dioxane. Oxygen was exchanged by nitrogen by five freeze-pump-thaw cycles. Polymerization was carried out at 70℃ for 15 h. The polymer was purified by dissolving in THF and precipitating in hexane for three times. 1.1 g of rose polymer was collected (54% yield). M_n(GPC) = 17300 g/mol, PDI = 1.20. δ_H(100 MHz; $CDCl_3$; Me_4Si) 3.54 (3H. s. O-CH_3), 1.84 (2H, m, CH_2), 0.96 (1H, s, CH), 0.80 (3H, m, CH_3).

For the second block, 200 mg ($1.16*10^{-5}$ mol) of the polymer, 1 mg ($5.4*10^{-6}$ mol) AIBN and 122 mg ($1.16*10^{-3}$ mol) 4-vinylpyridine were dissolved in 2 ml dioxane. Oxygen was exchanged by nitrogen by five freeze-pump-thaw cycles. Polymerization was carried out at 70℃ for 4 days. The polymer was purified by dissolving in THF and precipitating in petrol ether for three times resulting in 170 mg of solid polymer **P(MMA-b-4VP)**. δ_H(100 MHz; $CDCl_3$; Me_4Si): 8.3 (2H, broad m,

pyridine-H), 6.4 (2H, broad m, pyridine-H), 3.54 (3H. s. O-CH_3), 1.84 (2H, m, CH_2), 0.96 (1H, s, CH), 0.80 (3H, m, CH_3). M_n(GPC) = 26400 g/mol, PDI = 1.15.

Acknowledgements

We would like to thank the “Graduate School of Excellence: Materials Science in Mainz” (stipend for S. Meuer) and Bayer MaterialScience AG for having funded this work.

References

1 Dresselhaus, M.; Dresselhaus, G.; Avouris, P., Eds. In *Carbon Nanotubes: Synthesis, Structure, Properties and Applications*; Springer: Berlin, 2001.

2 Baughman, R. H.; Zakhidov, A. A.; de Heer, W. A. *Science* **2002**, *297*, 787-792.

3 Sun, Y.-P.; Fu, K.; Lin, Y.; Huang, W. *Acc. Chem. Res.* **2002**, *35*, 1096-1104.

4 Dyke, C. A.; Tour, J. M. *Chem. Eur. J.* **2004**, *10*, 812-817.

5 Tasis, D.; Tagmatarchis, N.; Georgakilas, V.; Prato, M. *Chem. Eur. J.* **2003**, *9*, 4000-4008.

6 Szleifer, I.; Yerushalmi-Rozen, R. *Polymer* **2005**, *46*, 7803.

7 Wang, H.; Zhou, W.; Ho, D. L.; Winey, K. I.; Fischer, J. E.; Glinka, C. J.; Hobbie, E. K. *Nano Lett.* **2004**, *4*, 1789-1793.

8 Rouse, J. H. *Langmuir* **2005**, *21*,1055-1061.

9 Dieckmann, G. R.; Dalton, A. B.; Johnson, P. A.; Razal, J.; Chen, J.; Giordano, G. M.; Munoz, E.; Musselman, I. H.; Baughman, R. H.; Draper, R. K. *J. Am. Chem. Soc.* **2003**, *124*, 1770.

10 Star, A.; Steuerman, D. W.; Heath, J. R.; Stoddart, F. *Angew. Chem., Int. Ed. Engl.* **2002**, *41*, 2508;

11 Baskaran, D.; Mays, J. M.; Bratcher, M. S. *Chem. Mater.* **2005**, *17*, 3389-3397.

12 Nativ-Roth, E.; Shvartzman-Cohen, R.; Bounioux, C.; Florent, M.; Zhang, D.; Szleifer, I.; Yerushalmi-Rozen, R. *Macromolecules* **2007**, *40*, 3676-3685.

13 Chen, R. J.; Zhang, Y.; Wang, D.; Dai, H. *J. Am. Chem. Soc.* **2001**, *123*, 3838.

14 Zhu, W.; Minami, N.; Kazaoui, S.; Kim, Y. *J. Mater. Chem.* **2004**, *14*, 1924.

15 Chen, J.; Liu, Y.; Weimer, W. A.; Halls, M. D.; Waldeck, D. H.; Walker, G. C. *J. Am. Chem. Soc.* **2002**, *124*, 9034-9035.

16 Islam, M. F.; Rojas, E.; Bergey, D. M.; Johnson, A. T.; Yodh, A. G. *Nanoletters* **2003**, *3*, 269-273.

17 Hough, L. A.; Islam, M. F.; Hammouda, B.; Yodh, A. G.; Heiney, P. A. *Nanoletters* **2006**, *6*, 313-317.

18 Wenseleers, W.; Vlasov, I. I.; Goovaerts, E.; Obraztsova, E. D.; Lobach, A. S.; Bouwen, A. *Adv. Funct. Mater.* **2004**, *14*, 1105-1112.

19 Lou, X.; Daussin, R.; Cuenot, S.; Duwez, A.-S.; Pagnoulle, C.; Detrembleur, C.; Bailly, C.; Jérôme, R. *Chem. Mater.* **2004**, *16*, 4005–4011.

20 Bahun, G. J.; Wang, C.; Adronov, A. *J. Polym. Sci., Part A: Polym. Chem.* **2006**, *44*, 1941–1951.

21 Meuer, S.; Braun, L.; Zentel, R. *Chem. Comm.* **2008**, 3166 – 3168.

22 Eberhardt, M.; Theato, P. *Macromol. Rapid Commun.* **2005**, *26*, 1488.

23 Eberhardt, M.; Mruk, R.; Zentel, R.; Theato, P. *Eur. Polym. J.* **2005**, *41*, 1569-1575.

24 Koutsioubas, A. G.; Spiliopoulos, N.; Anastassopoulos, D.; Vradis, A. A.; Priftis, G. D. *J. Polym. Sci., Part B: Polym. Phys.* **2007**, *45*, 2060–2070.

25 Meuer, S.; Braun, L.; Schilling, T.; Zentel, R. *Soft Matter*, submitted.

26 Oosawa, F.; Asakura, S. *J. Chem. Phys.* **1954**, *22*, 1255.

27 Zakri, C.; Poulin, P. *J. Mater. Chem.* **2006**, *16*, 4095-4098.

28 Jungblut, S.; Tuinier, R.; Binder, K.; Schilling, T. *J. Chem. Phys.* **2007**, *127*, 244909.

C.3.2 Dispersion Stability and Depletion Phenomena

This chapter focuses on alpha pyrene functionalized polymers for the dispersion of CNT in organic and aqueous media. As different soluble polymers are needed to match both media, the alpha functionalized approach using a pyrene functionalized RAFT agent is more versatile. PMMA and PDEGMEMA were polymerized this way and the alpha pyrene functionalized polymers were investigated for the dispersion of CNTs in THF and water. In both systems depletion plays a major role, as adding more polymer results in unstable dispersions. This effect is known from theoretical considerations for mixtures of rods (CNT) and spheres (polymer coils). In a very simple, purely entropic model that is based on the Asakura-Oosawa model, the spheres entropically mediate an effective attraction between the rods. This effect is known as depletion and plays a very important role in all polymer stabilized colloidal systems. The quintessence of this phenomenon is that adding more stabilizing polymer than needed is counterproductive and results in poor or even unstable dispersions.

The CNT dispersions prepared with alpha pyrene functionalized PMMA were investigated for CNT concentrations from 0.1 to 18 mg/ml and polymer concentrations from 0 to 1 mg/ml. We found stable dispersions for c(CNT) smaller than 2.5 mg/ml and c(polymer) smaller than 0.5 mg/ml, unstable dispersions for more polymer rich (depletion) and more CNT rich (percolation of rods → aggregates) dispersions. Even gelled samples were found for CNT concentrations of 17 mg/ml and polymer concentrations of 0.5 mg/ml. The effect of depletion could also be induced by the addition of a neutral polymer as PEG of different molecular weight. PEG with lower molecular weight as the alpha functionalized PMMA did not harm the

dispersions at all, but PEG with equal or larger molecular weight induced depletion leading to precipitation of the CNTs.

CNT dispersions in water were stabilized by alpha pyrene functionalized PDEGMEMA. We investigated the phase diagram between CNT concentrations of 0.1 and 35 mg/ml and polymer concentrations between 0 and 14 mg/ml. Stable precipitate free dispersions were found for CNT concentrations smaller than 2.6 mg/ml and gelled samples were found for CNT concentrations of 25 mg/ml. For a given CNT concentration of 2.6 mg/ml a reentrant behavior is found: With increasing amount of polymer the dispersions are first unstable (0 up to 2.6 mg/ml), then stable (up to 8.3 mg/ml) and then unstable again (over 10 mg/ml). To investigate this effect, we determined the adsorption of the polymer as a function of feed concentration and found a strong impact. Thus, adsorption / desorption equilibria are present as the single anchor unit is probably not strong enough to hold the quite long PDEGMEMA (M_n = 63.000 g/mol) chain on the surface. This equilibrium can be forced to the adsorbed state by adding more polymer leading to an improvement of the dispersion stability. But this also leads to depletion when the polymer concentration reaches 8.3 mg/ml. In the aqueous system we found another unexpected behavior: the unstable and precipitating dispersions with large amounts of excess polymer (showing depletion) were passing a 5 µm syringe filter resulting in a black dispersion. This was unexpected and the dispersions started to sediment again after filtration. We investigated these dispersions by polarizing microscopy and found after evaporation of the water highly birefringent phases shown in figure C.34. We interpreted this behavior in combination with the filtration (LC phases show shear thinning which would allow the passage through the filter) as a lyotropic liquid crystalline phase of CNTs in solution. The next chapter focuses in more detail on liquid crystallinity.

C.3.2.1 Publication in Polymer 2008, submitted

α-pyrene polymer functionalized multiwalled carbon nanotubes: Solubility, stability and depletion phenomena

S. Meuer, L. Braun, T.Schilling, R. Zentel

Abstract

This paper presents a study on the stability of dispersions of multiwalled carbon nanotubes that are covered with α-pyrene functionalized polymers prepared via RAFT polymerization and dispersed in different solvents. We find that a rather small amount of these polymers ($M_{polymer}$ / M_{CNT} less than 0.1) is capable to stabilize a high concentration of CNTs (up to 2.5 mg/ml) in solution. Another strong evidence for well stabilized CNTs is the comparably low gel points of around 1 vol-% of CNTs in solution. We find that adding the α-pyrene functionalized polymer to CNTs has two counter playing effects: on the one hand, increased surface coverage of the carbon nanotubes increases their solubility; on the other hand increased concentration of free polymer in the solution enhances the depletion forces between the nanotubes.

Introduction

Carbon nanotubes (CNTs) have mechanical, electrical, thermal and optical properties that make them highly interesting for applications in materials science.[1,2] "Raw" nanotubes, however, are usually produced in the form of a disordered powder, in which the individual CNTs are highly entangled. This applies for single walled carbon nanotubes and for their – not as well defined, but easier accessible – multiwalled

form. In order to use them in technical applications, it is thus necessary to disperse them in a solvent. Once they are dispersed, they can be mixed with other substances to form composites, squeezed into fibers or deposited as a film on a substrate. Dispersing nanotubes is, however, not easy, as they strongly attract each other via van der Waals-forces. A variety of methods for chemical functionalization as well as physical methods have been used to disperse carbon nanotubes. The different strategies include chemical modification,[3] covalent attachment of monomers, oligomers and polymers,[4] adsorption of charged surfactants and polyelectrolytes,[5] wrapping with polymers,[6] non-wrapping adsorption of partially collapsed block copolymers[7] and complexation by π-π interactions.[8] A major drawback of the chemically functionalized and covalently modified CNTs is the change in their electronic structure by creating sp^3 centers (needed for both methods).[3,4] The same is unfortunately true for CNT that adsorbed charged molecules as they usually inject or withdraw electrons from the nanotube. Large aromatic systems like pyrene are electronically very similar to graphite as pyrene can be seen as a cut piece from a graphite sheet. In these systems the interaction between two CNTs or different layers of a multi walled carbon nanotube (MWCNT) and between pyrene and CNT is quite similar and does not interfere too much with their electronic structure.[9]

Surfactants have been used extensively to stabilize CNTs in water leading to very high solubilities of CNTs in water up to 20 mg/ml.[10,11,12] They usually use way more surfactant than CNTs having functionalization ratios of surfactant to CNT of 10 : 1, which is a consequence of strong adsorption / desorption equilibria. A serious drawback of electrostatically stabilized CNTs (either by oxidation or surfactant treatment) is that their solubility is limited to aqueous media and that the charges used for stabilization disable any use for electronic devices (short cuts created by the

counter ions). Therefore ion free dispersions in organic solvents are highly desired but require another stabilization approach.

For this purpose the particles have to be surface functionalized with a organically soluble corona to overcome the strong adhesion forces. This can be done using the concept of “hairy rods”, which was originally developed for stiff main chain liquid crystalline polymers and which is very promising for such inorganic nano-objects too.[13] In that concept, a stiff insoluble core is solubilised by linking long chains (the hairs) on its surface. In our case, polymer chains are these hairs leading to a steric stabilization as well as organic solubility. As polymers themselves are objects of nanometer dimensions, polymer coated surface are stabilized sterically up to distance of nanometers and not just for angstroms as with alkyl chains. In addition, new polymers designed for surface functionalisation have multiple anchor units for surface attachment. Therefore adsorption-desorption equilibria reactions are avoided and a robust fixation of the multi-dentate polymer ligand to the surface can be achieved. In addition polymers can be prepared with complex functions as stimuli responsive behavior or conductive properties. On the other hand, polymer functionalized CNTs can be incorporated into polymer matrices, which is not possible for surfactant stabilized systems as they are usually expelled from the polymer matrix.

Various polymers with pyrene anchor units have been investigated by Jérôme et al.[14] and Andronov et al.[15] and were used to disperse carbon nanotubes. Our approach is different from these ones as we use a pyrene functionalized RAFT agent to synthesize α-pyrene functionalized polymers. Thus we can use the same method to polymerize different monomers with exactly the same anchoring system. This method was used recently to disperse multi walled carbon nanotubes very efficiently and liquid crystalline ordering was found.[16]

In this article we present a study on the stability of dispersions of multiwalled carbon nanotubes (Baytubes®) that are functionalized with α-pyrene functionalized polymers in different solvents and in the presence of additional "free" polymer. We interpret our results within the framework of a "semi-flexible rod plus depletant" model. We find that adding the α-pyrene functionalized polymer to the suspensions has two counter playing effects on the nanotubes: on the one hand, increased surface coverage of the carbon nanotubes increases their solubility; on the other hand increased polymer concentration in the solution enhances the depletion attraction between the nanotubes.

Results and Discussion

Polymer Synthesis

The synthesis of the α-pyrene functionalized polymers is based on the reversible addition-fragmentation chain transfer (RAFT) polymerization, a controlled radical polymerization allowing the synthesis of polymers with polydispersities around 1.2 and the build up of block copolymers.[17] We use a pyrene-functionalized RAFT agent to mediate the polymerization of methyl methacrylate (MMA) and diethylene glycol monomethyl ether methacrylate (DEGMEMA). It is made by DCC (N,N'-dicyclohexyl carbodiimide) coupling of (4-cyanopentanoic acid)-4-dithiobenzoate (synthesized according to literature 18) with 4-pyren-1-yl-butan-1-ol. As the monomers are inserted into the carbon sulfur bond of the RAFT agent, the pyrene moiety stays at exactly one end of the polymer chain and α-pyrene functionalized polymers **pyrene-PMMA** and **pyrene-PDEGMEMA** are formed (see figure C.29).

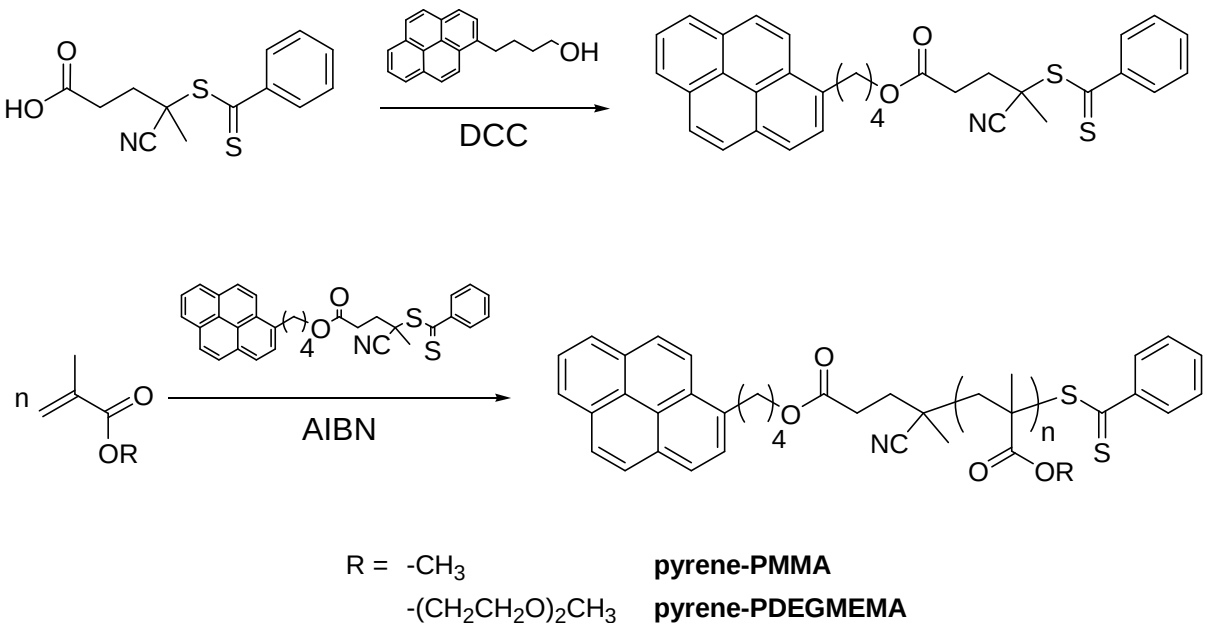

R = $-CH_3$ **pyrene-PMMA**

$-(CH_2CH_2O)_2CH_3$ **pyrene-PDEGMEMA**

Figure C.29: Synthesis of α-pyrene functionalized polymers.

The resulting end group functionalized polymers were analyzed by gel permeation chromatography (GPC) and polydispersity indices (PDI) around 1.2 were found, indicating a controlled polymerization mechanism with this functionalized RAFT agent (see figure C.30). Molecular weights and polydispersities are given in table C.9. The GPC elugram of **pyrene-PDEGMEMA** is showing a small shoulder on the left side indicating some side reactions occurring, but the polydispersity is still fairly low with 1.25. Remarkable is the fact that both detectors detect the polymers. Normally, PMMA and PDEGMEMA can only be detected by the refractive index detector, as no UV absorbing moiety is present at 255 nm. With the pyrene unit being covalently bound to the end of the polymer, the UV detection is now very easy and the signals can be recorded by both detectors equally. The tiny shift in elution volume is due to the fact, that the sample passes the UV detector prior to the refractive index detector.

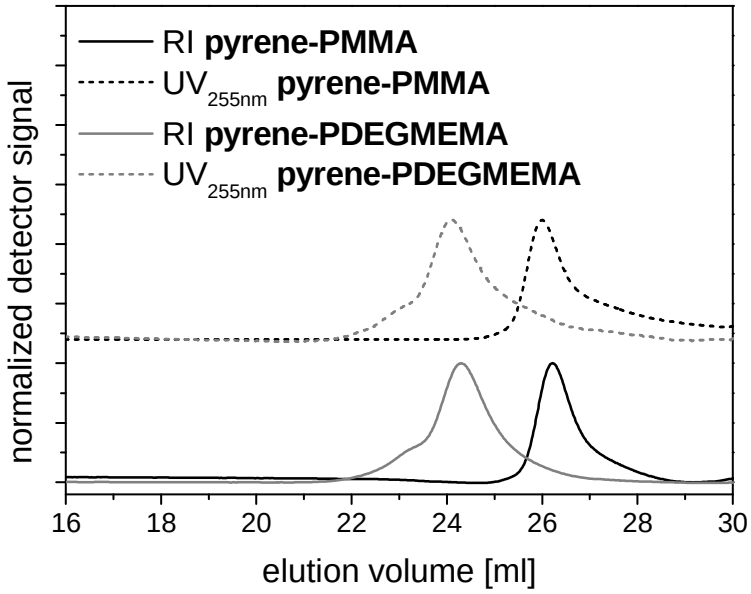

Figure C.30: GPC elugram of both α-functionalized polymers. The detectors shown are a refractive index (RI) detector and an UV detector (λ = 255 nm).

Table C.9: Polymer characterization.

polymer	M_n[a] [g/mol]	M_w[a] [g/mol]	PDI[a]
pyrene-PMMA	16,200	18,800	1.16
pyrene-PDEGMEMA	63,000	78,800	1.25

[a] determined by GPC in THF

PMMA functionalized carbon nanotubes in THF

The carbon nanotubes (CNT) used in this work are multi walled (3 to 15 walls) and in average 14.5 nm wide and 1 to 10 µm long. They were kindly donated by Bayer Material Science AG (Baytubes C 150 P) and were used as received. We focused on these less perfect CNTs as they can be produced in ton scale for a reasonable price making them very prominent for mass scale real world applications. In order to investigate the amount of adsorbed polymer chains, the pristine entangled CNTs (10mg) were added to a polymer solution in THF (10 mg in 2 ml) and stirred over night. The CNTs were separated by centrifugation and washed with fresh THF to

remove unbound polymer chains. The procedure was repeated three times. The CNTs were then dried and investigated by thermo gravimetry (TGA, under nitrogen atmosphere). The PMMA chains decompose between 300 – 400 ℃ and the weight loss is measured. Thus the amount of **pyrene-PMMA** that bounds per mg of CNTs is found to be 0.03 mg. We investigated this value for different concentrations of the functionalization polymer and found no concentration dependency when using more than 2 mg of **pyrene-PMMA** per 10 mg nanotubes. This value corresponds to an coverage of approximately 1200 polymer chains per nanotube and an inter-polymer distance of 14 nm (the calculations are based on a 5 µm long and 14.5 nm wide nanotube with a surface of $2.3*10^5$ nm^2 and a volume of $8.3*10^5$ nm^3. The density of the nanotubes is 1400 kg/m^3 so that there are around $8.7*10^{11}$ nanotubes present per mg).

To investigate the stability of **pyrene-PMMA** functionalized CNTs in solution we prepared samples with various concentrations of CNTs and **pyrene-PMMA** and sonified them for 5 minutes at 20 W (to disentangle the CNTs). The results are presented in figure C.31A. Starting from unstable dispersions at polymer concentrations too low to coat the CNTs, we found stable dispersions at higher polymer concentrations, where the CNTs could not be centrifuged down, but also unstable dispersions at still higher polymer concentrations, that precipitated quickly over an hour. These unstable dispersions do not pass a 5 µm meshed syringe filter indicating that the aggregates are larger than 5 µm. A stable dispersion passes the filter.

On the other hand we also found totally gelled samples on high CNT concentrations. With the known adsorption of **pyrene-PMMA** on the CNTs we were able to calculate the excess polymer concentration in solution (see figure C.31B).

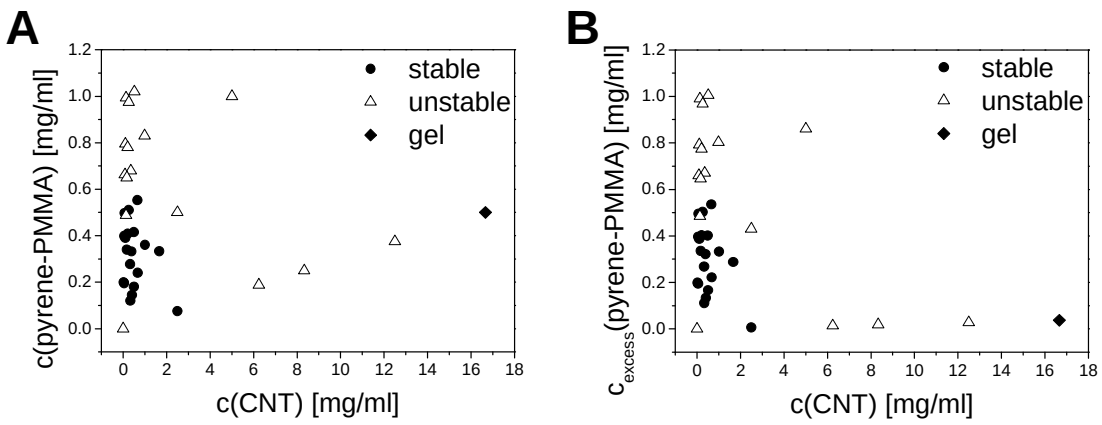

Figure C.31: Phase diagram of CNT versus **A**: **pyrene-PMMA** concentration; **B**: **pyrene-PMMA** excess concentration in THF solution.

At first: we found stable dispersions up to concentrations of PMMA functionalized CNTs larger than 2.5 mg/ml. Solubilities known from literature for polymer stabilized CNTs in organic solvents are as high as 0.65 mg/l and as low as 0.05 mg/l.[19,20] The solubility of these polymer stabilized dispersions was so far achieved with ratios of polymer to CNTs around 1-2.[14,15] We were able to achieve a solubility of 2.5 mg/l with a functionalization ratio less than 0.1 (0.075 mg **pyrene-PMMA** were sufficient to stabilize 2.5 mg CNTs). The solubility achieved with our system is higher than for other polymers, but lower than literature reported high score solubilities for surfactant stabilized CNTs in water, for which up to 10^{12} and 20^{10} mg/ml can be achieved with functionalization ratios of 1 : 1^{12} and 10 : 1^{10} (surfactant : CNT). However as already mentioned in the introduction, ion stabilized systems in water are not suitable for electronic applications or the incorporation of CNTs into polymers.

Secondly, we reached a gel region upon 16.6 mg/ml. This indicates that the CNTs are starting to fill the whole volume of the solution by a percolated network at volume fractions of around 1.2% (corresponding to 16.6 mg/ml as the density of the

CNTs is approximately 1.4 g/ml). This value is comparable to natural gelators as gelatin (forms stable gels at approx. 1 vol.-% in water).[21]

Interestingly the dispersion becomes unstable upon an excess polymer concentration of 0.6 mg/ml. This effect is known from theoretical considerations for mixtures of rods and spheres. In a very simple, purely entropic model that is based on the Asakura-Oosawa model,[22] the spheres entropically mediate an effective attraction between the rods. This effect is known as depletion and plays a very important role in all polymer stabilized colloidal systems. The quintessence of this phenomenon is that adding more stabilizing polymer than needed is counterproductive and results in poor or even unstable dispersions.[23] In the field of CNT dispersions a very interesting review on depletion was published by Poulin et al..[24]

In the diagrams shown in figure C.31, the excess polymer was unbound functionalization polymer. To generalize our observations we added polyethylene glycol (PEG) of different molecular weight to a stable dispersion from figure C.31 (0.18 mg/ml **pyrene-PMMA** and 0.5 mg/ml CNTs). The images of these dispersions are shown in figure C.32 and in each set of 2 ml vials 0.2, 1 and 10 mg of PEG 2,000, 5,000 or 20,000 were added. As PEG and PMMA are well known to have a Flory-Huggins interaction parameter of almost zero, one can be sure that the effects observed are of entropic nature only.[25]

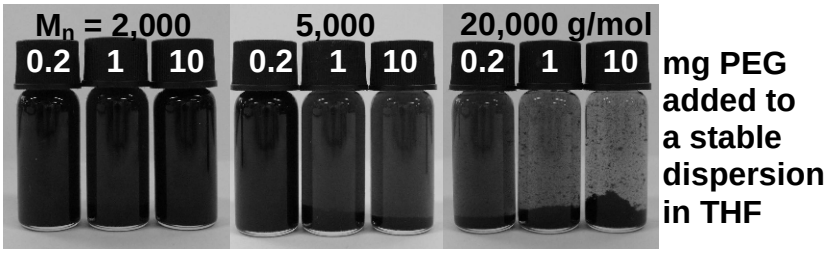

Figure C.32: Depletion of **pyrene-PMMA** functionalized carbon nanotubes by PEG.

Upon addition of PEG 2000 no change in stability can be observed, even upon addition of 10 mg. PEG 5,000 shows some concentration dependence as 0.2 mg do not disturb the stability, whereas upon 1 and 10 mg PEG 5,000 addition depletion starts. This can be explained by the fact, that the PEG 5,000 used is polydisperse so that the size of some chains is comparable to the size of the functionalization polymer on the CNT surface. For PEG 2,000 no chain is big enough to be hindered in its diffusion between PMMA grafted CNTs. For PEG 20,000 almost all chains are larger than the polymer corona around the CNTs and depletion sets in already for the smallest additions (0.2 mg).

PDEGMEMA functionalized carbon nanotubes in water

The adsorption of **pyrene-PDEGMEMA** was investigated with the same method as for **pyrene-PMMA** and an adsorption of 0.40 mg per mg of CNTs was found from THF solutions. This corresponds to a coverage of 4400 chains per nanotube and an inter-polymer distance of 7 nm (based on the same calculations as for **pyrene-PMMA**). This polymer adsorbs better on the CNTs and it can be assumed that unspecific binding of PDEGMEMA play a role too. PDEGMEMA offers the possibility to disperse CNTs not only in THF, but also in polar solvent like alcohols and it has a lower critical solution (LCST) behavior in water. The LCST temperature is around 25 °C and allows switching of the polymer corona from a theta-like dissolved to a collapsed precipitated state. Therefore we especially investigated the stability of **pyrene-PDEGMEMA** functionalized CNTs in aqueous solutions below 25 °C. We prepared various concentrations of CNTs and **pyrene-PDEGMEMA** and formed dispersions by sonification at 20 W for 5 minutes. We were able to find again stable, unstable and gelled dispersions as discussed before for **pyrene-PMMA** functionalized CNTs in THF. The solubility of the CNTs was 2.65 mg/ml at a polymer

concentration of 3.76 mg/ml, which is again significantly higher than literature known solubilities. The functionalization ratio is around 1.4, which is significantly larger than for **pyrene-PMMA**, but still in the typical range of literature known dispersions with much smaller CNT solubilities. At high concentrations of CNTs gelled samples are found (see figure C.33D). SEM images of the dried gel show large entangled structures indicating an unordered percolation of single nanotubes. The gel point is higher than for pyrene-PMMA but still fairly low around 25 mg/ml or 1.7 vol-%, which is reasonable as water is not an as good solvent for PDEGMEMA as THF for PMMA.

The whole phase diagram is shown in figure C.33A. It shows a re-entrant behavior, which is much more pronounced as discussed for the PMMA functionalized CNTs. With increasing amount of **pyrene-PDEGMEMA** the dispersions are first unstable (up to 2.6 mg/ml), then stable (up to 8.3 mg/ml) and then unstable again (over 10 mg/ml). To investigate this effect, we determined the adsorbed amount of **pyrene-PDEGMEMA** on nanotubes exposed to different concentrations of the polymer in water (constant concentration of nanotubes c(CNT) = 3 mg/ml). The CNTs were collected by centrifugation and washed from unbound polymer two times with water. In this case there is a clear dependency of the amount of bound polymer (see figure C.33B) on the preset ratio of polymer to CNT. This is different from the experiments in THF. We assume that this additional unspecific adsorption happens due to the following reasons: first, PDEGMEMA is soluble in water, but close to a LCST. This means that the polymer is not in a good solvent. Second, carbon nanotubes are hydrophobic leading to a high surface tension with polar solvents like water. This leads to additional unspecific adsorption of polymer and an adsorption/desorption equilibrium which is concentration dependent. This effect will not be present in good solvents for the functionalization polymer (like THF) and when the surface tension between CNT and solvent is moderate. With the adsorption

information from figure C.33C we rescaled the phase diagram to show the excess concentration of **pyrene-PDEGMEMA** in figure C.33B (the inset enlarges the re-entrant zone). In this rescaled diagram the re-entrant behavior is restored. It seems that a small amount of “free” or excess polymer is needed in solution to solubilise the nanotubes. We believe that this is due to the adsorption-desorption equilibrium. In order to coat the CNTs sufficiently some free polymer is needed in solution, but too much free polymer leads to segregation because of the depletion effect.

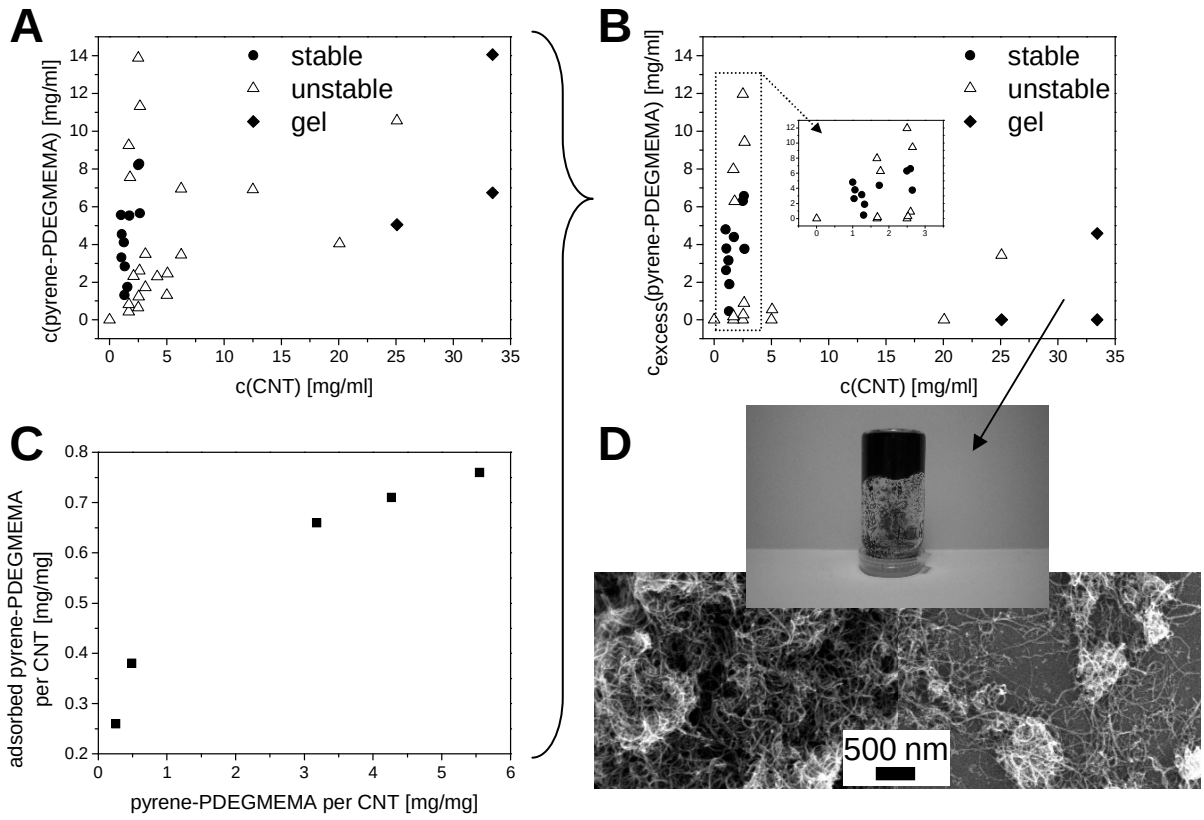

Figure C.33: **A**: Phase diagram CNT concentration versus **pyrene-PDEGMEMA** concentration; **B**: Adsorption behavior of **pyrene-PDEGMEMA** in water (used to calculate fig. C.33C); **C:** Phase diagram CNT concentration versus **pyrene-PDEGMEMA** excess concentration in water; **D**: Images of a sample in the gel region (lower images of a dried gel taken by a SEM).

Table C.10: Surface coverage of **pyrene-PDEGMEMA** on carbon nanotubes.

pyrene-PDEGMEMA per CNT [mg/mg][a]	chains per CNT[b]	A_{chain} [nm^2][b]	s [nm][b]	σ* [b]
0.26	2900	79	8.9	2.6
0.49	4200	55	7.4	3.8
3.18	7300	31	5.6	6.6
4.27	7900	29	5.4	7.2
5.55	8500	27	5.2	7.7

[a] measured by TGA; [b] assuming an average length of 5 µm and width of 14.5 nm.

Directly correlated to the results from figure C.33C (concentration dependent adsorption) are the results shown in table C.10. Here we calculated the number of chains per CNT out of figure C.33B as already done for **pyrene-PMMA**. The number of adsorbed chains increases from 2900 to 8500 chains and the inter-polymer distance is decreased from 8.9 to 5.2 nm in this concentration series. This is close to the radius of gyration of the functionalization polymer **pyrene-PDEGMEMA** (8.1 nm) so that the reduced coverage σ* (= πR_g^2 / A_{chain}) increases from 2.6 to 7.7.

There is an additional experiment, which has to be explained: We tried to filter three different samples from figure C.33C by a 5 µm meshed syringe filter. Images of the filtered dispersions are shown in figure C.34A. A sample being stable passes the filter unhindered and a completely black dispersion is found. An unstable dispersion with low concentration in polymer gave a completely clear filtrate. Obviously all carbon nanotubes were filtered away. An unstable dispersion with high polymer concentration passes the filter but the dispersion is less dark than before indicating the carbon nanotubes partially passed the filter. The filtered dispersion is not stable and precipitates slowly after one day. The question arises how the unstable and precipitating carbon nanotubes – at high polymer concentrations – were able to pass the filter. One possible explanation could be shear alignment of the carbon nanotube agglomerates which is known form lyotropic liquid crystalline phases. The results

from table 2 show that the surface coverage is significantly larger for this dispersion than for the other unstable dispersion that did not pass the filter. Thus we speculate that a larger surface coverage enhances the stiffness of the carbon nanotubes allowing them to shear align. In addition depletion forces the CNTs to a small-scale phase separation into CNT rich and poor domains. In another work we found a lyotropic liquid crystalline behavior of similar functionalized CNTs at high concentration[16] and therefore we investigated the unstable dispersion on liquid crystallinity. We redispersed the CNTs with ultra sound and allowed a drop to dry on a microscope slide (see figure C.34B). The dried droplets (too little material for the formation of a complete film) are birefringent indicating that it passed a lyotropic liquid crystalline phase.

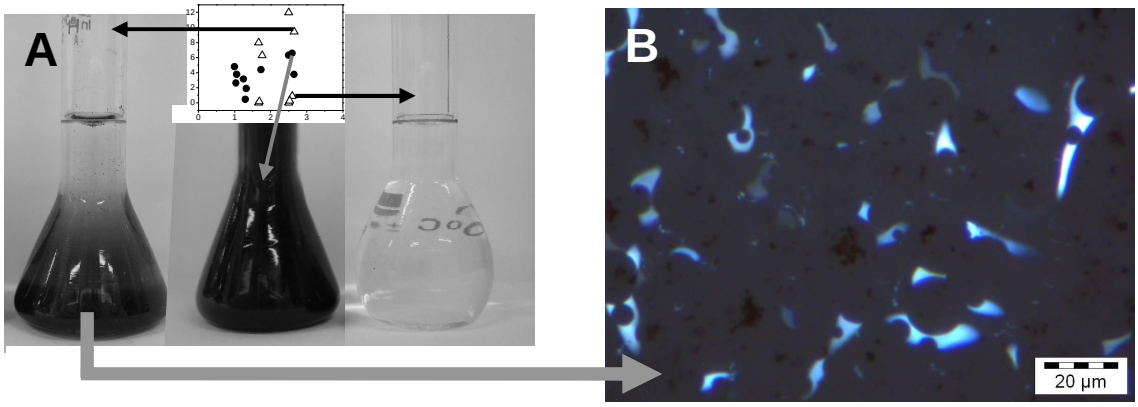

Figure C.34: **A**: Filtered dispersions (syringe filter: 5µm) from fig. C.33C inset: left: unstable dispersion above the stable region, middle: stable dispersion, right: unstable dispersion below the stable region; **B**: polarizing microscopy image of a dried droplet of the middle dispersion (crossed polarizers).

The observed results could thus be understood by the well known behavior of lyotropic rigid-rod dispersions.[26] The rigid-rods tend to segregate: They from a rigid-rod poor supernatant phase and a rigid-rod rich phase, that sediments due to its

larger density (this cannot be distinguished from an unstable dispersion without further experiments). Shear alignment and shear thinning are well know properties of lyotropic liquid crystals and would explain the observed filtration and self organization.[16,27]

Conclusion

Dispersions of polymer-functionalized carbon nanotubes show a rich phase behavior. Mainly, there are two counter playing effects of the amount of polymer added for functionalization: With increasing amount of polymer the nanotubes become better coated (the grafting density increases). Hence their solubility increases and their gel point decreases. On the other hand, excess polymer in the solution causes depletion attraction between the nanotubes and hence increases their tendency to aggregate. In detail, we showed that a very little amount of **pyrene-PMMA** ($M_{polymer}$ / M_{CNT} less than 0.1 compared to literature known ratios of 1 to 2)[14,15] is capable to stabilize very large concentrations of CNTs (up to 2.5 mg/ml compared to literature known 0.5 – 0.65 mg/ml)[19,20] in solution. We found that functionalization ratios of 1 or 2 already lead to a strong depletion force and unstable dispersions are formed. Another strong evidence for well stabilized CNTs are the comparably low gel points of around 1 vol-% in solution. As this can only be achieved by fully disentangled nanotubes, the stabilization must have been very good.

The differences between **pyrene-PMMA** and **pyrene-PDEGMEMA** can be rationalized by the following scenario: **Pyrene-PMMA** in THF is selectively linked at one end of the chain via the pyrene unit to the CNT and extends therefore highly into the solution. Therefore we observed stable dispersions with small amounts of **pyrene-PMMA**. For PDEGMEMA, however, binding to the CNTs might be different as we found a.) that a significantly larger amount of **pyrene-PDEGMEMA** binds to

the surface and b.) that the adsorption is concentration dependent. Thus we believe, that **pyrene-PDEGEMEMA** does not only adsorb selectively via the terminal pyrene unit, but also unspecifically via the diethylene glycol side group moieties of the chains. Under these conditions the conformation of a **pyrene-PDEGMEMA** chain on the surface of a CNT will be different from **pyrene-PMMA**. It might wrap around the CNTs and extend only little into the solution. Thus more adsorbed polymer would be needed to stabilize the nanotubes as we found experimentally. Water as solvent for PDEGMEMA is also a special case: As the CNTs are rather hydrophobic the unspecific adsorption is enhanced and a concentration dependence is found. This is due to an adsorption-desorption equilibrium and a stable polymer adsorption requires the presences of free excess polymer in solution. This is – of course – also leading to depletion, as we found for larger polymer concentrations.

We hope that these effects can be used to tailor the properties of carbon nanotube suspensions towards specific technological applications.

Experimental

The CNTs were kindly donated by Bayer MaterialScience AG (Baytubes C 150 P) and used as received. They are to our best knowledge and according to Bayer MaterialScience AG free of amorphous carbon and fullerenes and have a carbon purity of more than 95%. All solvents were dried and distilled before use. Methyl methacrylate (from Acros) and (diethylene glycol monomethyl ether) methacrylate ((2-methoxy-ethoxy)-ethyl methacrylate from Aldrich) was distilled before usage, αα'-azoisobutyronitrile (AIBN, from Fluka) was recrystalized from diethyl ether, dioxane and tetrahydro furan (THF) were dried and distilled before usage, all other solvents were used without further purification. Gel permeation chromatography (GPC) was carried out in THF as solvent and the detector system contained refractive index

(Jasco RI 1570), UV-Vis (Jasco UV 1575) and light scattering (Wyatt miniDAWN) detectors. Thermo gravimetry (TGA) was carried out in a Perkin Elmer Pyris 6 TGA under nitrogen atmosphere and analyzed by the Pyris software. Sonication was done using a Branson Digital Sonifier (model 250-D) tip-generator with a power of 10W for 15 minutes.

Synthesis of 4-cyano-4-methyl-4-thiobenzoylsulfanyl-butyric acid 4-pyren-1-yl-butyl ester (pyrene functionalized RAFT agent, modified from ref. 18): 204 mg (0.73 mol) (4-cyanopentanoic acid)-4-dithiobenzoate (synthesized according to ref. 18), 200 mg (0.73 mol) 4-(1-pyrenyl)-butanol and 9 mg (0.073 mol) 4-(dimethylamino)-pyridine were dissolved in 5 ml THF and a solution of 151 mg (0.73 mol) DCC (N,N'-dicyclohexylcarbodiimide) in 3 ml CH_2Cl_2 was added at 0 ℃. The mixture was stirred and allowed to warm up to room temperature over night. The suspension with white precipitate was filtered over Celite, washed with chloroform and purified by column chromatography (pure chloroform). The product, 4-cyano-4-methyl-4-thiobenzoylsulfanyl-butyric acid 4-pyren-1-yl-butyl ester was freeze dried from benzene (366 mg, 95%). δ_H(100 MHz; $CDCl_3$; Me_4Si) 8,23 (1H, d, pyrene-H), 8,13 (4H, q, pyrene-H), 8,01 (3H, s, pyrene-H), 7,84 (3H, m, phenyl-H + pyrene-H), 7,53 (1H, t, phenyl-H), 7,35 (2H, t, phenyl-H), 4,16 (2H, t, C_4H_8), 3,37 (2H, t, C_4H_8), 2,72 - 2,58 (2H, m, C_4H_8), 2,01 – 1,66 (9H, m, C_4H_8 + CH_3 + C_2H_4).

Synthesis of α-pyrene functionalized polymers ***pyrene-PMMA*** *and* ***pyrene-PDEGMEMA****:* General procedure: Monomer, RAFT agent (4-cyano-4-methyl-4-thiobenzoylsulfanyl-butyric acid 4-pyren-1-yl-butyl ester) and AIBN (αα'-azoisobutyronitrile) were dissolved in 2 ml dioxane. Oxygen was exchanged by nitrogen by five freeze-pump-thaw cycles. Polymerization was carried out at 70℃ for 20 h. The polymers were purified by dissolving in THF and precipitating in methanol for **pyrene-PMMA** and hexane for **pyrene-PDEGMEMA** for three times. Molecular

weights and PDIs are given in table C.9. For **pyrene-PMMA** 1.02 g (10.2 mmol) methyl methacrylate, 107.2 mg (0.2 mmol) RAFT agent and 8 mg ($4.9*10^{-5}$ mol) AIBN were used. After precipitation, 997 mg (97 %) rose colored polymer powder was collected. δ_H(100 MHz; $CDCl_3$; Me_4Si) 3.54 (3H. s. O-CH_3), 1.84 (2H, m, CH_2), 0.96 (1H, s, CH), 0.80 (3H, m, CH_3). For **pyrene-PDEGMEMA** 1.08 g (5.8 mmol) (diethylene glycol monomethyl ether) methacrylate ((2-methoxy-ethoxy)-ethyl methacrylate) and 1.2 mg ($7.2*10^{-6}$ mol) AIBN were used. After precipitation, 886 mg (82 %) rose colored jelly polymer was collected. δ_H(100 MHz; $CDCl_3$; Me_4Si) 4.4–3.5 (4d, 8H, -C*H*$_2$-C*H*$_2$-O-C*H*$_2$-C*H*$_2$-O-CH_3), 3.3 (s, 3H, -CH_2-CH_2-O-C*H*$_3$), 2.0–1.6 (m, 2H, [-C*H*$_2$-CRCH_3-]n), 1.3–0.7 (m, 3H, [-CH_2-CR(C*H*$_3$)-]$_n$).

Acknowledgements

We would like to thank the “Fonds der Chemischen Industrie” and the “Graduate School of Excellence: Materials Science in Mainz” for having funded this work (stipend for S. M.). T. S. acknowledges financial support by the DFG (Emmy Noether Program). We thank XXXXX for helpful advice. SEM images were kindly taken by XXXXX from the “Max Planck Institute for Polymer Research, Mainz / Germany”.

References

1 M. Dresselhaus, G. Dresselhaus, Ph. Avouris, Eds. “Carbon Nanotubes: Synthesis, Structure, Properties and Applications”, Springer, Berlin, 2001

2 R. H. Baughman, A. A. Zakhidov, W. A. de Heer, *Science*, 2002, **297**, 787-792

3 Y.-P. Sun, K. Fu, Y. Lin, W. Huang, *Acc. Chem. Res.*, 2002, **35**, 1096-1104; C. A. Dyke, J. M. Tour, *Chem. Eur. J.*, 2004, **10**, 812-817.

4 D. Tasis, N. Tagmatarchis, V. Georgakilas, M. Prato, *Chem. Eur. J.*, 2003, **9**, 4000-4008.

5 I. Szleifer, R. Yerushalmi-Rozen, *Polymer*, 2005, **46**, 7803; H. Wang, W. Zhou, D. L. Ho, K. I. Winey, J. E. Fischer, C. J. Glinka, E. K. Hobbie, *Nano Lett.*, 2004, **4**, 1789-1793.

6 J. H. Rouse, *Langmuir*, 2005, **21**,1055-1061; G. R. Dieckmann, A. B. Dalton, P. A. Johnson, J. Razal, J. Chen, G. M. Giordano, E. Munoz, I. H. Musselman, R. H. Baughman, R. K. Draper, *J.*

Am. Chem. Soc., 2003, **124**, 1770; A. Star, D. W. Steuerman, J. R. Heath, F. Stoddart, *Angew. Chem., Int. Ed. Engl.*, 2002, **41**, 2508; D. Baskaran, J. M. Mays, M. S: Bratcher, *Chem. Mater.*, 2005, **17**, 3389-3397.

7 E. Nativ-Roth, R. Shvartzman-Cohen, C. Bounioux, M. Florent, D. Zhang,I. Szleifer, R. Yerushalmi-Rozen, *Macromolecules*, 2007, **40**, 3676-3685.

8 R. J. Chen, Y. Zhang, D. Wang, H. Dai, *J. Am. Chem. Soc.*, 2001, **123**, 3838; W. Zhm, N. Minami, S. Kazaoui, J. Kim, *J. Mater. Chem.*, 2004, **14**, 1924; J. Chen, Y. Liu, W. A. Weimer, M. D. Halls, D. H. Waldeck, G. C. Walker, *J. Am. Chem. Soc.*, 2002, **124**, 9034-9035.

9 F. Tournus, S. Latil, M. I. Heggie and J.-C. Charlier, *Phys. Rev. B*, 2005, **72**, 075431; F. J. Gómez, R. J. Chen, D. Wang, R. M. Waymouth, H. Dai, *Chem. Commun.*, 2003, **2**, 190–191; R. J. Chen, Y. Zhang, D. Wang, H. Dai, *J. Am. Chem. Soc.*, 2001, **123**, 3838–3839; W. Z. Yuan, Y. Mao, H. Zhao, J. Z. Sun, H. P. Xu, J. K. Jin, Q. Zheng, B. Z. Tang, *Macromolecules*, 2008, **41**, 701–707.

10 M. F. Islam, E. Rojas, D. M. Bergey, A. T. Johnson, A. G. Yodh, *Nano Letters*, 2003, **3**, 269-273.

11 L. A: Hough, M. F. Islam, B. Hammouda, A. G. Yodh, P. A. Heiney, *Nano Letters*, 2006, **6**, 313-317

12 W. Wenseleers, I. I. Vlasov, E. Goovaerts, E. D. Obraztsova, A. S. Lobach, A. Bouwen, Adv. Funct. Mater., 2004, 14, 1105-1112.

13 M. Ballauff, *Angew. Chem.*, 1989, **101**, 261.

14 X. Lou, R. Daussin, S. Cuenot, A.-S. Duwez, C. Pagnoulle, C. Detrembleur, C. Bailly and R. Jérôme, *Chem. Mater.*, 2004, **16**, 4005–4011.

15 G. J. Bahun, C. Wang and A. Adronov, *J. Polym. Sci., Part A: Polym. Chem.*, 2006, **44**, 1941–1951.

16 S. Meuer, L. Braun, R. Zentel, *Chem. Comm.*, 2008, **DOI** 10.1039/b803099e.

17 G. Moad, E. Rizzardo, S. H. Thang, *Polymer*, 2008, **49** 1079-1131.

18 M. Eberhardt, Ph.D. Thesis, University of Mainz, 2006; M. Eberhardt, P. Theato, *Macromol. Rapid Commun.*, 2005, **26**, 1488.

19 W. Z. Yuan, J. Z. Sun, Y. Dong, M. Häussler, F. Yang, H. P. Xu, A. Qin, J. W. Y. Lam, Q. Zheng, B. Z. Tang, *Macromolecules*, 2006, **39**, 8011-8020

20 W. Z. Yuan, Y. Mao, H. Zhao, J. Z. Sun, H. P. Xu, J. K. Jin, Q. Zheng, B. Z. Tang, *Macromolecules*, 2008**, 41***,* 701-707

21 A. Veis, “The macromolecular chemistry of gelatin”, Academic Press, New York, 1964

22 F. Oosawa, S. Asakura, *J. Chem. Phys.*, 1954, **22**, 1255

23 S.Jungblut, R.Tuinier, K.Binder, T.Schilling, *J. Chem. Phys.*, 2007, **127**, 244909

24 C. Zakri, P. Poulin, *J. Mater. Chem.*, 2006, **16**, 4095-4098

25 H. Ito, T. P. Russell, *Macromolecules*, 1987, **20**, 2213-2220

26 A. Dessombz, D. Chiche, P. Davidson, P.Panine, C. Chanéac, J.-P. Jolivet, *J. Am. Chem. Soc.*, 2007, **129**, 5904

27 M. Lukaschek, D. A. Grabowski, C. Schmidt, *Langmuir*, 1996, **11**, 3590-3594

C.3.3 Liquid Crystalline Phases

Finally the PMMA functionalized CNTs were integrated into organic matrices: excess alpha functionalized PMMA and PEG 400. As already shown in the former chapter, adding excess functionalization polymer to a solution results in depletion but oriented phases were found in these dispersions. We wanted to investigate this effect in more detail performing the following experiments: we filtered highly diluted alpha pyrene PMMA stabilized CNT dispersions with polymer excess and evaporated the solvent (i) fast by spin coating and (ii) slowly between glass slides. The idea is that rearrangement of the CNTs is not possible when the solvent is evaporated fastly, which disables depletion effects, while evaporating the solvent slowly enables depletion effects. Thus, films prepared by both methods should differ in their CNT distribution along the film: the first film should have a homogeneous distribution of the CNTs while the second one should show CNT-rich and -poor domains.

A spin coated film was prepared and the CNT distribution in the film was investigated by scanning electron microscopy (SEM) after plasma etching to remove the polymer film. The resulting CNTs were nicely dispersed, forming a percolated network over the entire film. Thus, spin coating of dilute dispersions allows the incorporation of polymer functionalized CNTs into polymer films without running into depletion problems. But as a drawback, only thin films are available as spin coated dilute dispersions cannot be used for the fabrication of thick films.

The slowly evaporated films between glass slides show a very interesting behavior under a polarizing microscope: They showed birefringent domains that were optically well-oriented. Depletion enriched the CNTs locally and we believe that this induced a lyotropic liquid crystalline phase of the CNTs. This would explain the birefringence of the phases and the alignment could have happened in the drying

step as the LC phase might be stressed leading to shear alignment. This would also explain why neighboring patches were aligned in the same direction.

As the formation of lyotropic liquid crystalline phases had been found, we wanted to investigate such a phase in more detail. Therefore we used the same "solvent" used for the PMMA functionalized TiO_2 nanorod LCs, PEG 400. The advantages of PEG 400 are again that it does not evaporate, prevents sedimentation, is unable to produce depletion effects (molecular weight is far too small, see previous chapter) and is a suitable solvent for the PMMA corona. We prepared such a mixture and found, as expected, a lyotropic LC phase. As the mixture was done by evaporation of a dilute solution, small droplets were formed instead of a continuous film. After tempering, they were showing a texture typical for nematic droplets. A clearing temperature was also found around 48 °C, indicating again the impact of the polymer corona. When removing the analyzer in the microscopy, the orientation of the nanorods within the droplets could be analyzed. As the CNTs adsorb light specifically along their long axis, this can be used to determine the CNT orientation within the droplets: The droplets adsorb light along the direction of incident linear polarized light for all given angles. This can only be achieved for a radial conformation of the CNTs in the droplets.

C.3.3.1 Publication in Chemical Communications 2008, 3166-3168

Solubilisation of multi walled carbon nanotubes by α-pyrene functionalized PMMA and their liquid crystalline self-organization

Stefan Meuer, Lydia Braun, Rudolf Zentel

Introduction

Since the discovery of carbon nanotubes (CNT) and their unique mechanical and electrical properties many researchers have investigated ways to soluble them. The different strategies include chemical modification,[1] covalent attachment of monomers, oligomers and polymers,[2] adsorption of charged surfactants and polyelectrolytes,[3] wrapping with polymers,[4] nonwrapping adsorption of partially collapsed block copolymers[5] and complexation by π-π interactions.[6] A mayor drawback of the chemically functionalised and covalently modified CNTs is the change in their electronic structure by creating sp^3 centres (needed for both methods).[1,2] The same is unfortunately true for CNT that adsorbed charged molecules as they usually inject or withdraw electrons from the nanotube. π-π interactions can also change the electronic structure of the nanotubes, especially when heteroatom doped aromatic systems are used. But undoped aromatic systems like pyrene are electronically very similar to graphite as pyrene can be seen as cut piece from a graphite sheet. In these systems the interaction between two CNTs or different layers of a multi walled carbon nanotube (MWCNT) and between pyrene and CNT is quite similar and does not interfere too much with

their electronic structure.[7] Various diblock and statistical copolymers with pyrene anchor units have been investigated by Jérôme et al.[8] and Andronov et al.[9] who found a strong influence of block architecture, block length and distribution of the anchor units.

From their geometry, CNTs are semi flexible rod-like objects with large persistence length. Thus it should be possible to use them as mesogens in highly concentrated solutions to obtain a liquid crystalline (LC) phase. The experimental observation of the lyotropic phase requires mobility of the nano-objects at high concentration. Thus a neat material of highly anisotropic nano-objects usually does not form LC-phases due to lack of mobility, but LC-phases are formed, if highly concentrated and stable solutions can be obtained. This requires the "solubilisation" of the nano-objects and the choice of a suitable solvent. Thus the concept of "hairy rods", which was originally developed for stiff main chain liquid crystals, is also promising for inorganic nano-objects.[10] In that concept, a stiff insoluble core is solubilised by long alkyl chains (the hairs) on its surface. It has recently been used successfully for the functionalisation of TiO_2 nanorods, which act as mesogens at higher concentration.[11]

Results and Discussion

For the functionalisation of MWCNTs we decided to work with pyrene functionalised polymers.[8,9] As it is known that the molecular weight of the grafts is less important than their grafting density to solubilise nanoobjects successfully with polymers we focused on polymer chains that carry exactly one pyrene unit at one end to maximise the number of adsorbed chains. We prepared them using a RAFT (radical addition fragmentation transfer) polymerisation of methyl methacrylate using the pyrene functionalised RAFT agent 4-cyano-4-methyl-4-

thiobenzoylsulfanyl-butyric acid 4-pyren-1-yl-butyl ester. Thus each PMMA chain is end capped with exactly one pyrene unit (see fig. C.35A). The polymers were analyzed by gel permeation chromatography (GPC) with molecular weights and polydispersity indices reported in table C.11.

A

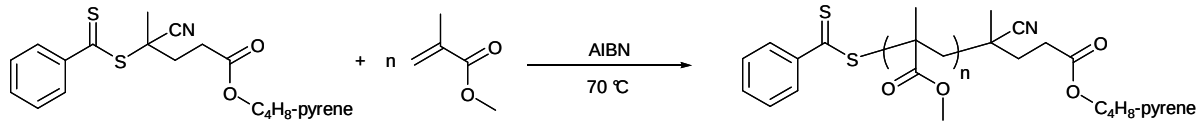

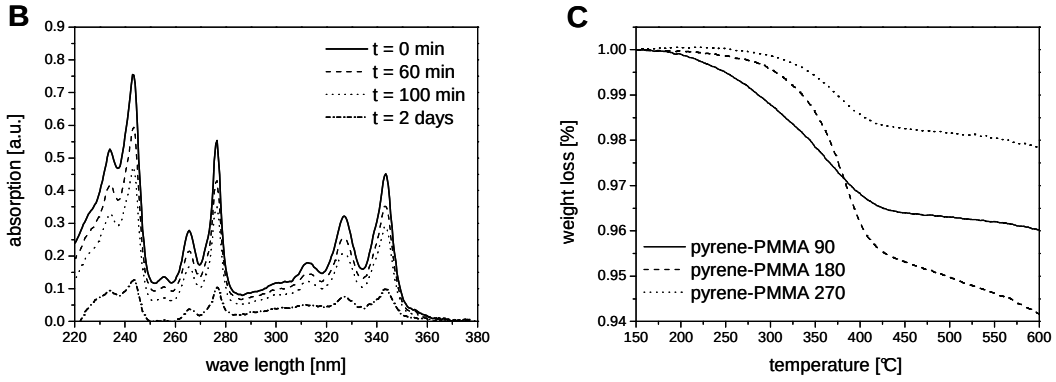

Figure C.35: **A**: Synthesis of **pyrene-PMMA**; **B**: UV-Vis absorption kinetic of **pyrene-PMMA 90** on MWCNTs; **C**: TGA analysis of **pyrene-PMMA** functionalized MWCNTs.

Table C.11: Molecular weight and adsorption characteristics of α-functionalized PMMA.

name	repeat units	M_n [g/mol]	PDI	adsorbed polymer on MWCNTs [weight %]	chains per MWCNT	s [nm]
pyrene-PMMA 90	90	8900	1.18	3.8	3000	9
pyrene-PMMA 180	180	18100	1.31	4.1	1550	12
pyrene-PMMA 270	270	27200	1.35	1.8	500	22

The MWCNTs were kindly donated by Bayer Material Science (Baytubes C 150 P, for SEM images of the pristine powder see fig. C.36A and B) and were in average 14.5 nm wide and 1 to 10 µm long and were used as received. The adsorption process can be monitored using UV-Vis spectroscopy (see fig. C.35B). For this purpose we prepared a cuvette with pristine MWCNTs lying at the bottom of the

cell with a dilute polymer solution above. The absorption of the pyrene units in solution decreases over time as the polymers adsorb on the MWCNTs at the bottom of the cell. As we worked in very dilute polymer solution, the adsorption is rather slow. In order to investigate the amount of adsorbed polymer chains, the pristine MWCNTs (10mg) were added to a polymer solution in THF (2 mg in 2 ml) and stirred over night. The MWCNTs were separated by centrifugation and redispersed in fresh THF to remove unbound polymer chains. The procedure was repeated three times. The MWCNTs were then dried and investigated by thermo gravimetry (TGA, under nitrogen atmosphere, see fig. C.35C). The PMMA chains decompose between 300 – 400 °C and the weight loss is measured. Out of this mass, the number of chains that adsorbed per MWCNT can be calculated (see tab. C.11). For the calculations we assumed an average surface per MWCNT of around $2.3*10^5$ nm^2 (assuming an average length of 5 µm and width of 14.5 nm). The number of MWCNTs is estimated to $8.6*10^{11}$ mg^{-1} (assuming a density of 1400 kg/m^3 and a volume of $8.3*10^5$ nm^3 per MWCNT). The interpolymer distance *s* between adsorbed polymers can be calculated as square root of the surface area per polymer chain.[12]

On the first view, the **pyrene-PMMA 180** was adsorbed best as by TGA analysis 4.1 weight % polymer was adsorbed. For **pyrene-PMMA 90** 3.8 weight % and for **pyrene-PMMA 270** 1.8 weight % polymer were found after functionalisation of the MWCNTs. But the total number of adsorbed chains is due to the different molecular weights largest for **pyrene-PMMA 90** with around 3000 chains. For **pyrene-PMMA 180** around 1550 and for **pyrene-PMMA 270** around 500 adsorbed chains per MWCNT were found (see tab. C.11). The interpolymer distance *s* was calculated to be 9 nm for **pyrene-PMMA 90** and increased to 22 nm for **pyrene-PMMA 270**. Thus the shortest polymer adsorbs

significantly better than the longer polymer chains. This effect might be due to a stronger tendency of longer polymer chains to desorb from the surface as the hydration enthalpy increases with growing chains length and overcomes the binding energy of the single anchor unit. This phenomenon was also found in grafting from polymers started by a pyrene anchored ROMP catalyst. With increasing polymer chain length the polymer films got instable and vanished into solution.[13] This cannot be detected in our systems but a weakening of the interaction can be stated from the TGA data. Nevertheless all polymers were capable to stabilise MWCNT dispersions in THF. The amount of polymer needed for a stable dispersion is just around 10 weight % of the carbon nanotubes (ratio $M_{MWCNT} : M_{\textbf{pyrene-PMMA}} = 10 : 1$) which is much less than reported in literature.[5,8,9]

Starting with the pristine and highly entangled MWCNTs (see fig. C.36A and B) is challenging as the disentanglement is crucial for all applications. Figure C.36C shows a dried solution of **pyrene-PMMA 90** stabilised MWCNTs. The MWCNTs have been disentangled in polymer solution and were forming a spreaded film of individual nanotubes upon solvent evaporation. The **pyrene-PMMA 90** polymer chains were able to functionalise and mobilise the nanotubes sufficiently that they disentangled upon ultra sonification. Moreover they were then stabilised in solution and formed dispersion in THF that were completely stable (no sedimentation observable over weeks). When more polymer is added than needed for the surface functionalisation (ratio $M_{MWCNT} : M_{\textbf{pyrene-PMMA}} = 1 : 30$), polymer films can be fabricated by spin coating from solution with well dispersed MWCNTs as filler material. In order to visualise the carbon nanotubes, the PMMA excess was etched away by oxygen plasma and the MWCNTs remained on the substrate

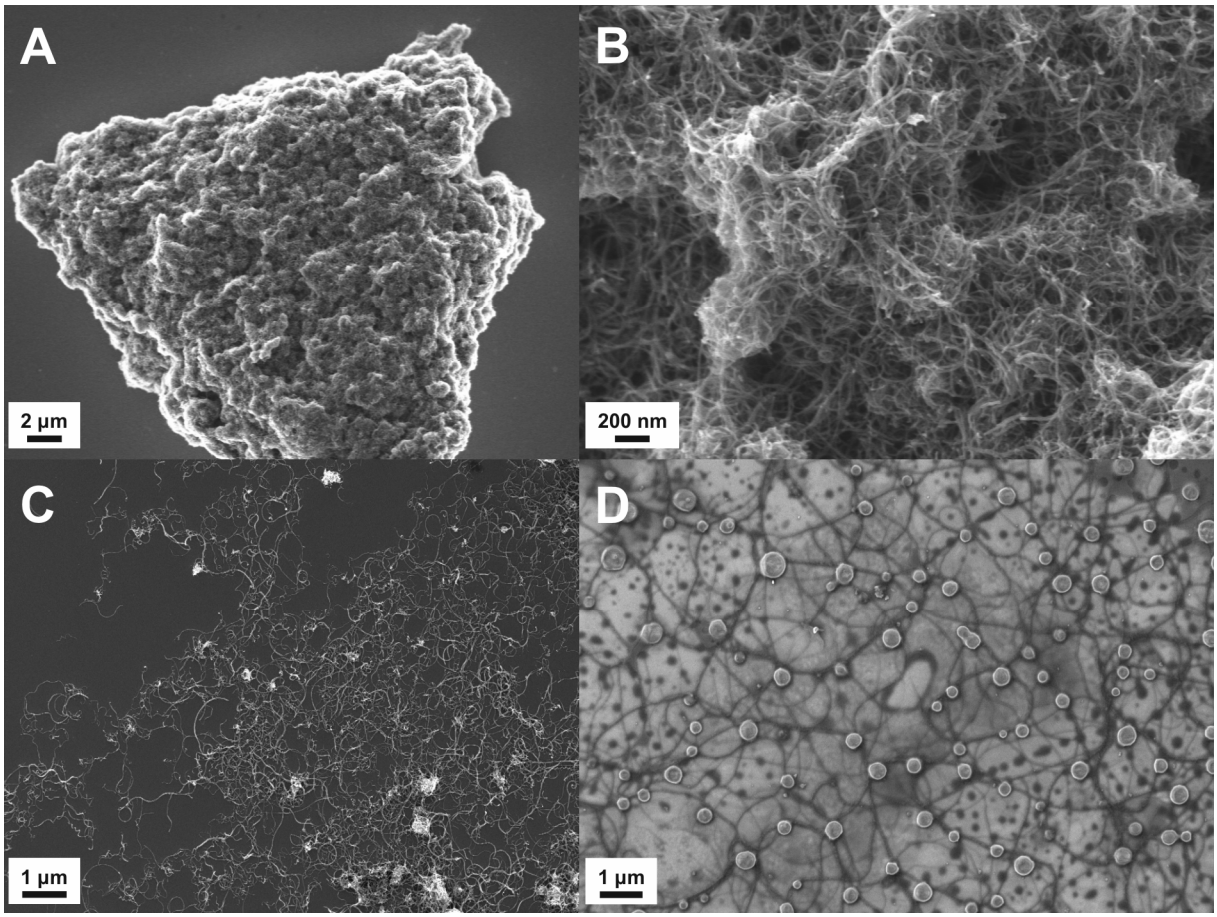

Figure C.36: SEM images of **A**, **B**: pristine multi walled carbon nanotubes; **C**: **pyrene-PMMA 90** functionalized MWCNTs drop coated from solution; **D**: **pyrene-PMMA 90** functionalized MWCNTs that were distributed in a PMMA film (etched away by O_2 plasma).

(see fig. C.36D). Residual polymer droplets can be seen and a percolation network of carbon nanotubes appears after etching. This is an absolute necessity to enhance the mechanical and electrical properties of the matrix with carbon nanotubes as filler.[14-18] Thus we were able to mediate successfully between the MWCNTs and the PMMA film and obtained a homogeneous film with embedded percolated nanotubes.

As the MWCNTs resemble semi flexible rod-like objects it should be possible to use them as mesogens to obtain a liquid crystalline phase in analogy to what is known

from solutions of rigid-rod polymers. Really highly concentrated solutions of polymer functionalized MWCNTs in PMMA (excess **pyrene-PMMA 90** polymer, $M_{MWCNT} : M_{\textbf{pyrene-PMMA}}$ = 1 : 1 or 3 : 1) prepared via solvent casting give inhomogeneous films, which show highly birefringent areas (figure C.37A and B) in an isotropic matrix.

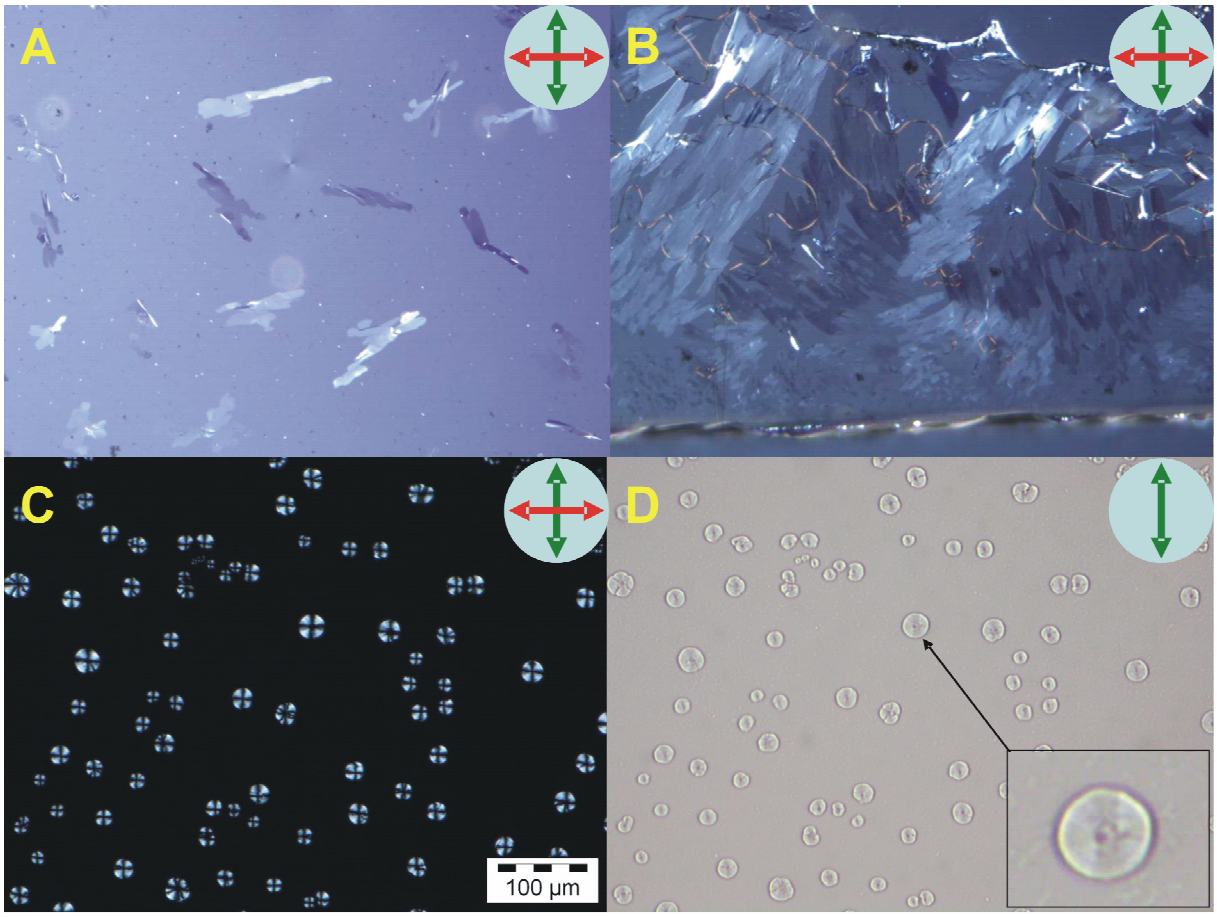

Figure C.37: Polarizing microscopy images (green arrow: polarizer plane, red arrow: analyzer plane) of **A**, **B**: **pyrene-PMMA 90** functionalized MWCNTs in PMMA films (crossed polarizers); **C**: liquid crystalline droplets of **pyrene-PMMA 90** functionalized MWCNTs in PEG 400 (crossed polarizers); **D**: same area as in C but without analyzer (transmission of linear polarized light). (The scale bar is the same for all images).

These areas are oriented as the birefringence is angle dependant and they became completely dark for a certain angle. These patches cannot result from the end group functionalised atactic polymer as it does not crystallise and therefore it can only be build up by oriented and densely packed MWCNTs. In the films with lower ratio of MWCNTs to functionalised polymer (M_{MWCNT} : $M_{\textbf{pyrene-PMMA}}$ = 1 : 1, see fig. C.37A), the patches have a quite irregular shape and the birefringence vanishes for certain angles. In the films with the higher ratio of MWCNTs to functionalised polymer (M_{MWCNT} : $M_{\textbf{pyrene-PMMA}}$ = 3 : 1), the patches start to interact with each other. We observed areas where many close lying patches are oriented into the same direction (their birefringence vanishes for the same angle, see fig. C.37B).

As the nanotubes are frozen in these PMMA films after solvent evaporation, their dynamic behaviour could not be investigated. This can be changed by using oligomeric matrices that are still mobile but on the other hand do not evaporate like a solvent. In another work, we found PEG 400 (M_n = 400 g/mol) to be a suitable matrix for PMMA functionalised TiO_2 nanorods[11]. Also **pyrene-PMMA 90** is miscible with PEG 400 (see electronic supplementary information). We prepared a mixture with a ration of $M_{\textbf{pyrene-PMMA 90}@MWCNT}$: M_{PEG400} = 1 : 1 in THF and evaporated the solution on a glass slide. We found a birefringent phase by polarised microscopy which was viscous but still mobile and showed a loss of the birefringence upon heating over 48 °C. The birefrin gence recovered after cooling and tempering around 20 °C produced liquid crystall ine droplets. The formation of droplets was – in this case – simply due to a lack of material in order to form a complete film. These droplets show textures that are common for nematic phases with a radial orientation of the mesogens (MWCNT).[19] When the analyzer is removed, the droplets show a darker area parallel to the incident polarisation

plane (see fig. C.37C). This is due to the ability of carbon nanotubes to absorb light along their long axis.[20] Assemblies of carbon nanotubes are known as potential materials for the polarisation of light which could be found in these droplets as well as in literature known organic liquid crystals that were filled with carbon nanotubes.[21] Thus we were able to solubilise and mobilise the MWCNTs sufficiently to create a liquid crystalline phase out of the nanotubes themselves.

To conclude, we presented a synthetic route to α-functionalised polymers via a pyrene functionalised RAFT agent. We showed that thus functionalised MWCNTs get disentangled and separated nanotubes are found.

At high concentration the functionalized MWCNTs self organize into oriented domains in PMMA as well as in PEG 400 matrices. In the PEG 400 matrix we found a liquid crystalline phase of the nanotubes, that act as mesogens. This offers the potential to align carbon nanotubes at high volume fractions.

Experimental

The MWCNTs were kindly donated by Bayer Material Science (Baytubes C 150 P) and used as received. All solvents were dried and distilled before use. Methyl methacrylate (from Acros) was distilled before usage, αα'-azoisobutyronitrile (AIBN, from Fluka) was recrystalized from diethyl ether, dioxane and tetrahydro furan (THF) were dried and distilled before usage, all other solvents were used without further purification. Gel permeation chromatography (GPC) was carried out in THF as solvent and the detector system contained refractive index (Jasco RI 1570), UV-Vis (Jasco UV 1575) and light scattering (Wyatt minDAWN) detectors. Differential scanning calorimetry (DSC) was carried out using a Pyris DSC 7 and analyzed by the Pyris Software.

Synthesis

Synthesis of 4-cyano-4-methyl-4-thiobenzoylsulfanyl-butyric acid 4-pyren-1-yl-butyl ester (RAFT reagent, modified procedure from ref. 22): 204 mg (0.73 mol) (4-cyanopentanoic acid)-4-dithiobenzoate (synthesized according to ref. 22), 200 mg (0.73 mol) 4(1-pyrenyl)butanol and 9 mg (0.073 mol) 4-(dimethylamino)-pyridine were dissolved in 5 ml THF and a solution of 151 mg (0.73 mol) N,N'-dicyclohexylcarbodiimide in 3 ml CH_2Cl_2 was added at 0 ℃. The mixture was stirred and allowed to warm up to room temperature over night. The suspension with white precipitate was filtered over Celite, washed with chloroform and purified by column chromatography (pure chloroform). The product, 4-cyano-4-methyl-4-thiobenzoylsulfanyl-butyric acid 4-pyren-1-yl-butyl ester was freeze dried from benzene (366 mg, 95%). δ_H(100 MHz; $CDCl_3$; Me_4Si) 8,23 (1H, d, pyrene-H), 8,13 (4H, q, pyrene-H), 8,01 (3H, s, pyrene-H), 7,84 (3H, m, phenyl-H + pyrene-H), 7,53 (1H, t, phenyl-H), 7,35 (2H, t, phenyl-H), 4,16 (2H, t, C_4H_8), 3,37 (2H, t, C_4H_8), 2,72 - 2,58 (2H, m, C_4H_8), 2,01 – 1,66 (9H, m, C_4H_8 + CH_3 + C_2H_4).

Synthesis of **pyrene-PMMA X**: 1g (10mmol) of methyl methacrylate, **X = 90**: 29.4 mg ($5.5*10^{-5}$ mol); **X = 180**: 53.9 mg ($1.0*10^{-4}$ mol); **X = 270**: 107.2 mg ($2.0*10^{-4}$ mol) (4-cyano-4-methyl-4-thiobenzoylsulfanyl-butyric acid 4-pyren-1-yl-butyl ester and **X = 90**: 2.2 mg ($1.34*10^{-5}$ mol); **X = 180**: 4.1 mg ($2.5*10^{-5}$ mol); **X = 270**: 8.0 mg ($4.87*10^{-5}$ mol) AIBN were dissolved in 2 ml dioxane in a schlenk-tube and oxygen was exchanged by nitrogen by five freeze-pump-thaw cycles. Polymerization was carried out at 70℃ for 20 h. The polymers were pur ified by dissolving in THF and precipitating in methanol for three times to yield **pyrene-PMMA X = 90**: 996.5 mg, 97%; **X = 180**: 992.0 mg, 99%; **X = 270**: 788.5 mg, 79%. δ_H(100 MHz; $CDCl_3$; Me_4Si) 3.54 (3H. s. O-CH_3), 1.84 (2H, m, CH_2), 0.96 (1H, s, CH), 0.80 (3H, m, CH_3). Molecular weights and PDIs are given in table C.11.

Miscibility of PEG and PMMA

1.) The miscibility of PEG and PMMA has been extendedly investigated by H. Ito, T. P. Russell and G. D. Wignall (*Macromolecules* 1987, **20**, 2213-2220). They found out that PMMA chains were unperturbed in a PEG matrix and that the Flory-Huggins interaction parameter is almost zero (χ_{AB} varies from $-5*10^{-3}$ to $-1*10^{-3}$ as the fraction of PMMA increases from 0.3 to 0.7). Therefore they demonstrated that high molecular PEG (M_w = 145000 g/mol) and PMMA (M_w = 125000 g/mol) are completely miscible.

2.) In our former work on PMMA coated TiO_2 nanorods (see ref. 11) we demonstrated that also oligomeric PEG (M_n = 400 g/mol) disperses the PMMA coated nanorods. We found very stable dispersions that did not demix over time or upon heating.

3.) In the case of **pyrene-PMMA 90** we tested the miscibility with PEG 400 by a DSC experiments (scanning rate = 40 °C/min from -80 °C to 150 °C):

   a. The glass transition temperature (T_g) of **pyrene-PMMA 90** is 70 °C
   b. PEG 400 has a T_g of -63 °C and a melting temperature (T_m) of 5.5 °C
   c. A mixture of 2:1 PEG 400 : **pyrene-PMMA 90** has a single T_g of -56 °C and a T_m of -0.5 °C.

   The T_g of **pyrene-PMMA 90** is missing, the T_m(PEG 400) is lowered by 6 °C and the T_g(PEG 400) is raised by 7 °C in the mixture. Thus we believe that both polymers are also miscible in the low molecular weight regime.

Aknowledgement

We would like to thank the “Fonds der chemischen Industrie” for funding (stipend for S. Meuer) and Bayer Material Science AG for donation of Baytubes C 150 P. SEM

pictures were taken by XXXXXXX (Max Planck Institute for Polymer Research, Mainz).

References

1 C. A. Dyke, J. M. Tour, *Chem. Eur. J.*, 2004, **10**, 812-817.

2 D. Tasis, N. Tagmatarchis, V. Georgakilas, M. Prato, *Chem. Eur. J.*, 2003, **9**, 4000-4008.

3 H. Wang, W. Zhou, D. L. Ho, K. I. Winey, J. E. Fischer, C. J. Glinka, E. K. Hobbie, *Nano Lett.*, 2004, **4**, 1789-1793.

4 J. H. Rouse, *Langmuir*, 2005, **21**,1055-1061.

5 E. Nativ-Roth, R. Shvartzman-Cohen, C. Bounioux, M. Florent, D. Zhang, I. Szleifer, R. Yerushalmi-Rozen, *Macromolecules*, 2007, **40**, 3676-3685.

6 W. Zhm, N. Minami, S. Kazaoui, J. Kim, *J. Mater. Chem.*, 2004, **14**, 1924.

7 F. Tournus, S. Latil, M. I. Heggie, J.-C. Charlier, *Phys. Rev. B*, 2005, **72**, 075431; F. J. Gómez, R. J. Chen, D. Wang, R. M. Waymouth, H. Dai, *Chem. Comm*., 2003, **2**, 190–191; R. J. Chen, Y. Zhang, D. Wang, H. Dai, *J. Am. Chem. Soc*., 2001, **123**, 3838-3839; W. Z. Yuan, Y. Mao, H. Zhao, J. Z. Sun, H. P. Xu, J. K. Jin, Q Zheng, B. Z. Tang, *Macromolecules*, 2008, **41**, 701-707

8 X. Lou, R. Daussin, S. Cuenot, A.-S. Duwez, C. Pagnoulle, C. Detrembleur, C. Bailly, R. Jérôme, Chem. Mater., 2004, **16**, 4005 4011.

9 G. J. Bahun, C. Wang, A. Adronov, *J. Polym. Sci., Part A: Polym. Chem.*, 2006, **44**, 1941–1951.

10 M. Ballauff, *Angew. Chem*., 1989, **101**, 261.

11 S. Meuer, P. Oberle, P. Theato, W. Tremel, R. Zentel, *Adv. Mater.*, 2007, **19**, 2073-2078.

12 A. G. Koutsioubas, N. Spiliopoulos, D. Anastassopoulos, A. A. Vradis, G. D. Priftis, *J. Polym. Sci., Part B*, 2007, **45**, 2060-2070.

13 F. J. Gómez, R. J. Chen, D. Wang, R. M. Waymouth, H. Dai, *Chem. Commun.*, 2003, **2**, 190–191.

14 J. N. Coleman, S. Curran, A. B. Dalton, A. P. Davey, B. McCarthy, W. Blau, R. C. Barklie, *Phys. Rev. B*, 1998, **58**, R7492.

15 J. Sandler, M. S. P. Shaffer, T. Prasse, W. Bauhofer, K. Schulte, A. H. Windle, *Polymer*, 1999, **40**, 5967.

16 J. M. Benoit, B. Corraze, O. Chauvet, *Phys. Rev. B,* 2002, **65**, 241405(R).

17 P. Pötschke, S. Dudkin, I. Alig, *Polymer*, 2003, **44**, 5023.

18 B. Vigolo, A. Pénicaud, C. Coulon, C. Sauder, R. Pailler, C. Journet, P. Bernier, P. Poulin, *Science*, 2000, **290**, 1331.

19 M. Stegemeyer, Guest Ed., *Liquid crystals*, Steinkopf, Darmstadt, Germany/ Springer, New York, USA 1994

20 G. Scalia, J. P. F. Lagerwall, S. Schymura, M. Haluska, F. Giesselmann, S. Roth, *Phys. Status Solidi B*, 2007, **244**, 4212–4217.

21 G. Scalia, C. von Bühler, C. Hägele, S. Roth, F. Giesselmann, J. P. F. Lagerwall, *Soft Matter*, 2008, DOI: 10.1039/b715683a

22 M. Eberhardt, Ph.D. Thesis, University of Mainz, 2006; M. Eberhardt, P. Theato, *Macromol. Rapid Commun.*, 2005, **26**, 1488.

C.3.4 Carbon Nanotube reinforced Polymers

The history of fiber reinforced plastics is almost as old as the history of polymers themselves. First natural fibers like cotton or hemp, later glass fibers and asbestos were used to prepare very tough hybrid materials. The combination of the soft and elastic polymers with the tough and brittle fibers results in a material combining the best of both worlds. The hybrids are usually highly tough but still elastic, which is not achievable by either one or the other component alone. The mechanical properties of CNTs are expected and/or measured to be exceptional good (better than steal), making them very prominent for the preparation of CNT reinforced plastics. But not only the mechanical but also the conductive properties of CNTs are very interesting. CNTs are expected to show a similar performance compared to conductive carbon black with lower volume fractions as their anisotropy is much larger. Thus, the expected percolation of nanotubes should happen at very low volume fractions of the CNTs.

Concerning the CNTs, tensile tests on poly(vinyl alcohol) doped with six different types of carbon nanotubes (single-, double- and multi-walled CNTs of different diameters) revealed that MWCNTs show a superior mechanical toughness compared to single- and double-walled CNTs . Moreover, the strengthening of the film scales with the inverse of the radius of the CNTs used.[1] The authors claim that therefore small diameter multi-walled CNTs are the best CNTs for mechanical reinforcement. The MWCNT used for this experiment (Baytubes®) have an average radius of 14.5nm (smallest 5nm, largest 20nm) and are therefore expected to show a good mechanical reinforcement. On the other hand, the impact of CNT perfectness (Baytubes® are not very perfect) on the mechanical properties was investigated and no impact was found.

C.3.4.1 CNT reinforced PMMA: Collaboration with XXXXX from the DKI (Deutsches Kunststoff Institut, Darmstadt)

The advantages of polymer functionalization compared to surfactant stabilization of nanoobjects are solubility in organic media and mediation to polymeric matrices. Therefore, PMMA functionalized CNTs investigated in the previous chapters, should be miscible with a PMMA matrix. We investigated the reinforcement of commercially available PMMA films by the addition of PMMA functionalized CNTs. As depletion is expected to happen, we investigated two molecular weights of PMMA matrices. Concerning the first one, depletion should not be a problem as its molecular weight is smaller than the grafted PMMA chains ($M_{n,graft}$ = 18.000 g/mol, M_n = 9.000 g/mol, PDI = 1.5, PMMA 15k) whereas for the second one depletion is expected to happen (M_n = 420.000 g/mol, PDI = 1.6, PMMA 350k). The latter was also chosen as the low molecular weight PMMA 15k is not suitable for any application as it is very brittle whereas the PMMA 350k is a more typical PMMA (tough, glassy and little brittle).

As one can imagine, the volume fraction of CNTs incorporated into the film should alter the physical properties strongly. But as the CNTs do only alter the electrical conductivity and mechanical toughness efficiently when they form a percolated network, there is a threshold volume fraction of CNTs. When the volume of CNTs is lower, the CNTs will just act as a filler material without altering the properties too much. In the range of the percolation threshold, small variations of the volume fraction will have a big influence on the film properties whereas volume fractions far above the threshold will not alter the system too much either.[2]

The percolated network can be destroyed vertically (this is the measurement direction of the conductivity and shear modulus) by shearing the sample above its T_g

but recovers over time, as the entropically driven diffusion of the shear aligned CNTs leads back to a percolated 3D network.[3]

The following samples were prepared by dissolving all components in chloroform, treating the dispersion with ultrasound, evaporating the solvent and pressing polymer plates (2.5 cm diameter, ≈ 1 mm thickness) in a melting vacuum press at 120℃ (PMMA 15k) or 160℃ (PMMA 350k) and a pressure of 50 kN under vacuum (see table C.12).

Table C.12: Sample compositions of CNT reinforced PMMA plates.

Sample Code	Matrix	Weight percent CNTs	Stabilized with **pyrene-PMMA 180**
A	PMMA 15k	4.76	**–**
B		4.76	**+**
C		1.96	**+**
D		1.96	**–**
E	PMMA 350k	4.76	**–**
F		4.76	**+**
G		1.96	**+**
H		1.96	**–**

The samples were analyzed by SEM to reveal the distribution of CNTs in the plates. Figure C.38 shows SEM images of PMMA plates containing 4.76 wt% CNTs (samples A, B, E and F). The differences are rather obvious: first, CNT distributions obtained in PMMA 15k matrix are much more homogeneous than in PMMA 350k. Second, the addition of stabilizing polymer **pyrene-PMMA 180** (CNT to **pyrene-PMMA 180** = 10 : 1 by weight) results in a significant disentanglement of the CNTs, leading to a better dispersion. But the stabilized dispersion in PMMA 350k is not as homogeneous as in PMMA 15k, which was expected and is due to depletion. The unstabilized CNT dispersion in PMMA 350k is the worst one, as almost all CNTs are highly entangled and badly distributed over space.

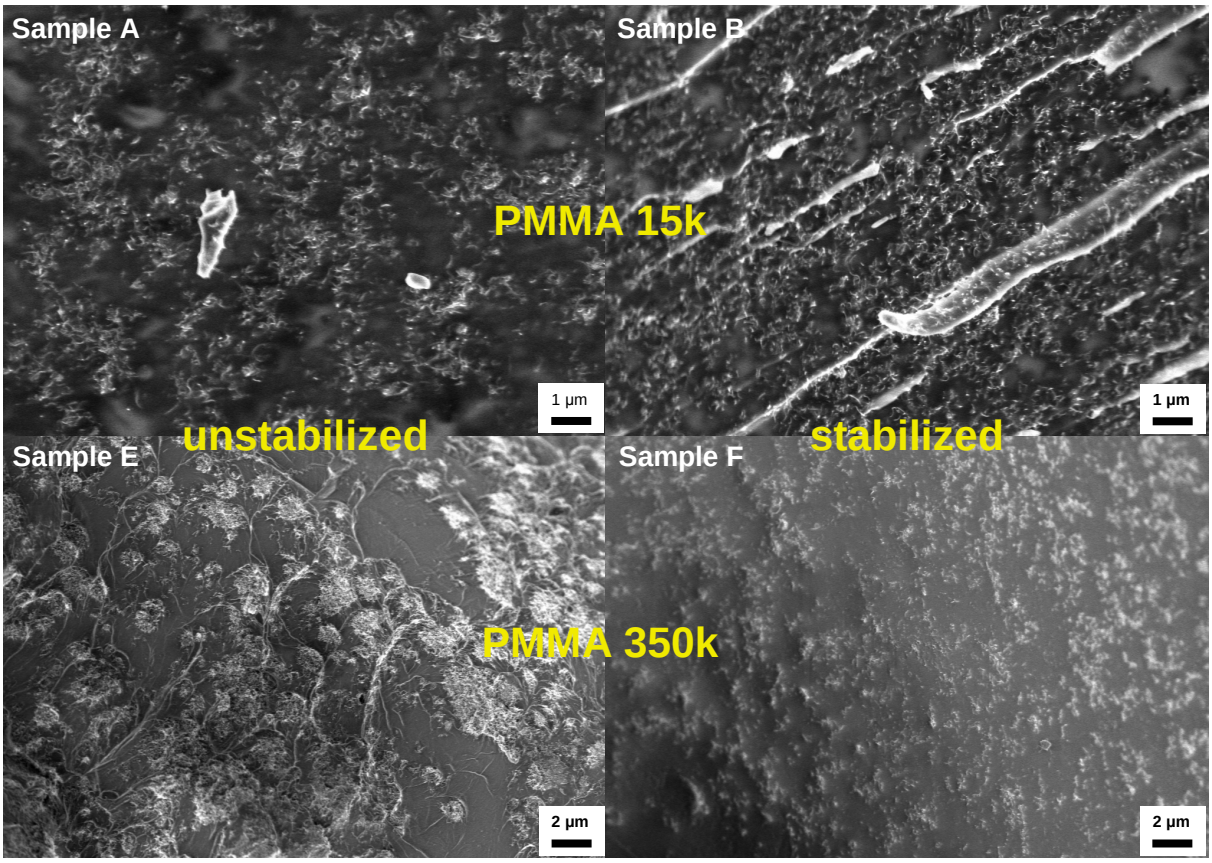

Figure C.38: SEM images of stabilized and unstabilized samples of 4.76 wt% CNTs in PMMA films (samples A, B, E and F from Tab. C.12).

The samples were then investigated by XXXXX, using a self-made setup combining a rheometer and a dielectric spectrometer. The primary setup is a typical rheometer measuring in plate-plate geometry. In the insulating plates a conductive metal ring is implanted which is connected to a dielectric spectrometer. The PMMA plates are heated well above their glass temperature (170℃ for PMMA 15k and 200℃ for PMMA 350k samples) and tempered for 1 hour. After that the samples are sheared once for 6 rad (≈340°) and the recoverage of the electric conductivity is measured by the dielectric spectrometer (10^3–10^6 Hz). Parallel to the dielectric spectroscopy the mechanical properties are measured using an oscillating (1 rad/s) strain of 10% for 2 hours. The results are presented in figure C.39 (PMMA 15k) and C.40 (PMMA 350k).

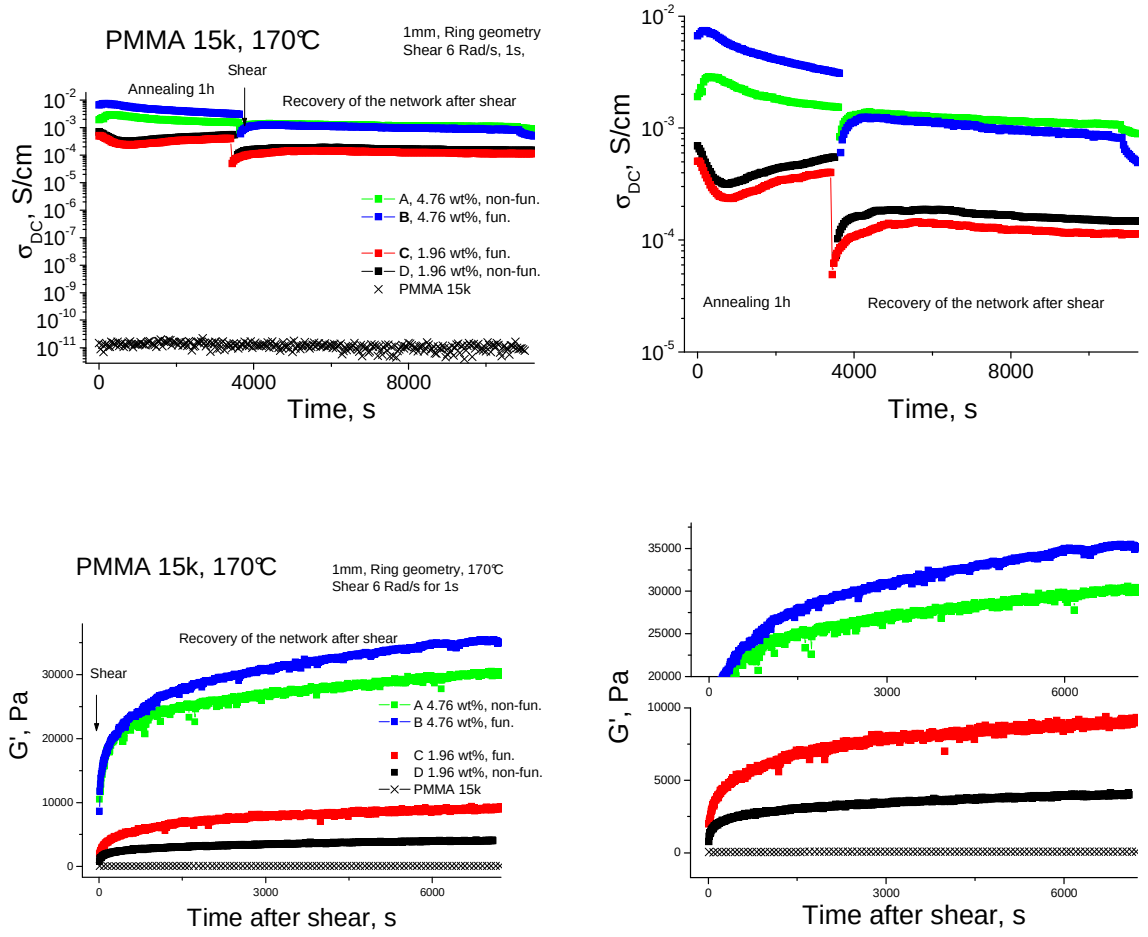

Figure C.39: Conductivity (σ_{DC}) and shear modulus (G') of PMMA 15k samples A, B, C and D.

Figure C.39 shows the conductivity and shear modulus obtained in such a shear experiment. The conductivity of all CNT reinforces PMMA 15k samples is dramatically enhanced by 7 to 8 orders of magnitude. The best conductivity was obtained for the samples with 4.76 wt% CNTs with 10^{-3} S/cm. For comparison, undoped silicon has a conductivity of $2.5*10^{-6}$ S/cm and germanium of $1.5*10^{-2}$ S/cm. This conductivity is therefore very well in the range of semiconductors. Unfortunately, the polymer functionalization of the CNTs has no influence on the conductivity. This was unexpected as the CNT distribution should be influenced by the polymer functionalization. This is also true for the samples with 1.96 wt% of stabilized and

unstabilized CNTs. They show conductivities around 10^{-4} S/cm and are also identically within the experimental error. As both conductivities of the 1.96 and 4.76 wt% doped samples are far above the conductivity of pure PMMA 15k (10^{-11} S/cm), we believe that both sets are far beyond the electrical percolation threshold.

Contrary to the electrical behavior are the mechanical properties: Here the polymer functionalization has a strong influence on the shear modulus and the stabilizing polymer enhances the modulus by 20% (4.76 wt%) to 100% (1.96 wt%). The absolute values are small for 1.96 wt% CNTs (3 / 8 kPa) and increase up to 30 / 35 kPa (4.76 wt%). These values are of course not optimal, but compared to the very low toughness of the PMMA 15k matrix (0.08 kPa), this is a large enhancement. The change is dramatic between 1.96 and 4.76 wt% and therefore, we believe that the mechanical percolation threshold lies in between those values. The mechanical percolation threshold is expected to be higher than the electrical one, as the terms of percolation are different. For electronic percolation, the conditions are less strict concerning direct contact of the tubes as charge hopping can also happen if the CNTs are only close to each other. The mechanical percolation needs hard contact and entanglement of the CNTs for the build-up of a percolated network and thus higher weight fractions. Another notable property of both sets is a strong shear thinning, as the mechanical toughness drops drown strongly after the 6 rad shearing and recovers over time. This can be understood by shear alignment of the CNTs, which breaks the percolated network vertically (this is the measurement direction of the conductivity and shear modulus). This is followed by the entropically driven diffusion back to a random orientation of the CNTs leading back to a vertically percolated network again.

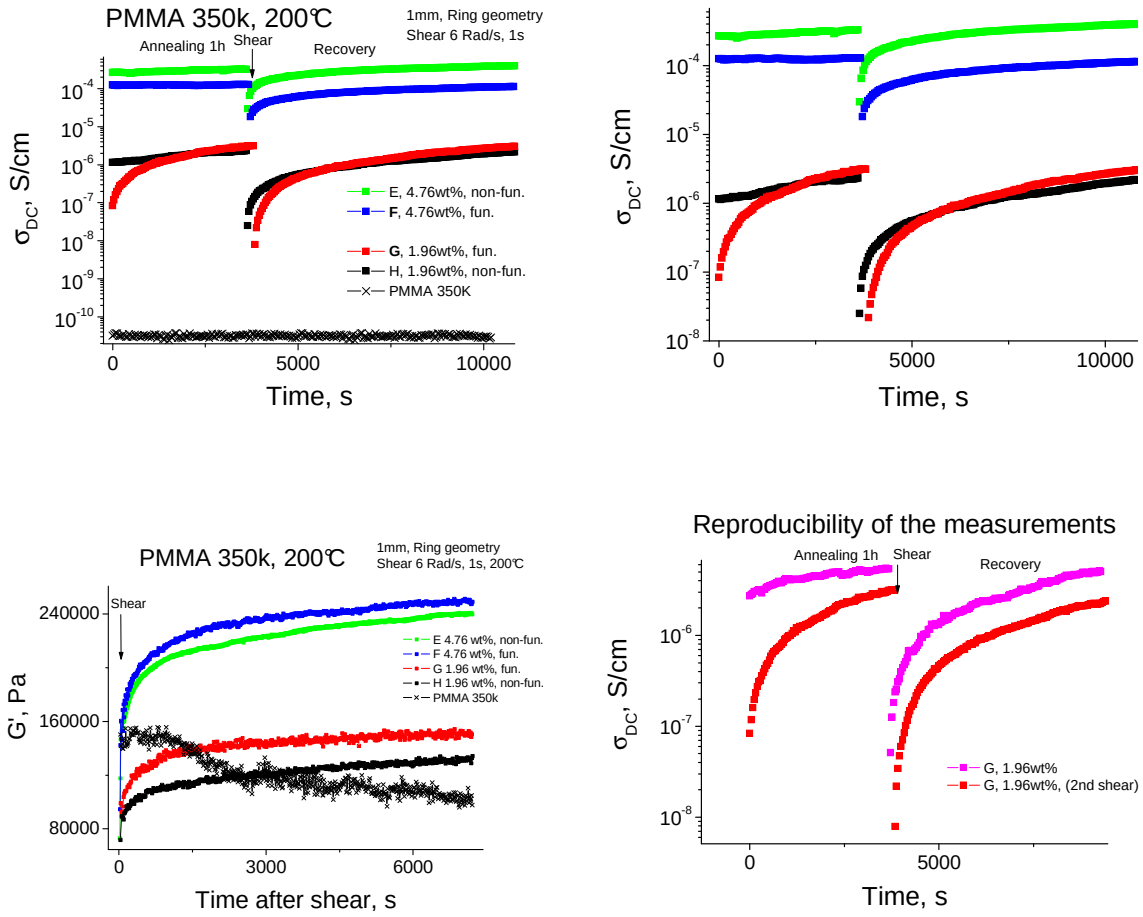

Figure C.40: Conductivity (σ_{DC}) and shear modulus (G') of PMMA 350k samples E, F, G, H and reproducibility of the measurements (sample G).

Figure C.40 shows the results obtained with PMMA 350k as matrix polymer. On the first glance, the electrical conductivity is lower but the shear modulus is dramatically larger than in the PMMA 15k matrix. The lower electrical conductivity might be due to an inferior dispersion of the CNTs in the matrix, as already seen in the SEM images (figure C.38). The electrical conductivity is again – within the experimental error – independent of the addition of stabilizing polymer and the shear modulus is only enhanced slightly (1 (4.76 wt%) to 15% (1.96 wt%)). The electrical percolation in this matrix is expected to be in the range of 1.96 wt% as the conductivity is in between the bulk and 4.76 wt% value. The mechanical percolation threshold is similar to the

PMMA 15k matrix expected between 1.96 and 4.76 wt%, as the lower doped sample shows almost the same modulus as the PMMA 350k matrix. Interestingly, pure PMMA 350k is shear thickening (higher module after shearing) but the CNT doped samples are shear thinning (lower module after shearing). Shear thickening can be explained by entanglement of the polymer chains leading to rubber elasticity. This causes a counterforce upon deformation of the physically cross-linked (entangled) system and results in shear thickening. This effect is obviously suppressed by the addition of the CNTs.

References

1 M. Cadek, J. N. Coleman, K. P. Ryan, V. Nicolosi, G. Bister, A. Fonseca, J. B. Nagy, K. Szostak, F. Béguin, W. J. Blau, *Nano Letters* **2004**, 4, 353-356.

2 P. Pötschke, S. M. Dudkin, I. Alig, *Polymer* **2003**, 44, 5023–5030.

3 I. Alig, T. Skipa, M. Engel, D. Lellinger, S. Pegel, P. Pötschke, *Phys. Stat. Sol. B* **2007**, 244, 4223–4226.

D Summary

D.1 Polymer Functionalized TiO_2 Nanorods

To summarize the results, we successfully applied the concept of polymer functionalization (hairy rod model) to prepare stable organic dispersions of TiO_2 nanorods. We used the highly versatile RAFT polymerization to build up functional diblock copolymers. The soluble blocks used in this work were polymethyl methacrylate (PMMA) and poly((diethylene glycol monomethyl ether) methacrylate) (PDEGMEMA), which were polymerized as the first block with low polydispersities (1.1 to 1.2). For the second block, we used pentafluorophenol methacrylate, a reactive ester monomer. The reactive ester moiety is not destroyed while polymerization and was used afterwards to introduce the anchor units polymer-analogously. The very efficient catechole anchor unit was used since it binds very strongly to oxidic surface and was introduced amine-functionalized as dopamine. The polydispersity of the final block copolymers was still low (around 1.2).

The block copolymers were optimized concerning the lengths of soluble and anchor block and a maximal adsorption of polymers was found for short anchor blocks (≈ 20 units) and short soluble blocks (≈ 40 – 100). The expected trends were confirmed experimentally: Increasing the soluble block length at a given anchor block length and increasing the anchor block length for a given soluble block both decreases the grafting density. The first one is due to the hydrodynamic radius of the soluble block limiting the accessibility of the surface and the second one is due to the limitation of free surface by larger anchor blocks.

After polymer functionalization the solution properties were investigated. The solubility was – as expected – good in suitable solvents for the polymer corona (for PMMA: chloroform, THF, dioxane, etc.; for PDEGMEMA: H_2O (LCST), alcohols,

chloroform, THF, dioxane). We investigated the organic dispersions by dynamic as well as static light scattering and found a hydrodynamic radius and a radius of gyration of approximately the same size as the length average. As this is not expected from theoretical considerations for uniform, monodisperse cylinders, we included a distribution function in the calculations and were able to reproduce the experimental values theoretically. Thus, the nanorods are ideally dispersed as single objects in the organic solvents. For PDEGMEMA functionalized nanorods in water, we observed the LCST-switching of the polymer corona microscopically by dynamic light scattering and macroscopically by turbidity measurements. We found that the dispersion stability is – as predicted – a function of temperature and the dispersion was totally unstable above the LCST. Thus, also stimuli responsive polymers can be addressed even when immobilized as corona on the nanorod surface.

AFM was used to visualize the PDEGMEMA polymer corona. The measurements were done in the tapping mode, in which the phase image is sensitive for the viscoeleastic properties of the sample. The inorganic nanorod is expected to be very hard, but the PDEGMEMA corona is very soft (low T_g polymer). Experimentally, we also found a strong contrast in the phase image between nanorod and polymer corona.

Directly correlated to the polymer corona is the thermotropic behavior of the lyotropic liquid crystal found in PEG 400 as “solvent”. PEG 400 is a suitable solvent for PMMA that does not evaporate and is thermally stable up to 180°C. The phase diagram of PMMA functionalized TiO_2 nanorods in PEG 400 was investigated and a lyotropic liquid crystalline phase was found for nanorod volume fractions between 0.2 and 0.65. Interestingly, all of them showed a clearing temperature (thermal transition to an isotropic phase), which increased with increasing nanorod volume fraction. This is not expected when considering only hard-body interactions between the rods and

must be due to soft interactions induced by the polymer corona. The thermotropic phase behavior was investigated for a mixture with a nanorod volume fraction of 0.2 and a rich phase behavior was found. We analyzed the sample in polarizing microscopy equipped with a heating stage and in a DSC to determine the transition temperatures as well as the textures of the phases. The sample showed two smectic and a nematic phase before reaching the isotropic phase. The phase sequence upon cooling was isotropic to nematic: 63 °C; nematic to smectic A: 52 °C; smectic A to smectic 2: 42 °C. The transition temperatures were broad, also indicating the polydispersity of the nanorods. The phases were first assigned according to their texture in polarizing microscopy and afterwards by SEM and SAXS. SEM pictures of dried nematic phases were investigated and well-ordered phases were found. The SAXS experiments were very hard to perform as the reflections are very close to the beam stopper (very small angles) and we could only record the scattering of the first smectic phase. It showed a reflection corresponding to a layer distance of 55 nm which is reasonable for the shorter nanorods used in this experiment. The peak was rather broad also indicating a distribution of layer distances. This together with size separation effects found by SEM indicate that the polydisperse rods form a smectic phase by orientation of size separated the rods to a layered structure.

The lyotropic phase can also be used for the alignment of the nanorods. For this purpose, an evaporating solvent has to be used. We used a dilute methanolic dispersion of PDEGMEMA stabilized nanorods and drew a structured substrate very slowly out of this dispersion. The substrate had small channels that controlled the meniscus. Inside the meniscus, solvent evaporates faster (higher curvature → higher vapor pressure), which accumulates the nanorods. This forces the nanorods to form a lyotropic liquid crystalline phase, which forms perpendicular to the meniscus and leads to an orientation of the nanorods in drawing direction. By this method, oriented

films were prepared and analyzed by SEM. The images show a dried nematic orientation of TiO_2 nanorods over several micrometers and the order parameter of the film was calculated using an image software and seizing each nanorod by hand. The order parameter was 0.7 (zero = unordered; one = perfectly ordered), which is a typical value for well-ordered nematic phases. Thus the macroscopic orientation of TiO_2 nanorods was realized using an intermediate lyotropic liquid crystalline phase.

D.2 Polymer Functionalized Carbon Nanotubes

Carbon nanotubes can also be functionalized following the hairy rod approach. Again functional polymers, which were prepared by RAFT polymerization, were used for their functionalization. In this case two synthetic routes were compared leading first to an alpha functionalized polymer and second to a block copolymer. For the first approach, an anchor unit functionalized RAFT agent is synthesized first and used to polymerize the monomer for the soluble block. This leads to an alpha anchor unit functionalized polymer. The second approach is the same as described above for TiO_2 nanorods and an anchor block copolymer is synthesized. For CNTs, pyrene units have been found to be suitable anchor units and this group is very well compatible with radical reactions, which allows to compare alpha functionalized polymers versus block copolymers. Both systems were synthesized with low polydispersities (around 1.2) and compared for their adsorption behavior on MWCNTs. The alpha pyrene functionalized polymers showed an adsorption that decreased with increasing soluble block length. This effect was expected and is due to sterical hindrance of the soluble blocks and to desorption of the chains, which is more likely for a longer soluble block (entropy win of the soluble block vs. the binding enthalpy of the anchor unit). The binding enthalpy of pyrene units on CNTs is not as

strong as for catecholes on oxidic surface, leading to adsorption / desorption equilibria. This can be avoided by using anchor block copolymers as they show a stronger adsorption. The adsorption increased with increasing block length and got best for 13 to 20 repeat units in the pyrene containing block. This can be interpreted by suppression of desorption when enough anchor units bind simultaneously.

Stable dispersions were prepared in THF and water and the impact of polymer and CNT concentration on the stability was investigated. Stable dispersions up to 2.5 mg nanotubes per ml of solvent were found, but only for specific polymer concentrations. When too little polymer is added, the dispersions are instable due to insufficient surface coverage. This can be overcome by adding a polymer excess leading to a stable surface coverage. But on the other hand, adding too much polymer results in unstable dispersions again. This effect can be understood as depletion, which is an entropically driven demixing of spheres (polymer coils) and rods (CNTs). Thus adding more polymer is counterproductive and leads to CNT aggregates. Depletion can be induced either by an excess of the functionalization polymer or by a neutral polymer. The latter effect was investigated with PEG of different molecular weight and the result was that depletion is only occurring when PEG of equal or larger molecular weight than the stabilizing polymer (grafted on the CNTs) was used.

Interestingly, the depletion forces may orient the CNTs into a lyotropic liquid crystalline phase. Such a phase was found in an aqueous dispersion of PDEGMEMA stabilized CNTs. The lyotropic phase sedimented as its density was increased but passed a syringe filter by shear alignment. The filtered dispersion sedimented again and showed a birefringent texture upon evaporation of the water. Therefore we investigated the lyotropic phase behavior in more detail.

We prepared organic dispersions of PMMA stabilized CNTs in THF with large excess of stabilizing polymer and filtered them. Then we prepared hybrid films first by rapid evaporation of the solvent done by spin coating and second by slow evaporation of the solvent between glass slides. The spin coated film showed no birefringence and the CNTs were distributed homogeneously over the PMMA film. The slowly evaporated films demixed and showed highly birefringent domains of oriented CNTs within the polymer matrix. For low CNT concentrations, the domains were statistically oriented in space but for larger CNT concentrations, the birefringence of neighboring domains was strongly correlated. This is probably due to shear alignment of the lyotropic phase while drying, leading to the same orientation of the CNTs in neighboring domains.

To investigate this phenomenon in the liquid crystalline phase, PMMA functionalized CNTs were investigated in PEG 400. The PMMA functionalized CNTs were dispersed in THF and PEG 400 was added. Then the THF was evaporated again leading to the lyotropic liquid crystalline phase. Birefringent droplets formed and were investigated by polarizing microscopy. They had a texture usually found for nematic droplets and showed a clearing to the isotropic phase around 48 °C. The orientation of the CNT within the droplets could be revealed by their adsorption of linear polarized light along their long axis. Therefore the analyzer was removed and the transmission of linear polarized light investigated. The droplets showed an adsorption of light parallel to the incident linear polarized light which followed the rotation of the polarizer. Therefore the orientation of the CNTs is radial within the droplets. The lyotropic liquid crystalline phase can therefore be used to orient carbon nanotubes similar to the results shown for TiO_2 nanorods.

A totally other topic is the reinforcement of polymers by CNT. As CNTs have a very good mechanical toughness combined with large electrical conductivity, they are

highly interesting fillers for polymers. As depletion is a critical factor for the homogeneous distribution of CNTs, we investigated PMMA functionalized CNTs in commercially available PMMAs of different molecular weights. One was chosen with a molar mass smaller than those of the grafted PMMA chains on the CNT surface (M_n = 9.000 g/mol, $M_{n,graft}$ = 18.000 g/mol) and another one with a higher molecular weight (M_n = 420.000 g/mol). To investigate the impact of the stabilizing polymer, two sets were prepared: One with stabilizing polymer (ratio of CNT to polymer = 10 : 1) and the other one without stabilizing polymer. The amount of CNTs added was also varied and samples with 1.96 and 4.76 wt% CNTs were prepared. Overall, eight different samples were investigated. The distribution of CNTs was analyzed by SEM images taken at the breaking-edge. The samples in the low molecular weight PMMA matrix were distributed very well with and without stabilizing polymer, whereas the distribution was much worse in the high molecular weight matrix. In the latter matrix, the CNTs were not distributed well without stabilizing polymer (large clusters of aggregated CNTs). The mechanical and electrical investigation of the sample was performed at the DKI in Darmstadt and the results can be summarized as follows: The addition of stabilizing polymer had only little effect on the conductivity but enhanced the mechanical toughness up to 100%. This is an important result as the absolute amount of stabilizing polymer in the matrix was very small (around 0.5 wt%) and shows that controlling the interface between CNT and polymer matrix is very important.

Overall, the concept of polymer functionalization was successfully applied for the stabilization of inorganic, anisotropic nanoparticles in organic media. The anisotropic nanoparticles were forming lyotropic liquid crystalline phases, as predicted from theory, with an additional thermotropic behavior induced by the polymer corona. This

opened the possibility to align the anisotropic nanoparticles macroscopically, which is a key requirement for the build-up of nano-scaled devices. In addition polymer functionalization allows their incorporation into polymeric matrices leading to highly interesting hybrid materials.

E Acknowledgement

First of all, I would like to thank my girlfriend, my parents, my advisor and all co-authors of the publications for their tremendous support. Especially the Max Planck Institute for Polymer Research (Mainz), the Institute for physical Chemistry (Mainz) and the Institute for physical Chemistry (Stuttgart), where a couple of experiments were done, need to be acknowledged.

Financial support of this work came mainly by the “Fonds der chemischen Industrie” and the “Graduate School of Excellence: Mainz” (Materials Science in Mainz) subdivision “POLYMAT” (polymers in advanced technologies) granting stipends, numerous summer schools and soft skill trainings for me. Additionally financial support come from the “International Research Training Group: Self-organized Materials for Optoelectronics”, a DFG (german science foundation) funded cooperation of the Seoul National University, Hannam University (both Korea) and the University of Mainz (Germany). Non-financial support came also from the “Studienstiftung des deutschen Volkes”, also allowing the participation in summer school.

F Appendix

Figure, Table and Equation Index